

ON THE NUMERICAL CONSTRUCTION OF  
HYPERBOLIC STRUCTURES FOR COMPLEX  
DYNAMICAL SYSTEMS

A Dissertation

Presented to the Faculty of the Graduate School

of Cornell University

in Partial Fulfillment of the Requirements for the Degree of

Doctor of Philosophy

by

Jennifer Suzanne Lynch Hruska

August 2002

© 2002 Jennifer Suzanne Lynch Hruska  
ALL RIGHTS RESERVED

# ON THE NUMERICAL CONSTRUCTION OF HYPERBOLIC STRUCTURES FOR COMPLEX DYNAMICAL SYSTEMS

Jennifer Suzanne Lynch Hruska, Ph.D.  
Cornell University 2002

Our main interest is using a computer to rigorously study  $\epsilon$ -pseudo orbits for polynomial diffeomorphisms of  $\mathbb{C}^2$ . Periodic  $\epsilon$ -pseudo orbits form the  $\epsilon$ -chain recurrent set,  $\mathcal{R}_\epsilon$ . The intersection  $\bigcap_{\epsilon>0}\mathcal{R}_\epsilon$  is the chain recurrent set,  $\mathcal{R}$ . This set is of fundamental importance in dynamical systems.

Due to the theoretical and practical difficulties involved in the study of  $\mathbb{C}^2$ , computers will presumably play a role in such efforts. Our aim is to use computers not only for inspiration, but to perform rigorous mathematical proofs.

In this dissertation, we develop a computer program, called *Hypatia*, which locates  $\mathcal{R}_\epsilon$ , sorts points into components according to their  $\epsilon$ -dynamics, and investigates the property of *hyperbolicity* on  $\mathcal{R}_\epsilon$ . The output is either “yes”, in which case the computation *proves* hyperbolicity, or “not for this  $\epsilon$ ”, in which case information is provided on numerical or dynamical obstructions.

A diffeomorphism  $f$  is *hyperbolic on a set  $X$*  if for each  $x$  there is a splitting of the tangent bundle of  $x$  into an *unstable* and a *stable* direction, with the unstable (stable) direction expanded by  $f$  ( $f^{-1}$ ). A diffeomorphism is *hyperbolic* if it is hyperbolic on its chain recurrent set.

Hyperbolicity is an interesting property for several reasons. Hyperbolic diffeomorphisms exhibit *shadowing* on  $\mathcal{R}$ , *i.e.*,  $\epsilon$ -pseudo orbits are  $\delta$ -close to true orbits. Thus they can be understood using combinatorial models. Shadowing also implies *structural stability*, *i.e.*, in a neighborhood in parameter space the behavior is constant. These properties make hyperbolic diffeomorphisms amenable to computer investigation via  $\epsilon$ -pseudo orbits.

We first discuss *Hypatia* for polynomial maps of  $\mathbb{C}$ . We then extend to polynomial diffeomorphisms of  $\mathbb{C}^2$ . In particular, we examine the class of Hénon diffeomorphisms, given by

$$H_{a,c}: (x, y) \rightarrow (x^2 + c - ay, x).$$

This is a large class of diffeomorphisms which provide a good starting point for understanding polynomial diffeomorphisms of  $\mathbb{C}^2$ . However, basic questions about the complex Hénon family remain unanswered.

In this work, we describe some Hénon diffeomorphisms for which *Hypatia* verifies hyperbolicity, and the obstructions found in testing hyperbolicity of other examples.

## BIOGRAPHICAL SKETCH

Jennifer Suzanne Lynch Hruska moved to Ithaca, New York, in May 1997. Here she lived, for the first time, away from her home state of Missouri, away from her parents, sisters, grandparents, great grandmother, aunts, uncles and cousins. Suzanne had just completed her B.S. in applied mathematics from the University of Missouri at Rolla, only 30 miles from her childhood town of Waynesville. In Ithaca she attended Cornell University with the intention of earning her Ph.D. in mathematics, an intention which has been realized with the submission of this dissertation. She agrees with Cornell's Director of Graduate Studies in mathematics, who explained at the May 2002 commencement exercises that graduate students are to learn, to learn how to learn, to learn how to impart knowledge to others, and to learn how to create knowledge. Cornell and Ithaca have provided an excellent environment for Suzanne to achieve these goals.

During this process, she also earned her M.S. in mathematics from Cornell (August 1999) and met and married fellow mathematics graduate student Geoffrey Christopher Hruska (June 2000). She became a vegetarian and learned to cook, swing dance and program a computer. She traveled to Barcelona, Marseilles and Paris.

In August 2002, Suzanne will move to Long Island to be a (VIGRE) postdoctoral fellow at the State University of New York at Stony Brook.

For Terry and Jan Primas

## ACKNOWLEDGEMENTS

During my five years at Cornell, many people have provided encouragement and support. Friends, family, and colleagues have all contributed to my finishing this process with my sanity intact. I would like to individually acknowledge a few who stand out as having been particularly helpful. My advisor, John Smillie, has patiently shared his knowledge and wisdom during many many meetings. He has provided sound guidance in each phase of my studies, from the formation of my dissertation topic to securing a good position for after I leave Cornell. John Hamal Hubbard's enthusiasm, apparent on my first visit to Cornell as a prospective graduate student, brought me to the subject of holomorphic dynamical systems. His suggestions led to this dissertation topic and have been useful for studying the problem. Greg Buzzard helped me to gain an improved perspective on mathematics and life any time I was starting to feel overwhelmed by the process. We had many useful discussions when I was first reading papers on the Hénon family, and in the early stages of my dissertation. John Guckenheimer provided feedback on this dissertation and served on my special committee, and Clifford Earle introduced me to complex analysis in the graduate course he taught my first year at Cornell, as well as served as a member of my special committee. I also had helpful conversations with Yulij Ilyashenko, Eric Bedford, John Erik Fornæss, Mattias Jonsson, Ricardo Oliva, and Roland Roeder. I would also like to thank Adrien Douady, for invitations and hospitality.

Harnessing the power of a computer has been a central theme in my work. Warwick Tucker introduced me to a key technique in rigorous computing, interval arithmetic. Karl Papadantonakis, along with other members of Cornell's "Hénon working group" (Smillie, Hubbard, Guckenheimer, Ilyashenko, Buzzard, Tucker, Ricardo Oliva, David Brown, Yutaka Ishii, and occasionally Bedford, Douady, and Peter Papadopol), opened a world of fascinating possibilities in the dynamics of the Hénon family through the development and examination of new computer programs `FractalAsm` and `SaddleDrop` ([1]). Additionally, Bob Terrell has often provided technical support in his capacity as System Administrator for the Cornell mathematics department's excellent computing facilities. My work benefited from the use of computers purchased with funds from a SCREMS grant from the NSF (National Science Foundation).

As a graduate student, I received financial support through a variety of sources, most notably Cornell University and the NSF. Various sources of funds supported my participation in conferences and allowed increased time for working on mathematical research.

Graduate school is extremely rewarding overall, but at times can be incredibly frustrating. My parents, my sisters, my closest friends, and most of all my husband deserve high praise for not only putting up with me these five years, but making my time here better in myriad ways.



## TABLE OF CONTENTS

<b>1</b>	<b>Introduction and Background</b>	<b>1</b>
1.1	The Hénon family . . . . .	1
1.2	Invariant sets of interest . . . . .	2
1.3	Hyperbolicity . . . . .	8
1.4	Overview of this dissertation: <i>Hypatia</i> . . . . .	19
<b>2</b>	<b>The box-chain recurrent set</b>	<b>21</b>
2.1	Trapping regions for $\mathcal{R}_\delta$ . . . . .	21
2.2	The box-chain recurrent graph . . . . .	23
2.3	Algorithm to build a box-chain recurrent graph . . . . .	28
<b>3</b>	<b>Hyperbolicity in one complex dimension</b>	<b>31</b>
3.1	Introduction: box-expansion . . . . .	31
3.2	Algorithm to build a metric showing box-expansion . . . . .	32
3.3	Box-expansion implies continuous expansion . . . . .	34
3.4	Finding a good expansion amount . . . . .	35
3.4.1	An optimal, yet impractical solution . . . . .	36
3.4.2	An approximate, efficient solution . . . . .	38
3.5	Building a better metric . . . . .	39
3.5.1	An optimal, yet very impractical solution . . . . .	40
3.5.2	An approximate, realistic solution . . . . .	44
3.6	Examples of running <i>Hypatia</i> for polynomial maps . . . . .	47
<b>4</b>	<b>Hyperbolicity in two complex dimensions</b>	<b>65</b>
4.1	Introduction: box-hyperbolicity . . . . .	65
4.2	Algorithm to show box-hyperbolicity . . . . .	66
4.2.1	Defining stable and unstable directions . . . . .	66
4.2.2	Defining a metric on the directions . . . . .	68
4.2.3	Defining a cone field . . . . .	70
4.3	Characterizing box-hyperbolicity . . . . .	71
4.3.1	Checking box-hyperbolicity with Hermitian forms . . . . .	71
4.3.2	Box-hyperbolicity implies hyperbolicity . . . . .	73
4.4	Examples of running <i>Hypatia</i> for Hénon diffeomorphisms . . . . .	77
4.4.1	A generic run of <i>Hypatia</i> for a Hénon diffeomorphism . . . . .	77
4.4.2	Box-hyperbolic Hénon diffeomorphisms . . . . .	86
4.4.3	Describing box covers which are not box-hyperbolic . . . . .	86
<b>5</b>	<b>Analysis of <i>Hypatia</i>'s performance</b>	<b>97</b>
5.1	Separating $J$ from a fixed sink . . . . .	97
5.2	Conclusions . . . . .	107
<b>A</b>	<b>Interval arithmetic</b>	<b>109</b>

<b>B Pseudo-code</b>	<b>111</b>
<b>References</b>	<b>114</b>

## LIST OF TABLES

3.1	Examples of running <i>Hypatia</i> for $P_c(x) = x^2 + c$ . . . . .	55
3.2	Examples of running <i>Hypatia</i> for $P_{c,a}(z) = z^2 - 3a^2z + c$ . . . . .	64
4.1	Data from verifying hyperbolicity with <i>Hypatia</i> . . . . .	87
4.2	Data on subdivision for Example 4.4.4. . . . .	88
4.3	Data on stable/unstable directions for Example 4.4.4. . . . .	89
4.4	Data on first metric and cones for Example 4.4.4. . . . .	90
4.5	Data on subdivision for Example 4.4.5. . . . .	92
4.6	Data on stable/unstable directions for Example 4.4.5. . . . .	93
4.7	Data on subdivision for Example 4.4.6. . . . .	94
4.8	Data on stable/unstable directions for Example 4.4.6. . . . .	95
4.9	Data comparing Examples 4.4.5 and 4.4.6. . . . .	96
5.1	Constants for sink/ $J$ separation estimates for Example 5.1.1. . . .	107



## LIST OF FIGURES

1.1	$\epsilon$ -recurrence . . . . .	3
1.2	Examples of Julia sets for $P_c(x) = x^2 + c$ . . . . .	4
1.3	A sketch of $J^\pm \cap \mathbb{R}^2$ for a Hénon diffeomorphism . . . . .	5
1.4	A parametrized slice of $K$ for a Hénon diffeomorphism . . . . .	7
1.5	The Mandelbrot set . . . . .	9
1.6	Julia sets for $P_c$ illustrating structural stability . . . . .	9
1.7	Julia sets for Hénon diffeomorphisms illustrating structural stability	13
1.8	A Hénon parameter space slice: the $c$ -plane with $a = .3$ . . . . .	14
1.9	A parametrization of $W^u(p)$ for $H_{a,c}, c = -1.1875, a = .15$ . . . . .	16
1.10	A parametrization of $W^u(p)$ for $H_{a,c}, c = -1.05, a = .05$ . . . . .	16
1.11	A parametrization of $W^u(p)$ , for $H_{a,c}, c = -1.17, a = .3$ . . . . .	17
1.12	A parametrization of $W_p^u$ for $H_{a,c}, c = -3.5, a = .57$ . . . . .	17
1.13	A blow-up of the left region of Figure 1.12, for maps on the loop. .	18
2.1	Subdivision of box cover . . . . .	29
3.1	Graph illustrating Example 3.4.5 . . . . .	37
3.2	Diagram illustrating proof of Proposition 3.5.5 . . . . .	42
3.3	Graph, with box multipliers, for Examples 3.5.6, 3.5.7, and 3.5.8 .	43
3.4	Graph with optimal edge expansion. . . . .	44
3.5	Graph with badly guessed edge expansion. . . . .	45
3.6	Graph illustrating another way of badly guessing edge expansion. .	45
3.7	Graph illustrating a good way of guessing edge expansion. . . . .	46
3.8	A box cover of $\mathcal{R}$ for $P_c, c = -1$ . . . . .	48
3.9	A box cover of $\mathcal{R}$ for $P_c, c = -.123 + .745i$ . . . . .	49
3.10	A coarser box cover of $\mathcal{R}$ for $P_c, c = -.123 + .745i$ . . . . .	50
3.11	A box cover of $\mathcal{R}$ for $P_c, c = -1.31$ . . . . .	50
3.12	A box cover of $\mathcal{R}$ for $P_c, c = -.504 + .563i$ . . . . .	51
3.13	A box cover of $J$ for $P_c, c = .388 + .22i$ . . . . .	52
3.14	A box cover of $J$ for $P_c, c = -1.755$ . . . . .	52
3.15	A box cover of $J$ for $P_c, c = -.1588 + 1.033i$ . . . . .	53
3.16	A box cover of $J$ , for $P_c, c = -.75 + .3i$ . . . . .	54
3.17	A box cover of $J$ for $P_c, c = .3$ , for a (mostly) $2^8 \times 2^8$ grid. . . . .	54
3.18	Legend for metric constant shading in Figures 3.19 and 3.20 . . . .	57
3.19	Shading illustrates the first box-expanded metric found . . . . .	58
3.20	Shading illustrates improvements made with <b>BetterMetric</b> . . . .	58
3.21	A box cover of $J$ for $P_{c,a}, c = i, a = 0.1i$ . . . . .	59
3.22	A box cover of $J$ for $P_{c,a}, c = .75i, a = 0.5i$ . . . . .	60
3.23	A box cover of $J$ for $P_{c,a}, c = -.19 + 1.1i, a = 0.1i$ . . . . .	61
3.24	A box cover of $J$ for $P_{c,a}, c = -.54 + .54i, a = 0.1i$ . . . . .	61
3.25	A box cover of $J$ for $P_{c,a}, c = -.44 - .525i, a = .3i$ . . . . .	62
3.26	A box cover of $J$ for $P_{c,a}, c = -.44 - .525i, a = .3i$ . . . . .	62

3.27	A box cover of $J$ for $P_{c,a}, c = -.38125 + .40625i, a = 0.5i$ . . . . .	63
4.1	A box cover of $\mathcal{R}$ for $H_{a,c}, c = -.3, a = .1$ . . . . .	79
4.2	A box cover of $\mathcal{R}$ for $H_{a,c}, c = -1.05, a = .05$ . . . . .	80
4.3	A box cover of $\mathcal{R}$ for $H_{a,c}, c = -1.1875, a = .15$ . . . . .	81
4.4	A finer box cover of $\mathcal{R}$ for $H_{a,c}, c = -1.1875, a = .15$ . . . . .	81
4.5	Shading indicates where reasonable cones cannot be defined . . . . .	83
4.6	Shading indicates where reasonable cones cannot be defined . . . . .	83
4.7	Legend for the shading of Figures 4.5 and 4.6 . . . . .	84
4.8	Shading indicates where the cone condition failed . . . . .	85
4.9	A FractalAsm picture of $W_p^u \cap K^+$ for $H_{a,c}, c = -3, a = -.25$ . . . . .	86
4.10	Shading indicates the weakest unstable direction expansion . . . . .	91
5.1	A box cover of $\mathcal{R}$ for $H_{a,c}, c = -1.17, a = .3$ . . . . .	98

# Chapter 1

## Introduction and Background

We give relevant background on dynamical systems and the dynamics of polynomial maps of  $\mathbb{C}$  and polynomial diffeomorphisms of  $\mathbb{C}^2$  in Sections 1.1, 1.2, and 1.3. In Section 1.4, we give an overview of the remainder of the dissertation.

### 1.1 The Hénon family

Thirty years ago, Hénon [37, 38] initiated the study of the diffeomorphism  $H_{a,c}$  of  $\mathbb{R}^2$ , defined by

$$H_{a,c}(x, y) = (x^2 + c - ay, x)$$

because it exhibits the qualitative behavior of a certain Poincaré section of the Lorenz differential equation. Since then,  $H_{a,c}$  has been widely studied as a diffeomorphism of  $\mathbb{R}^2$  with  $a, c$  real parameters. About fifteen years ago, John H. Hubbard began the study and promotion of  $H_{a,c}$  as a holomorphic diffeomorphism of  $\mathbb{C}^2$ , allowing  $a, c$  to be complex. There are several motivations for studying the complex Hénon family, which bring mathematicians with different backgrounds into this field.

The complex Hénon family generalizes the quadratic family,  $P_c: \mathbb{C} \rightarrow \mathbb{C}$ , defined by  $P_c(z) = z^2 + c$ . Many questions have been answered about the dynamics of polynomial maps of  $\mathbb{C}$ , and often an understanding of that area aids in at least an intuitive understanding of the complex Hénon family. Hubbard and colleagues tend utilize this approach ([43, 44, 42]). In this dissertation, we often describe  $P_c$  behavior before describing Hénon family behavior, in order to explain the motivations and results from a simpler viewpoint.

On the other hand, the real dynamics are contained in the complex dynamics, so we may learn about the real system of interest while utilizing the tools of complex analysis. John Smillie, whose background is smooth dynamical systems on  $\mathbb{R}^n$ , and Eric Bedford, coming from classical several complex variables, have made progress doing this ([3]), and have developed many fundamental tools for the complex theory ([4, 5, 6, 7, 2, 8, 9, 10, 11]).

Other members of the field of several complex variables have become interested in the Hénon family. Nessim Sibony and Eric Bedford initiated the use of pluripotential theory as a tool for studying the Hénon family, which was further developed by Sibony and John Erik Forneaess in [23]. Another direction in complex dynamics in several variables is the study of holomorphic self maps of  $\mathbb{C}P^n$ , which has been largely developed by Hubbard and Papadopol ([45]) and Forneaess and Sibony ([34, 33, 32, 30, 31, 28, 29, 27, 26, 25, 24]).

Hénon diffeomorphisms are fundamental to the dynamical study of polynomial diffeomorphisms of  $\mathbb{C}^2$ . Polynomial diffeomorphisms of  $\mathbb{C}^2$  necessarily have polynomial inverses, thus are often called polynomial automorphisms. Friedland and Mil-

nor ([35]) showed that polynomial automorphisms of  $\mathbb{C}^2$  break down into two categories. *Elementary* automorphisms have simple dynamics, and are polynomially conjugate to a diffeomorphism of the form  $(x, y) \rightarrow (ax+b, cy+p(x))$  ( $p$  polynomial,  $a, c \neq 0$ ). *Nonelementary* automorphisms are all conjugate to finite compositions of *generalized Hénon mappings*, which are of the form  $f(x, y) = (p(x) - ay, x)$ , where  $p(x)$  is a monic polynomial of degree  $d > 1$  and  $a \neq 0$ . A generalized Hénon mapping  $f$  has inverse  $f^{-1}(x, y) = (y, (p(y) - x)/a)$ , and derivative

$$\begin{bmatrix} p'(x) & -a \\ 1 & 0 \end{bmatrix},$$

with  $\det(Df) = a$ .

To clarify the situation, one can define a *dynamical degree* of a polynomial automorphism of  $\mathbb{C}^2$ . If  $\deg(f)$  is the maximum of the degrees of the coordinate functions, the dynamical degree is

$$d = d(f) = \lim_{n \rightarrow \infty} (\deg(f^n))^{1/n}.$$

This degree is a conjugacy invariant. Elementary automorphisms have dynamical degree  $d = 1$ . A nonelementary automorphism is conjugate to some automorphism whose polynomial degree is equal to its dynamical degree. In this dissertation, we restrict our attention to automorphisms  $f$  which are nonelementary. Without loss of generality, we assume such  $f$  are finite compositions of generalized Hénon mappings, rather than simply conjugate to mappings of this form.

Thus, the quadratic, complex Hénon family  $H_{a,c}(x, y) = (x^2 + c - ay, x)$  represents the dynamical behavior of the simplest class of nonelementary polynomial automorphisms; those of dynamical degree two. Most of the ideas in this dissertation are extremely general, but we shall often concentrate on the illustrative examples  $P_c(x) = x^2 + c$  and  $H_{a,c}(x, y) = (x^2 + c - ay, x)$ .

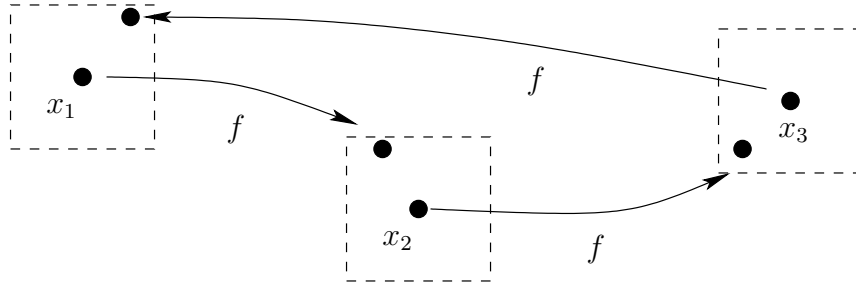
For more background in dynamics in one complex variable, see Milnor's textbook, [50]. For further reading on real dynamical systems, Katok and Hasselblatt provide a comprehensive guide in [47], while Shub in [61] provides a good source for classical theory. A basic textbook for analysis in several complex variables is Hörmander's, [40]. A recent survey of one and two dimensional complex dynamics is given in Morosawa, *et al*, [53].<sup>1</sup>

## 1.2 Invariant sets of interest

The *chain recurrent set*,  $\mathcal{R}$ , the *nonwandering set*,  $\Omega$ , and the *Julia set*,  $J$ , are all attempts at locating the points with dynamically interesting behavior. We define these sets and describe their relationship.

---

<sup>1</sup>This dissertation was typeset with L<sup>A</sup>T<sub>E</sub>X 2<sub>ε</sub>. We recommend the recent [36] for a comprehensive guide to typesetting mathematics with L<sup>A</sup>T<sub>E</sub>X 2<sub>ε</sub>.

Figure 1.1:  $\epsilon$ -recurrence

**Definition 1.2.1.** For a differentiable function  $f$ , the *orbit* of a point  $x_0$  under  $f$  is the sequence of images  $x_0, f(x_0), f^2(x_0), \dots$  under repeated application, or iteration, of the function.

## The chain recurrent set $\mathcal{R}$

Chain recurrence is a useful notion for studying points which are recurrent, as well as points which are approximately recurrent. For more information on using chain recurrence in dynamics, consult [60].

**Definition 1.2.2.** An  $\epsilon$ -chain of length  $n > 1$  from  $p$  to  $q$  is a sequence of points  $\{p = x_1, \dots, x_n = q\}$  such that  $|f(x_k) - x_{k+1}| < \epsilon$  for  $1 \leq i \leq n - 1$ .

**Definition 1.2.3.** A point  $p$  belongs to the  $\epsilon$ -chain recurrent set,  $\mathcal{R}_\epsilon$ , of a function  $f$  if there is an  $\epsilon$ -chain from  $p$  to  $p$  (Figure 1.1). Then the *chain recurrent set* is  $\mathcal{R} = \bigcap_{\epsilon > 0} \mathcal{R}_\epsilon$ .

Note the following facts about the chain recurrent set:

- For any  $\epsilon$ ,  $\mathcal{R} \subset \mathcal{R}_\epsilon$ .
- $\mathcal{R}$  is closed and invariant.
- If  $\epsilon_1 < \epsilon_2$ , then  $\mathcal{R}_{\epsilon_1} \subset \mathcal{R}_{\epsilon_2}$ .

We can decompose  $\mathcal{R}$  into components which do not interact with one another.

**Definition 1.2.4.** A point  $q$  is in the *forward chain limit set* of a point  $p$ ,  $\mathcal{R}(p)$ , if for all  $\epsilon > 0$ , for all  $n \geq 1$ , there is an  $\epsilon$ -chain from  $p$  to  $q$  of length greater than  $n$ .

Then put an equivalence relation on  $\mathcal{R}$  by:  $p \sim q$  if  $p \in \mathcal{R}(q)$  and  $q \in \mathcal{R}(p)$ . Equivalence classes are called *chain transitive components*.

Analogously we can define  $\mathcal{R}_\epsilon(p)$  and  $\epsilon$ -chain transitive components.

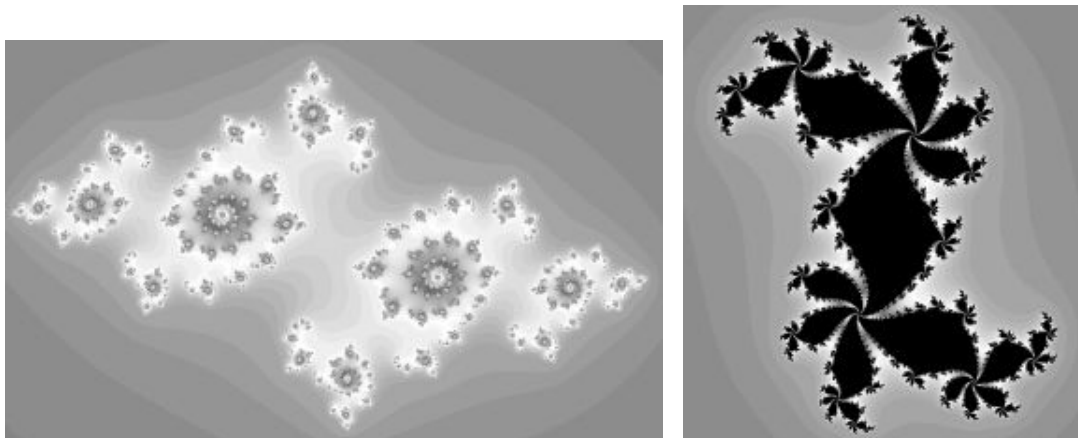


Figure 1.2: Examples of Julia sets for  $P_c(x) = x^2 + c$

**Definition 1.2.5.** Given  $\epsilon > 0$ , a point  $q$  is in the  $\epsilon$ -forward chain limit set of a point  $p$ ,  $\mathcal{R}_\epsilon(p)$ , if for some  $n > 1$ , there is an  $\epsilon$ -chain from  $p$  to  $q$  of length  $n$ .

Then put an equivalence relation on  $\mathcal{R}_\epsilon$  by:  $p \sim q$  if  $p \in \mathcal{R}_\epsilon(q)$  and  $q \in \mathcal{R}_\epsilon(p)$ . Equivalence classes are called  $\epsilon$ -chain transitive components.

These are sets of dynamical interest which are very natural to study using a computer.

## The Julia set $J$

**Definition 1.2.6.** For a polynomial map  $f$  of  $\mathbb{C}$ , the *filled Julia set*,  $K$ , is the set of points whose orbits are bounded under  $f$ ; the *Julia set*,  $J$ , is the topological boundary of  $K$ .

See Figure 1.2 for examples of Julia sets. Note that  $J$  is an invariant set for  $f$ . To see more such pictures, download one of the many programs for drawing these pictures, like Fractint for Windows, or FractalAsm for Macintosh (available at [1]).

**Definition 1.2.7.** For a polynomial diffeomorphism  $f$ , like  $H_{a,c}$ , there are corresponding Julia sets:

- $K^+(K^-)$  is the set of points whose orbits are bounded under  $f(f^{-1})$  and  $K = K^+ \cap K^-$  is called the *filled Julia set*;
- $J^\pm = \partial K^\pm$  (the topological boundary) and  $J = J^+ \cap J^-$  is called the *Julia set*.

See Figure 1.3 for an drawing of  $J^+$  and  $J^-$  for a Hénon diffeomorphism in  $\mathbb{R}^2$ .

Of course we cannot see all of a Julia set in  $\mathbb{C}^2$ , but methods for visually understanding it have been developed. Intuitively, one may try to merge Figures 1.2

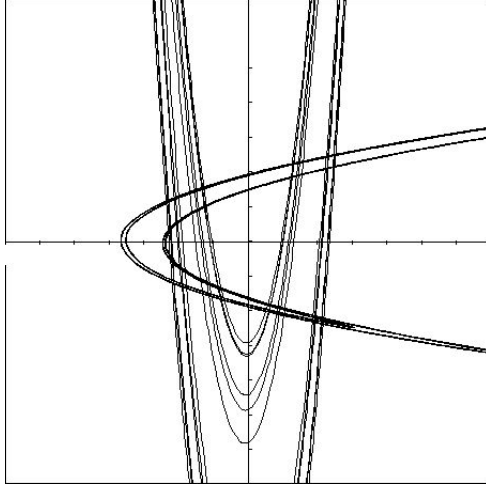


Figure 1.3: A sketch of  $J^\pm \cap \mathbb{R}^2$  for a Hénon diffeomorphism

and 1.3 to imagine complexifying the curved lines of  $J^+$  and  $J^-$  and inserting a  $P_c$ -like Julia set in each of them. More precise ways of visualizing complex Hénon Julia sets are discussed a few pages below.

## Relating $\mathcal{R}$ , $J$ , and $\Omega$

**Definition 1.2.8.** A point  $p$  belongs to the *nonwandering set*,  $\Omega$ , of a diffeomorphism  $f$  if for every neighborhood  $U$  of  $p$ , there is an  $n > 1$  such that  $f^n(U)$  intersects  $U$ .

**Theorem 1.2.9 ([6]).** *Let  $f$  be a polynomial diffeomorphism of  $\mathbb{C}^2$ , with  $d(f) > 1$ . Then  $J \subset \Omega \subset \mathcal{R} \subset K$  and  $J$  is contained in a single chain transitive component of  $\mathcal{R}$ .*

**Theorem 1.2.10 ([6]).** *Let  $f$  be a polynomial diffeomorphism of  $\mathbb{C}^2$ , with  $d(f) > 1$ . Assume  $|\det Df| < 1$ . Let  $O_j$  for  $j = 1, 2, \dots$  denote the sink orbits of  $f$ .*

1.  $\Omega$  is the union of  $J$ , all rotational domains, and all  $O_j$ .
2.  $\mathcal{R}$  is the set of bounded orbits (in forward/backward time) not in punctured basins, where if  $p$  is a sink, the punctured basin of  $p$  is  $W^s(p) - p$ .
3. The chain transitive components are the sink orbits,  $O_j$ , and the set  $\mathcal{R} - \cup_j O_j$ .

## Unstable manifolds and Connectivity of $J$

A useful strategy in the study of these two complex dimensional objects is to study dynamically significant one complex dimensional invariant manifolds.

**Definition 1.2.11.** A point  $p$  is *periodic* under a map  $f$  if there exists some integer  $n$ , called the *period* of  $p$ , such that  $f^n(p) = p$ .

**Definition 1.2.12.** Let  $f$  be a diffeomorphism of  $\mathbb{C}^2$ . If  $p$  is a periodic point of period  $m$ , and the eigenvalues  $\lambda, \mu$  of  $D_p f^m$  satisfy  $|\lambda| > 1 > |\mu|$  (or vice-versa), then  $p$  is a *saddle periodic point*. The large (small) eigenvalue is called the unstable (stable) eigenvalue.

**Definition 1.2.13.** If  $p$  is a saddle periodic point for an invertible  $f$ , then the *stable manifold* of  $p$  is  $W^s(p) = \{q: d(f^n(q), f^n(p)) \rightarrow 0 \text{ as } n \rightarrow \infty\}$ , and the *unstable manifold* of  $p$  is  $W^u(p) = \{q: d(f^{-n}(q), f^{-n}(p)) \rightarrow 0 \text{ as } n \rightarrow \infty\}$ .

Below are some basic properties of stable and unstable manifolds of saddle periodic points for Hénon diffeomorphisms, which illustrate why they are useful.

**Theorem 1.2.14.** *Let  $f$  be a polynomial diffeomorphism of  $\mathbb{C}^2$ , with  $d(f) > 1$ , and  $p$  a saddle periodic point of  $f$ .*

1.  $W^u(p)$  ( $W^s(p)$ ) is biholomorphically equivalent to  $\mathbb{C}$ , and on  $W^u(p)$  ( $W^s(p)$ ),  $f$  is conjugate to multiplication by the unstable (stable) eigenvalue of  $D_p f$  ([16]).
2.  $\overline{W^u(p)} = J^+$ , and  $\overline{W^s(p)} = J^-$  ([6]).
3. Assume  $|a| \leq 1$ . Then  $J$  is connected if and only if for some (equivalently, any) periodic saddle point  $p$ , some (equivalently, each) component of  $W^u(p) \cap (\mathbb{C}^2 - K^+)$  is simply connected ([9]).

The last item above indicates that we can “see” the connectivity of  $J$  for a Hénon diffeomorphism,  $H$ , simply by looking into an unstable manifold. Hubbard has suggested a method for doing so, which we will explain below. This method has been implemented by Karl Papadantonakis in FractalAsm ([41]). All of the complex dynamics pictures in this dissertation not produced by programs of the author were drawn using programs of Papadantonakis available at [1]. See Figure 1.4 for an example.

To draw an unstable manifold, we need first to find a saddle periodic point.

**Proposition 1.2.15** ([41]). *When  $|a| \neq 1$ , except on the curve of equation  $4c = (1 + a)^2$ , the Hénon diffeomorphism  $H$  has at least one fixed point with one expanding and one contracting eigenvalue.*

Then we need to compute a linearizing coordinate  $\gamma$ .

**Proposition 1.2.16** ([41]). *Let  $p$  be a saddle fixed point of  $H$ . The unstable manifold  $W^u(p)$  has a natural parametrization  $\gamma: \mathbb{C} \rightarrow W^u(p)$  given by*

$$\gamma(z) = \lim_{m \rightarrow \infty} H^m \left( p + \frac{z}{\lambda_1^m} \mathbf{v}_1 \right),$$

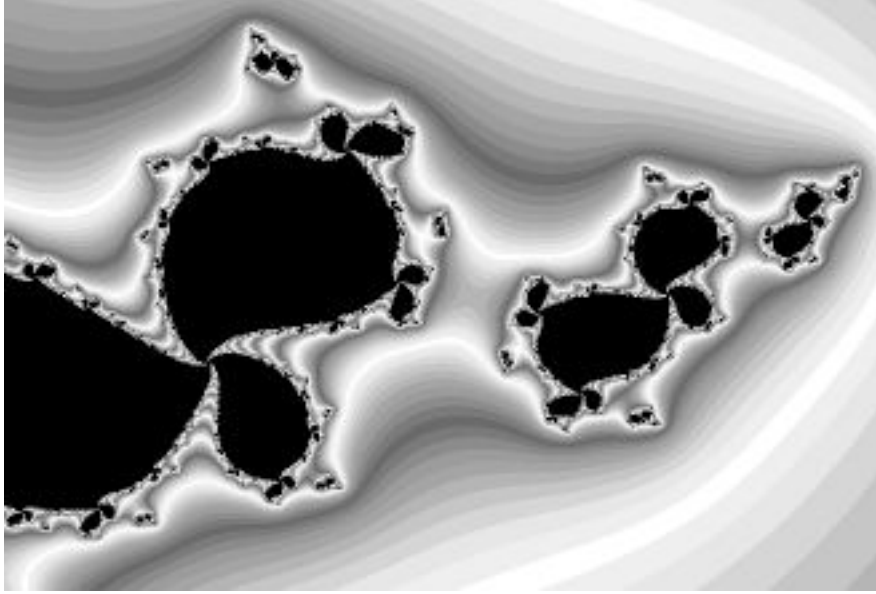


Figure 1.4: A parametrized slice of  $K$  for a Hénon diffeomorphism

where  $\lambda_1$  is the unstable eigenvalue of  $D_p H$  and  $\mathbf{v}_1$  is the associated eigenvector. This parametrization has the property that  $H(\gamma(z)) = \gamma(\lambda z)$ , and any two parametrizations with this property differ by scaling the argument.

Not only does  $\gamma$  give us a way to draw pictures of Hénon diffeomorphisms, but this proposition suggests a way to compare these to pictures of polynomial maps in one variable. Compute a repelling fixed point  $p$  of  $P_c$ , and its multiplier  $\lambda$ . A  $\gamma_p: \mathbb{C} \rightarrow \mathbb{C}$  which satisfies the functional equation  $P_c(\gamma_p(x)) = \gamma_p(\lambda x)$  is called a linearizing coordinate, and coloring a region in the  $z$ -plane based on  $\gamma_p(z)$  will yield one dimensional pictures analogous to the unstable manifold pictures. One can see an approximation to this kind of picture by zooming in very close to a repelling fixed point in a standard Julia set picture for  $P_c$ .

To actually compute the unstable manifold picture, we must approximate  $\gamma$  by choosing a large box  $T$  in  $\mathbb{C}$ , (for example, of side length 100) and a value for  $m$  (say 10). The accuracy of such approximation is discussed in [41]. We then compute a saddle fixed point  $p$ , and its unstable eigenvalue  $\lambda_1$  and eigenvector  $\mathbf{v}_1$ . Next, we split the large box into pixels by putting a  $P \times P$  grid on  $T$ . For each pixel  $Z$ , we compute  $g(Z) = H^m(p + \mathbf{v}_1(Z/\lambda_1^m))$ . We then choose a color for pixel  $Z$  based on  $g(Z) \in \mathbb{C}^2$ . For example, if  $H^{100}(g(Z)) < R$ , we may decide  $g(Z) \in K^+$  and color it black. Otherwise, color according to which iterate  $H^n(g(Z))$  first surpassed  $R$ .

### 1.3 Hyperbolicity

#### Hyperbolicity in one complex dimension

In  $\mathbb{C}$ , the condition of *hyperbolicity* reduces to expansion of tangent vectors over  $J$ .

**Definition 1.3.1** ([50]). A rational map  $f$  of the Riemann sphere  $\hat{\mathbb{C}}$  is *hyperbolic* if there exists a (continuous) riemannian metric  $\mu$ , defined on some neighborhood of  $J$ , such that the derivative  $D_z f$  at every point  $z$  in  $J$  satisfies

$$|D_z f(\mathbf{v})|_\mu > |\mathbf{v}|_\mu$$

for every nonzero vector  $\mathbf{v}$  in the tangent space  $T_z \hat{\mathbb{C}}$ .

The following theorem gives two properties which characterize the condition of hyperbolicity in one dimension. In this case, the behavior of the orbit of the critical points of a map is the key to understanding the dynamics of the map.

**Theorem 1.3.2** ([50]). *A rational map of degree  $d \geq 2$  is hyperbolic iff every critical point with bounded orbit is contained in the basin of attraction of an attracting periodic orbit. In fact, if  $f$  is hyperbolic then every point in the complement of  $J$  is contained in the basin of attraction of some attracting periodic orbit.*

Douady and Hubbard ([21]) developed a theory which gives a combinatorial description of the dynamics of *all* hyperbolic quadratic polynomial maps. Using results of Thurston, Hubbard and Schleicher to developed and implemented an algorithm to find the  $c$  value for which a specified combinatorial behavior occurs ([22, 46]).

Many fundamental dynamical questions concern how the dynamics of  $P_c$  vary with the parameter  $c$ . Douady and Hubbard ([21]) and others made substantial progress toward understanding the parameter space for  $P_c$ . Many mathematicians have contributed to this area of research, and many, though not all, questions have been answered.

The Mandelbrot set is the set of all parameters  $c$  such that  $J_c$  is connected; see Figure 1.5. In many ways, the Mandelbrot set provides a catalog of Julia sets. The location of a  $c$  inside the Mandelbrot set reveals much more about the dynamics of  $P_c$  than simply the fact that  $J_c$  is connected. The exterior of  $M$  consists entirely of hyperbolic maps whose Julia sets are Cantor sets, and which are conjugate on  $J$  to the one-sided 2-shift. These are easily understood. The cardioid and balls off of the cardioid, and analogous components in baby Mandelbrot sets, are hyperbolic connected components of the interior of  $M$ .

Mañé, Sad, and Sullivan ([48]) show that *every* connected component of the interior of  $M$  is a region of *structural stability*, *i.e.*, for any two maps,  $P_{c_1}, P_{c_2}$ , in such a component, there is a homeomorphism,  $\varphi$ , which conjugates them (*i.e.*,  $P_{c_1} \circ \varphi = \varphi \circ P_{c_2}$ ) and which maps  $J_{c_1}$  to  $J_{c_2}$ . See Figure 1.6. Thus structural stability is dense in the family of quadratic polynomials. It is conjectured, but in fact remains one of a few substantial open problems in this area, that hyperbolicity is dense in this family.

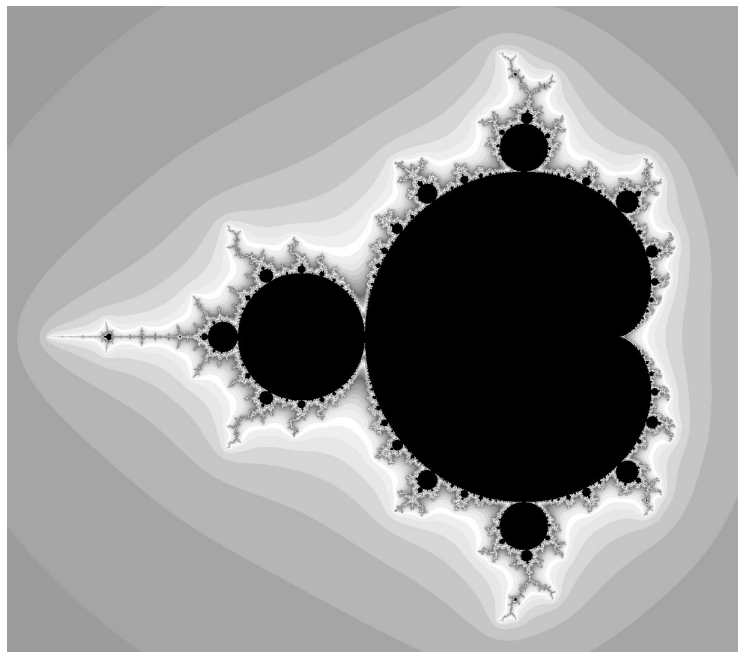


Figure 1.5: The Mandelbrot set

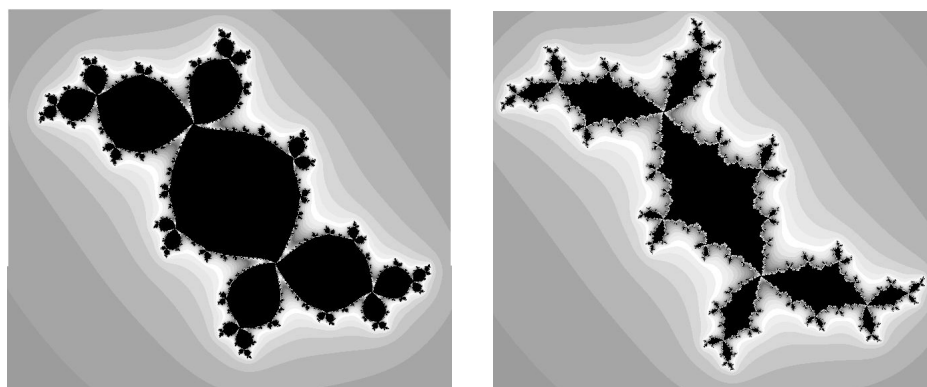


Figure 1.6: Julia sets for  $P_c$  illustrating structural stability

## Hyperbolicity in a general setting

We first define hyperbolicity as a property of an invariant set, then discuss implications of a function being hyperbolic on various invariant sets.

**Definition 1.3.3** ([54]). Let  $f$  be a  $C^1$  diffeomorphism of the compact manifold  $M$ , and let  $\Lambda \subset M$  be a closed  $f$ -invariant set. Then  $\Lambda$  is hyperbolic for  $f$  if there is a splitting of the tangent bundle,  $T_x M = E_x^s \oplus E_x^u$ , for each  $x$  in  $\Lambda$ , which varies continuously with  $x$  in  $\Lambda$ , a constant  $\lambda > 1$ , and a riemannian norm  $\|\cdot\|$  such that:

1.  $f$  preserves the splitting, *i.e.*,  $D_x f(E_x^s) = E_{fx}^s$ , and  $D_x f(E_x^u) = E_{fx}^u$ , and
2.  $Df(Df^{-1})$  expands on  $E^u(E^s)$  uniformly, *i.e.*, if  $\mathbf{w} \in E_x^u$  then  $\|D_x f(\mathbf{w})\| \geq \lambda \|\mathbf{w}\|$ , and if  $\mathbf{w} \in E_x^s$  then  $\|D_x f^{-1}(\mathbf{w})\| \geq \lambda \|\mathbf{w}\|$ .

*Remark.* The above definition is independent of choice of norm.

Hyperbolicity can also be described using a *cone field*. To define a cone field, we need a splitting  $T_x M = E_{1x} \oplus E_{2x}$  for  $x$  in  $\Lambda$ , and a positive real-valued function  $\epsilon(x)$  on  $M$ . Then define the  $\epsilon(x)$ -sector  $S_{\epsilon(x)}(E_{1x}, E_{2x})$  by

$$S_{\epsilon(x)}(E_{1x}, E_{2x}) = \{(\mathbf{v}_1, \mathbf{v}_2) \in E_{1x} \oplus E_{2x} : \|\mathbf{v}_2\| \leq \epsilon(x) \|\mathbf{v}_1\|\}.$$

Then  $C_x = S_{\epsilon(x)}$ .

**Theorem 1.3.4** ([54, 55]). Let  $f$  be a  $C^1$  diffeomorphism of the compact manifold  $M$ , and let  $\Lambda \subset M$  be a closed  $f$ -invariant set. Then  $\Lambda$  is hyperbolic for  $f$  iff there is a field of cones  $C_x$  in  $T_x M$  for  $x$  in  $\Lambda$ , a constant  $\lambda > 1$ , and a riemannian norm  $\|\cdot\|$  such that:

1.  $D_x f(C_x) = C_{fx}$ , and
2.  $D_x f$  expands  $C_x$  and  $D_x f^{-1}$  expands  $T_x M - C_x$ , *i.e.*,  $\|D_x f(\mathbf{v})\| \geq \lambda \|\mathbf{v}\|$  for  $\mathbf{v}$  in  $C_x$ , and  $\|D_x f^{-1}(\mathbf{v})\| \geq \lambda \|\mathbf{v}\|$  for  $\mathbf{v}$  in  $T_x M - C_x$ .

The field of cones  $x \rightarrow C_x$  need not be continuous.

This cone field condition for hyperbolicity yields a natural way to study the hyperbolic structure of a diffeomorphism using a computer.

Historically, a map is said to be hyperbolic if it is hyperbolic over its nonwandering set.

**Definition 1.3.5.** Let  $f$  be a  $C^1$  diffeomorphism of the compact manifold  $M$ .

1.  $f$  is *hyperbolic* if it is hyperbolic on  $\Omega$ .
2.  $f$  is *Axiom A* if it is hyperbolic and if periodic points are dense in  $\Omega$ .

However, if we instead follow Conley ([19]) as in [60] and study maps for which the chain recurrent set is hyperbolic, then we get Axiom A automatically.

**Definition 1.3.6.** A map  $f: X \rightarrow X$  is *topologically transitive* on an invariant set  $Y$  if the (forward) orbit of some point  $p$  is dense in  $Y$ . This is equivalent to the condition that given any two open sets  $U, V$  in  $Y$ , there is an  $N \geq 0$  such that  $f^N(U) \cap V \neq \emptyset$ . A stronger condition is *topologically mixing*: for any pair of open sets  $U, V$  there is an  $N > 0$  such that  $f^n(U) \cap V \neq \emptyset$  for all  $n > N$ .

**Definition 1.3.7.** Let  $\Lambda$  be a hyperbolic invariant set for a  $C^1$  diffeomorphism  $f$  of a compact manifold  $M$ . We say  $\Lambda$  has *local product structure* if for some  $\epsilon > 0$ ,  $W_\epsilon^s(p_1) \cap W_\epsilon^u(p_2) \subset \Lambda$  if  $p_1, p_2 \in \Lambda$ .

**Theorem 1.3.8 ([60]).** *Let  $f$  be a  $C^1$  diffeomorphism of a compact manifold  $M$ . If  $\mathcal{R}$  is hyperbolic for  $f$ , then there are a finite number of (disjoint) chain transitive components,  $\mathcal{R} = \mathcal{R}_1 \cup \dots \cup \mathcal{R}_m$ , such that each  $\mathcal{R}_j$  is closed, invariant under  $f$ , the periodic points are dense, and  $f$  is topologically transitive on  $\mathcal{R}_j$ . Further, each  $\mathcal{R}_j$  has local product structure. Such sets are often called basic sets for  $f$ .*

Hyperbolicity on an invariant set which either has local product structure or is locally isolated gives Anosov's shadowing lemma.

**Corollary 1.3.9 ([60]).** *Let  $f$  be a  $C^1$  diffeomorphism of a compact manifold  $M$ . If  $\mathcal{R}$  is hyperbolic for  $f$ , then for  $\gamma$  sufficiently small there is a constant  $\alpha$  and a neighborhood  $U$  of  $\mathcal{R}$  such that every (bi-infinite)  $\alpha$ -chain in  $U$  is  $\gamma$  shadowed by a (unique) point in  $\mathcal{R}$ .*

Shadowing is a very useful tool in the numerical study of diffeomorphisms, for studying a single diffeomorphism and small perturbations of it. A related property of hyperbolic diffeomorphisms is structural stability.

**Theorem 1.3.10 ([60]).** *Let  $f$  be a  $C^1$  diffeomorphism of the compact manifold  $M$ . If  $\mathcal{R}$  is hyperbolic for  $f$ , then  $f$  is structurally stable on  $\mathcal{R}$ , i.e., there is a neighborhood  $\mathcal{N}$  of  $f$  (in the  $C^1$  topology) such that for  $g \in \mathcal{N}$  there is homeomorphism  $\phi$  which conjugates  $f$  to  $g$  (i.e.,  $\phi \circ f = g \circ \phi$ ) and maps  $\mathcal{R}(f)$  onto  $\mathcal{R}(g)$ .*

Shadowing and structural stability on  $\mathcal{R}$ , plus the finite decomposition into chain transitive components, suggest that the dynamics of a hyperbolic diffeomorphism can be completely described by a computer, i.e., with a finite amount of data.

## Hyperbolic polynomial diffeomorphisms of $\mathbb{C}^2$

In examining hyperbolic Hénon diffeomorphisms, we want characterizations which involve the Julia set. Bedford and Smillie have shown that for hyperbolic Hénon diffeomorphisms, there is a simple relationship among  $\mathcal{R}, \Omega$  and  $J$ .

**Theorem 1.3.11 ([6]).** *Let  $f$  be a polynomial diffeomorphism of  $\mathbb{C}^2$ , with  $d(f) > 1$ . The following are equivalent:*

1.  $f$  is hyperbolic on its Julia set,  $J$ ;
2.  $f$  is hyperbolic on its nonwandering set,  $\Omega$ ;
3.  $f$  is hyperbolic on its chain recurrent set,  $\mathcal{R}$ .

We say  $f$  is hyperbolic if any of the above three conditions hold.

**Proposition 1.3.12 ([5]).** *Let  $f$  be a polynomial diffeomorphism of  $\mathbb{C}^2$ , with  $d(f) > 1$ . If  $f$  is hyperbolic, then  $\mathcal{R}$  and  $\Omega$  are both equal to  $J$  union finitely many attracting periodic orbits.*

Thus for hyperbolic polynomial diffeomorphisms of  $\mathbb{C}^2$ , the chain transitive components are  $J$  and the attracting periodic orbits, and thus the dynamical properties in Theorem 1.3.8, Corollary 1.3.9, and Theorem 1.3.10 apply to  $J$ .

In fact, we can say a bit more about  $J$ .

**Theorem 1.3.13 ([5]).** *Let  $f$  be a polynomial diffeomorphism of  $\mathbb{C}^2$ , with  $d(f) > 1$ . If  $f$  is hyperbolic then  $f|_J$  is topologically mixing.*

Structural stability can also be strengthened for Hénon diffeomorphisms. Mañé, Sad, and Sullivan ([48]) used holomorphic motions to prove structural stability on all of  $\mathbb{C}$  for polynomial maps of  $\mathbb{C}$ . Buzzard and Verma ([17]) extended the concept of holomorphic motions to two dimensions and showed that all maps in a neighborhood of a hyperbolic polynomial diffeomorphism of  $\mathbb{C}^2$  are conjugate via a homeomorphism on  $J^+ \cup J^-$  (not just  $J$ ). See Figure 1.7 for an illustration of structural stability on  $J$ .

The following is a partial analog to Theorem 1.3.2.

**Theorem 1.3.14 ([5]).** *Let  $f$  be a polynomial diffeomorphism of  $\mathbb{C}^2$ , with  $d(f) > 1$ . Assume  $|\text{Det}(Df)| < 1$ . If  $f$  is hyperbolic, then the interior of  $K^+$  consists of the basins of finitely many sink orbits, and the interior of  $K^-$  is empty.*

Oliva ([57]) describes a way to encode the dynamics of hyperbolic Hénon diffeomorphisms with connected Julia sets in a combinatorial model. However, a method for giving a combinatorial description of all hyperbolic Hénon diffeomorphisms is not yet known.

## Previous descriptions of specific hyperbolic Hénon diffeomorphisms

There are two classes of Hénon diffeomorphisms proven to be hyperbolic, and both have behavior which is essentially one dimensional.

**Theorem 1.3.15 (Small perturbations of hyperbolic polynomials, [44]).** *Let  $P_c(x) = x^2 + c$  be a hyperbolic polynomial. There exists an  $A$  such that if  $0 < |a| < A$ , then  $H_{a,c}$  is hyperbolic. In particular,  $H_{a,c}|_J$  is topologically conjugate to the function induced by  $P_c$  on the inverse limit  $\varprojlim (J, P_c)$ .*

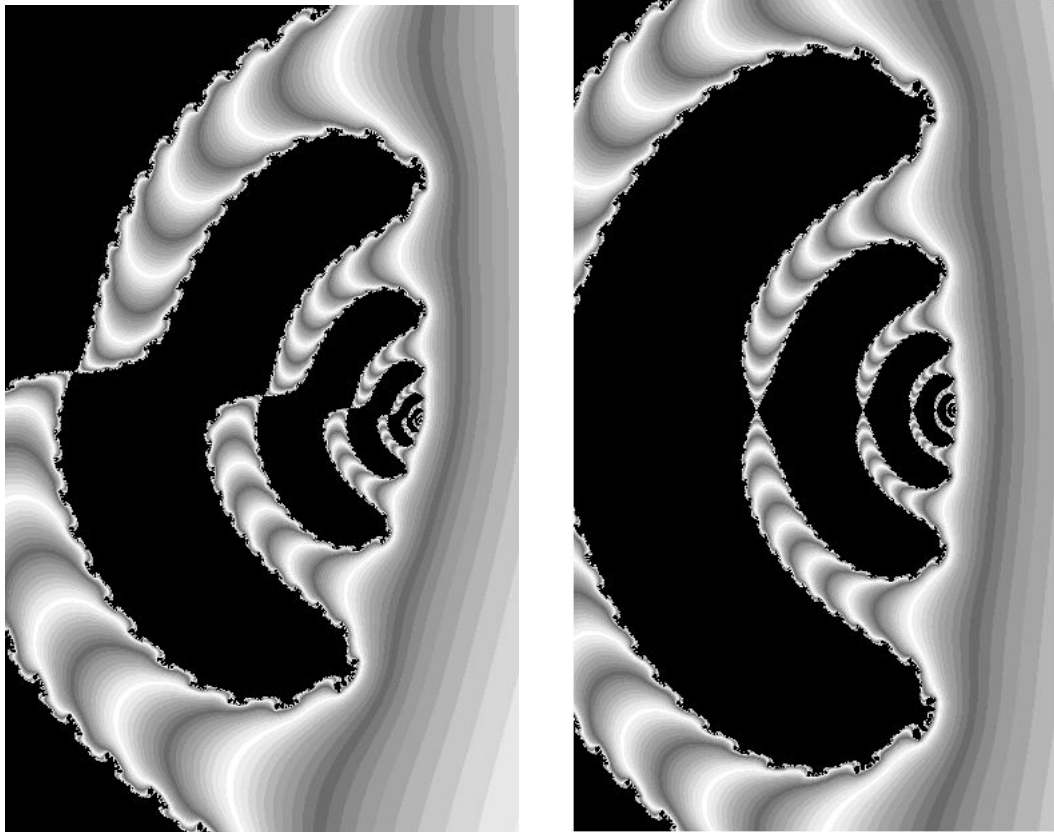


Figure 1.7: Julia sets for Hénon diffeomorphisms illustrating structural stability

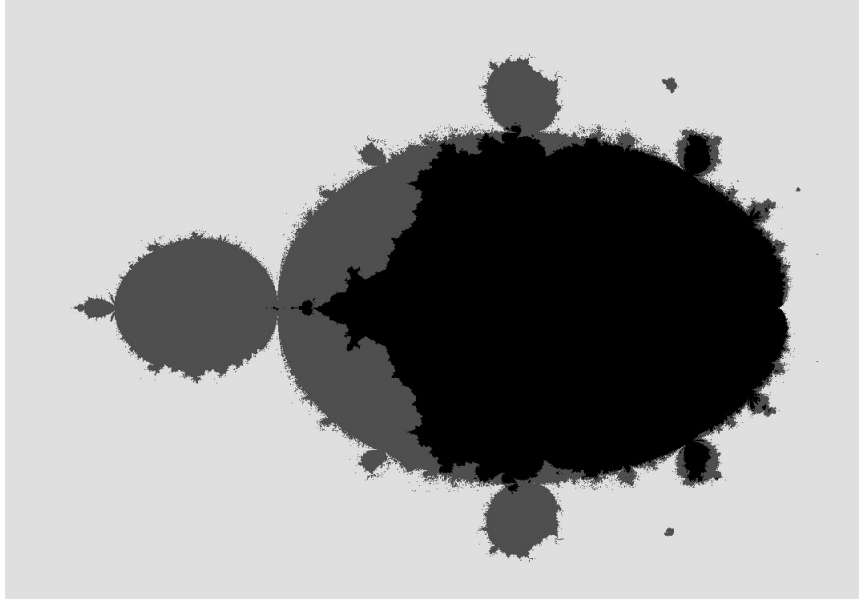


Figure 1.8: A Hénon parameter space slice: the  $c$ -plane with  $a = .3$ . Presumably, the inner dark set represents connected  $J_{a,c}$ 's, the slightly larger set represents all non-Cantor  $J_{a,c}$ 's, and the exterior represents Cantor  $J'_{a,c}$ 's.

**Definition 1.3.16.** We say  $f$  exhibits one dimensional behavior if  $f|_J$  is topologically conjugate to the function induced by  $f$  on the inverse limit  $\varprojlim(J, f)$ .

**Definition 1.3.17.** A *horseshoe* is a diffeomorphism  $f$  such that  $f|_J$  is topologically conjugate to the left shift operator on  $\Sigma_2$  (the symbol space of bi-infinite sequences of 0's and 1's). The *horseshoe locus* in the Hénon parameter space,  $\mathcal{H}$ , is the hyperbolic component of parameter space containing the set of horseshoes.

Since the full left shift on  $\Sigma_2$  is the inverse limit of the one-sided left shift, horseshoes also exhibit one dimensional behavior.

**Theorem 1.3.18 (Horseshoes, [56]).** *If  $|c|$  is sufficiently large compared to  $a$ , then  $H_{a,c}$  is a horseshoe, thus hyperbolic.*

See [53] for a proof of the above theorem. Horseshoes are topologically the same as Smale's Horseshoe, *i.e.*, the Julia set is a Cantor set, and the dynamics are well-understood.

Recent computer programs FractalAsm and SaddleDrop made by Karl Papadantonakis, under the direction of John Hubbard, have generated pictures of slices of the Hénon parameter space,  $\{a, c \in \mathbb{C}\} = \mathbb{C}^2$ , holding  $a$  or  $c$  fixed and drawing the other plane (programs available at [1], description in [41]). These programs draw pictures of either the connectivity locus or the non-Cantor locus.

They have revealed fascinating levels of detail. In Figure 1.8, the inner dark set represents  $\{a, c: J_{a,c} \text{ is connected}\}$ , and the slightly larger set represents  $\{a, c: J_{a,c} \text{ is not a Cantor set}\}$ .

Pictures produced by both programs suggest the dynamical behavior of complex Hénon diffeomorphisms can be rich and varied. The accuracy of these pictures is an interesting topic, see [41].

## Motivating examples

Next we describe some basic examples of Hénon diffeomorphisms which do not seem to exhibit one dimensional behavior. These diffeomorphisms have not been successfully analyzed theoretically.

**Example 1.3.19 (The alternate basilica).** The Hénon diffeomorphism  $H_{a,c}$  with  $c = -1.1875, a = .15$ , Figure 1.9, appears to be topologically conjugate to the diffeomorphism with  $c = -1.24, a = .125$ . Ricardo Oliva ([57]) gave evidence that the latter diffeomorphism is hyperbolic with a period two attracting cycle, but is not conjugate to the inverse limit of the basilica, Figure 1.10 ( $c = -1, a$  small). This seems to be one of the simplest Hénon diffeomorphisms which does not exhibit one dimensional behavior.

**Example 1.3.20 (The 3-1 map).** The Hénon map with  $c = -1.17, a = .3$ , Figure 1.11, is an interesting example because it appears to be hyperbolic with *two* attracting periodic cycles, one of period three and one of period one. This is not a phenomenon which appears for  $z^2 + c$ . This map was also analyzed in [57]. This seems to be the simplest example of a Hénon diffeomorphism with more than one attracting periodic cycle.

**Example 1.3.21 (Loops in the horseshoe locus).** We are also interested in studying the topology of the horseshoe locus,  $\mathcal{H}$  (Definition 1.3.17). Examining SaddleDrop ([41]) one can discover that this topology seems quite complicated.

Using SaddleDrop, one can search for such loops in  $\mathcal{H}$ . Hubbard and Papadantonakis suggest as a first example the loop in the  $c = -3.5$  plane passing through  $a = .57$  (9 o'clock),  $a = .52 + .04i$  (12 o'clock),  $a = .47$  (3 o'clock), and  $a = .52 - .04i$  (6 o'clock) ([1]). The parameters  $c = -3.5, a = .47$  define a real horseshoe, covered by Theorem 1.3.18. Figure 1.12 illustrates  $H_{a,c}, c = -3.5, a = .57$ . All of the pictures for this loop will look approximately like this one. The largest change in the pictures can be seen by zooming in on the center of the left region. Figure 1.13 shows this zoom for the four selected maps on the loop, with top to bottom order:  $a = .57$  (9 o'clock),  $a = .52 + .04i$  (12 o'clock),  $a = .47$  (3 o'clock), and  $a = .52 - .04i$  (6 o'clock). The vertical components seen in the topmost figure will switch places upon moving around this loop, by passing through the real line.

Hubbard conjectures that there exists a surjection from the fundamental group of  $\mathcal{H}$  to  $\text{Aut } \Sigma_2$ , where  $\text{Aut } \Sigma_2$  is the group of Automorphisms of  $\Sigma_2$  (the symbol

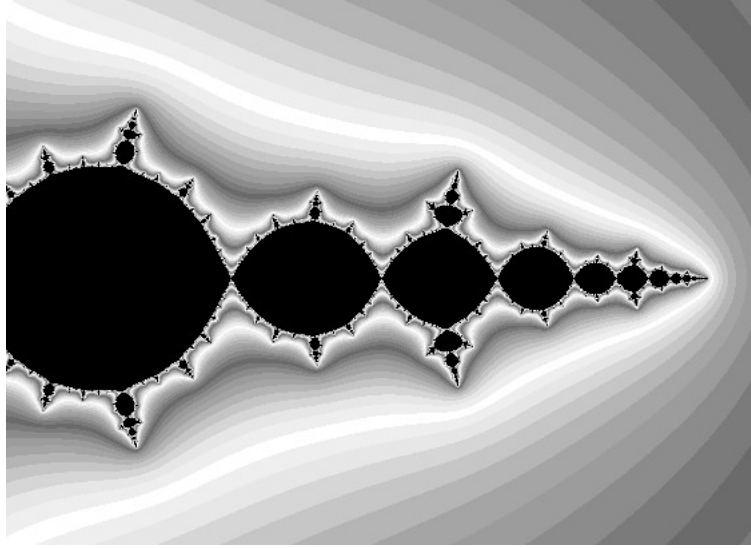


Figure 1.9: A parametrization of  $W^u(p)$  for  $H_{a,c}$ ,  $c = -1.1875$ ,  $a = .15$ . Black is  $W^u(p) \cap K^+$ . It appears that  $J$  is connected and  $H$  has an attracting 2-cycle, but is not conjugate to the inverse limit of the basilica.

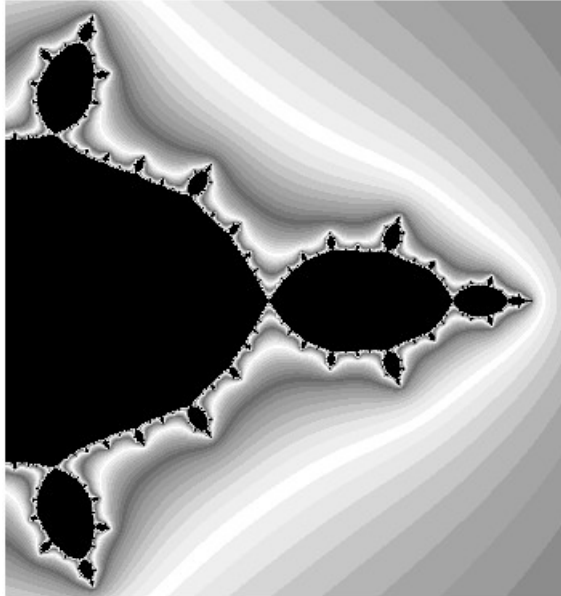


Figure 1.10: A parametrization of  $W^u(p)$  for  $H_{a,c}$ ,  $c = -1.05$ ,  $a = .05$ . Black is  $W^u(p) \cap K^+$ . It appears that  $J$  is connected and  $H$  is conjugate to the inverse limit of the basilica.

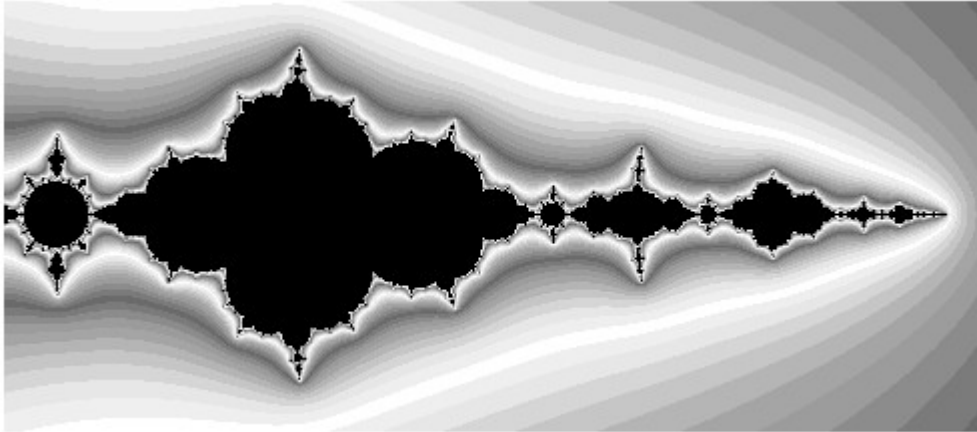


Figure 1.11: A parametrization of  $W^u(p)$  for  $H_{a,c}$ ,  $c = -1.17$ ,  $a = .3$ . Black is  $W^u(p) \cap K^+$ . It appears that  $J$  is connected and  $H$  has attracting cycles of periods one and three.

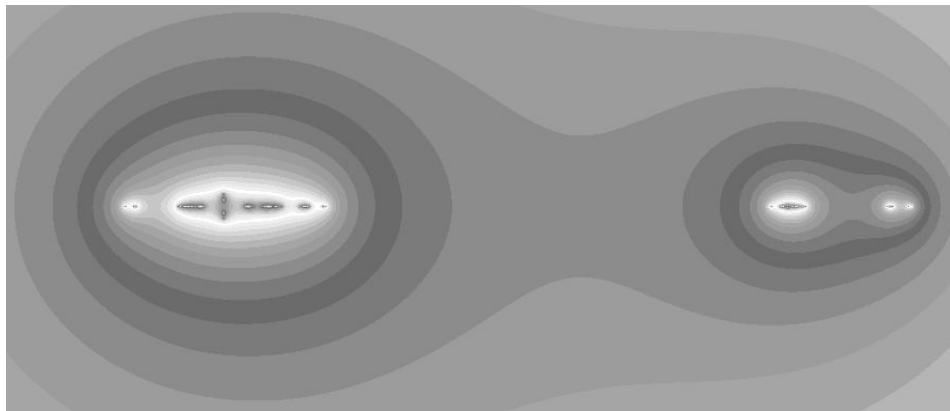


Figure 1.12: A parametrization of  $W_p^u$  for  $H_{a,c}$ ,  $c = -3.5$ ,  $a = .57$ . Black is  $W^u(p) \cap K^+$ .  $J$  appears to be a Cantor set.

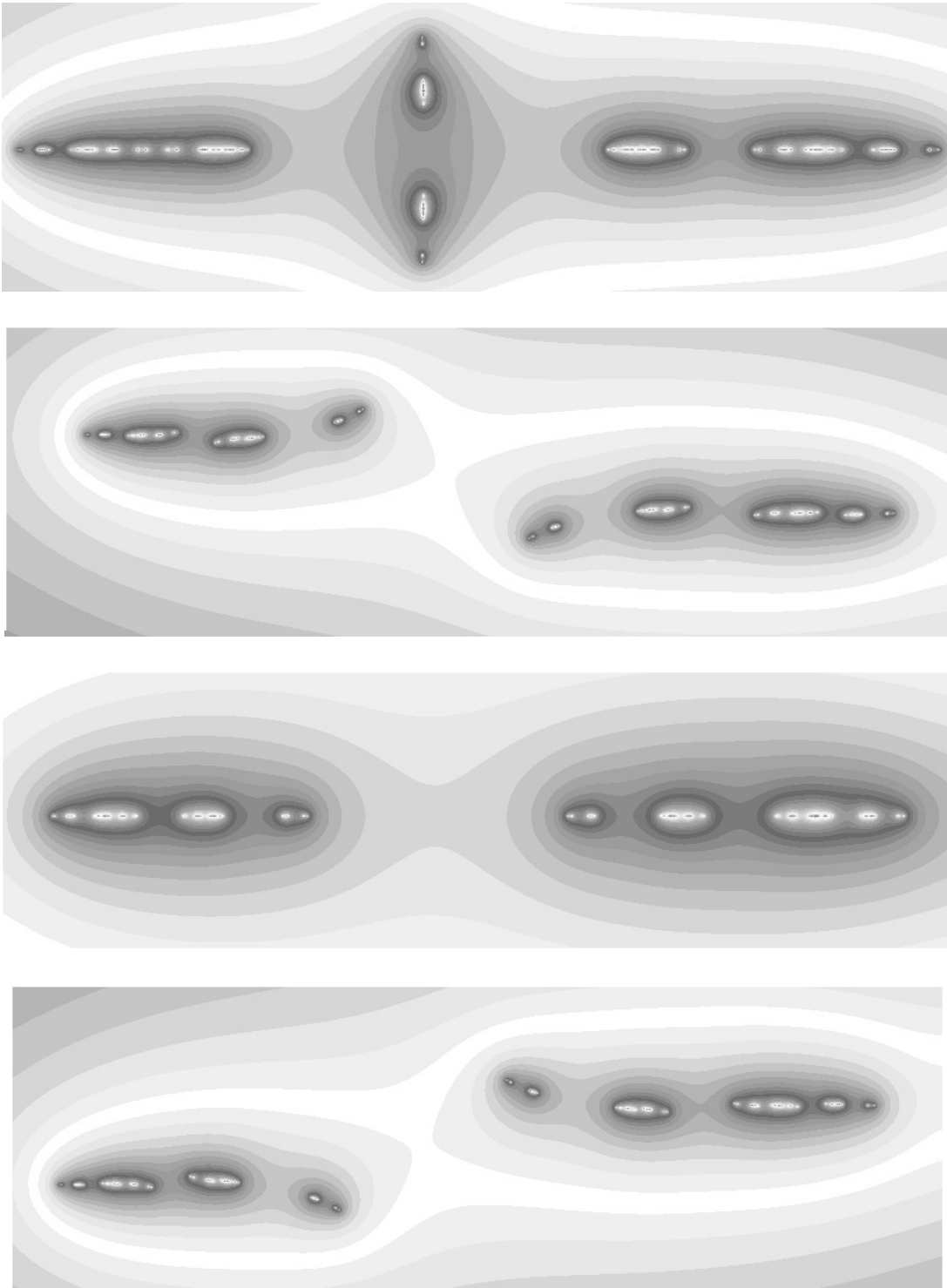


Figure 1.13: A blow-up of the left region of Figure 1.12. All have  $c = -3.5$ ;  
top to bottom:  $a = .57, .52 + .04i, .47, .52 - .04i$ .

space of bi-infinite sequences of 0's and 1's). Hubbard and Branner demonstrate the relationship between an element of  $\text{Aut } \Sigma_2$  and a loop in  $\mathcal{H}$  in [13, 14], where they show a similar result for cubic polynomials. Further, Blanchard, Devaney, and Keen develop a result for higher degree polynomials in [12]. SaddleDrop will compute the automorphism up to a certain depth for an inputted loop.

In addition to these examples, experience with zooming and further refinement suggests that the behavior is often even more complicated than it appears on a large scale first glance. Thus we learn that while pictures produced with this program show fascinating structures previously unimagined, they also may fail to clearly illustrate the complete dynamical picture. We cannot trust that what we see at one level determines the structure at a finer level. Further numerical and theoretical tools are needed to precisely clarify the situation.

*Thus we are led to the conclusion that a reasonable approach to the problem of understanding the dynamics of specific hyperbolic Hénon diffeomorphisms would be to develop a computer program to determine the hyperbolic structure on  $\mathcal{R}$ .*

## 1.4 Overview of this dissertation: *Hypatia*

In this dissertation, we develop a computer algorithm which can locate an  $\epsilon$ -chain recurrent set,  $\mathcal{R}_\epsilon$ , sort points into  $\epsilon$ -chain transitive components, and investigate the hyperbolicity of polynomial maps of  $\mathbb{C}$ , or polynomial diffeomorphisms of  $\mathbb{C}^2$ . The program is general enough to study a wide range of functions. We call it *Hypatia*, after the word “hyperbolicity” and the name of an early female mathematician. If the output is “yes”, then the computation has created structures which *prove* the diffeomorphism is hyperbolic. If the output is “not for this  $\epsilon$ ”, then it includes information on numerical and dynamical obstructions, and the user may try to overcome these obstacles by lowering  $\epsilon$  and re-testing. Appendix A explains how to control round-off error to make the computation rigorous.

In our discussion of each step of the algorithm, we make an effort to separate as much as possible the theoretical notions involved from the actual algorithm which is employed in *Hypatia*.

In Chapter 2 we develop and study a method for modeling  $\mathcal{R}$  and the chain transitive components. We define a graph  $\Gamma$ , called the *box-chain recurrent graph*, where the vertices of  $\Gamma$  are boxes in  $\mathbb{C}^n$ , and its edges encode the box-dynamics. We define the *box-chain recurrent set*,  $\mathcal{B}_\Gamma$ , as the union of the box vertices of  $\Gamma$ , and a *box-chain transitive component* as the set  $\mathcal{B}_{\Gamma'}$  for  $\Gamma'$  a connected component of  $\Gamma$ . We quantify how well the box-chain recurrent set and box-chain transitive components approximate  $\mathcal{R}$  and the chain transitive components, with explicit estimates for for  $f = P_c$  or  $H_{a,c}$ . We then explain how *Hypatia* finds a box-chain recurrent graph.

To investigate hyperbolicity, we first focus on polynomial maps of  $\mathbb{C}$ . Since the quadratic family is familiar, studying the case of  $P_c$  helps to verify the correctness of the algorithm and its implementation. Also, as already mentioned,  $P_c$  has many

similarities to the Hénon family, which eases the conversion from  $\mathbb{C}$  to  $\mathbb{C}^2$ . In Chapter 3 we describe a procedure for verifying hyperbolicity in one dimension. There we define and study the notion of *box-expansion*, describe how *Hypatia* checks for box-expansion, and prove that a box-expansive polynomial map is hyperbolic. We also give several examples of using *Hypatia* to verify expansion for quadratic and cubic polynomial maps.

In Chapter 4, we extend the algorithm in order to study polynomial diffeomorphisms of  $\mathbb{C}^2$ . We define and study the notion of *box-hyperbolicity*, describe the procedure *Hypatia* uses to verify box-hyperbolicity, and show a box-hyperbolic polynomial diffeomorphism of  $\mathbb{C}^2$  is hyperbolic. We give examples of some Hénon diffeomorphisms for which the program proves hyperbolicity. The memory required to prove hyperbolicity for certain interesting examples of Section 1.3 is more than currently available. We discuss this in Sections 4.4.3 and in Chapter 5, where we show that to some extent these memory limitations are intrinsic to the problem of studying  $\mathcal{R}_\epsilon$ , rather than being dependent on our particular algorithm.

The code for *Hypatia* is in a combination of **C** and **C++**. The source code can be downloaded at [1]. The computations described in this dissertation were run on a Sun Enterprise E3500 server with 4 processors, each 400MHz UltraSPARC (though the multiprocessor was not used) and 4 GB of RAM. When computations became overwhelming, memory usage was the limiting factor.

# Chapter 2

## The box-chain recurrent set

Recall that in general, a differentiable function  $f$  is hyperbolic if  $\mathcal{R}$  is a hyperbolic set for  $f$ , but for a complex polynomial (map or diffeomorphism), this is equivalent to whether  $J$  is a hyperbolic set for  $f$ . Theorem 1.2.9 gives us that even when  $f$  is not hyperbolic,  $J$  lies in a chain transitive component of  $\mathcal{R}$ . Thus, we need to find a cover of  $\mathcal{R}$ , and decompose it into its chain transitive components.

In Section 2.1, we find a large box  $V$  which is guaranteed to contain  $\mathcal{R}_\delta$ , proving Proposition 2.1.4.

We define the *box-chain recurrent graph*,  $\Gamma$ , the *box-chain recurrent set*,  $\mathcal{B}_\Gamma$ , and *box-chain transitive components*,  $\mathcal{B}_{\Gamma'}$ , in Section 2.2. We prove Theorems 2.2.6 and 2.2.9, quantifying how well  $\mathcal{B}_\Gamma$  approximates  $\mathcal{R}$ , and how well the  $\mathcal{B}_{\Gamma'}$  approximate the chain transitive components.

Finally, we describe in Section 2.3 how *Hypatia* constructs all of these box-chain recurrent objects, including a discussion of ways in which this procedure can be enhanced to more efficiently find a good box-chain recurrent set.

### 2.1 Trapping regions for $\mathcal{R}_\delta$

It is useful for computer calculations to consider vectors in  $\mathbb{R}^{2n}$ , rather than  $\mathbb{C}^n$ , and use the following alternate metric.

**Definition 2.1.1.** Let  $\|\cdot\|_\infty$  be the  $L^\infty$  norm on  $\mathbb{R}^{2n}$ , so that for a vector  $x = (x_1, \dots, x_n) \in \mathbb{C}^n$ ,

$$\|x\|_\infty = \max\{|\operatorname{Re}(x_k)|, |\operatorname{Im}(x_k)| : 1 \leq k \leq n\}.$$

Let  $\mathcal{N}_\infty(S, r)$  be the open  $r$ -neighborhood about the set  $S$  in the metric  $d_\infty$  induced by  $\|\cdot\|_\infty$ , *e.g.*,

$$\mathcal{N}_\infty(0, r) = \{x = (x_1, \dots, x_n) \in \mathbb{C}^n : |\operatorname{Re}(x_k)| < r \text{ and } |\operatorname{Im}(x_k)| < r\}.$$

We use the simpler notation  $|\cdot|_\infty$  for dimension  $n = 1$ .

This metric is *uniformly equivalent* to the euclidean metric on  $\mathbb{C}^n$ ,  $\|\cdot\|_e$ , since

$$\frac{1}{\sqrt{2n}} \|x\|_e \leq \|x\|_\infty \leq \|x\|_e.$$

Neighborhoods are slightly different with respect to two uniformly equivalent norms. However, the topology generated by them is exactly the same, thus they can practically be used interchangeably. Similarly, the  $\epsilon$ -chain recurrent set  $\mathcal{R}_\epsilon$  depends on choice of metric, but in effect, this will only mildly change the constant  $\epsilon$ . It is clear that the chain recurrent set  $\mathcal{R}$  is exactly the same for any metric uniformly equivalent to euclidean.

The following makes precise the idea that for polynomial diffeomorphisms of  $\mathbb{C}^2$ , infinity in the  $x$  direction is attracting, while infinity in the  $y$  direction is repelling for  $f$ , and vice-versa for  $f^{-1}$ .

**Lemma 2.1.2.** *Let  $f$  be a polynomial diffeomorphism of  $\mathbb{C}^2$ , with  $d(f) > 1$ . Then there is an  $R > 1$  such that for  $R' > R$ , there is an  $\eta_0 > 0$  such that if  $|x|_\infty \geq R'$  and  $|x|_\infty \geq |y|_\infty$ , then  $\|f(x, y)\|_\infty \geq |x|_\infty + \eta_0$ .*

*If  $f = H_{a,c}$ , then  $R = \frac{1}{2}(1 + |a|_\infty + \sqrt{(1 + |a|_\infty)^2 + 4|c|_\infty})$  and  $\eta_0 = (R')^2 - (1 + |a|)R' - |c|$ .*

A version of this lemma is given in [35] (also see [62]).

*Proof.* Assume  $f$  is a generalized Hénon mapping,  $f(x, y) = (z, x) = (p(x) - ay, x)$ , with  $\deg(p) > 1$ . Let  $q(r) = p(r) - (1 + |a|_\infty)r$ . Then there is an  $R > 0$  such that  $q$  is monotone increasing on  $[R, \infty)$ , with  $q(R) = 0$ . Note if  $r > R$ , then  $q(r) \geq r^d - r$ , thus the positive root  $R$  is at least one. Let  $R' > R$ , and set  $\eta_0 = q(R')$ . Then  $\eta_0 > 0$ . Let  $(x, y) \in \mathbb{C}$  satisfy  $|x|_\infty \geq R'$  and  $|x|_\infty \geq |y|_\infty$ . Then

$$|z|_\infty \geq |p(x)|_\infty - |a|_\infty |y|_\infty \geq |p(x)|_\infty - |a|_\infty |x|_\infty \geq |x|_\infty + \eta_0.$$

The case of  $H_{a,c}(x, y) = (x^2 + c - ay, x)$ , follows immediately from these calculations. If  $f = f_m \circ \dots \circ f_1$ , set  $\eta_0 = \eta_0(f_1) + \dots + \eta_0(f_m)$ .  $\square$

**Definition 2.1.3.** Following [5], we define the “trapping regions”, for  $R'$  large enough that Lemma 2.1.2 holds, by:

$$\begin{aligned} V &= \{|x|_\infty \leq R' \text{ and } |y|_\infty \leq R'\}; \\ V^- &= \{|x|_\infty > R' \text{ and } |x|_\infty > |y|_\infty\}; \\ V^+ &= \{|y|_\infty > R' \text{ and } |y|_\infty > |x|_\infty\}. \end{aligned}$$

The sets  $V, V^\pm$  were introduced to study  $K, K^\pm$ , and if defined using  $R$ , satisfy  $K^+ \subset V \cup V^+$ ,  $K^- \subset V \cup V^-$ , and  $K \subset V$  ([5]). Choosing  $R'$  larger than  $R$  allows us to trap  $\epsilon$ -pseudo orbits as well.

**Proposition 2.1.4.** *Let  $f$  be a polynomial diffeomorphism of  $\mathbb{C}^2$ , with  $d(f) > 1$ . Let  $\eta_0$  be as in Lemma 2.1.2 and let  $\eta = \eta_0/2$ . Then  $\mathcal{R}_\eta \subset V$ .*

*Proof.* Given Lemma 2.1.2, we have  $f(V^-) \subset V^-$  and  $f(V^-) \cap \mathcal{N}_\infty(V, \eta_0) = \emptyset$ . Thus if  $p \in V^-$ , then  $p$  is not in  $\mathcal{R}_{\eta_0/2}$ , since the images  $f(x_k)$  move by at least  $\eta_0$  out toward the  $x$  direction, and so the  $x_{k+1}$  coming back in by only  $\eta_0/2$  makes it impossible for  $x_n = p$ .

Similarly, we can look at the chain backward for  $p \in V^+$  to get a contradiction to  $\eta_0/2$ -chain recurrence.  $\square$

For polynomial maps of  $\mathbb{C}$ , Lemma 2.1.2 and Proposition 2.1.4 apply easily to give:

**Corollary 2.1.5.** *Let  $f$  be a polynomial map of  $\mathbb{C}$  of degree  $d > 1$ . Then there exist  $R' > 1, \eta > 0$  such that  $\mathcal{R}_\eta \subset V = \{|x|_\infty \leq R'\}$ . For  $P_c(x) = x^2 + c$ ,  $R', \eta$  are as in Proposition 2.1.4, except take  $a = 0$ .*

To get an idea of the size of  $R$ , note that  $R = 2$  for  $c = 2$ . Since the Mandelbrot set is contained in  $\{x : |x| \leq 2\}$ , for the parameters we are likely to be examining we will have  $1 \leq R \leq 2$ . For the Hénon map, the values of  $R$  are also close to this range.

## 2.2 The box-chain recurrent graph

When we say *box*, we mean a neighborhood in the norm  $\|\cdot\|_\infty$ . That is, if  $(x_1, \dots, x_n)$  and  $(y_1, \dots, y_n)$  are vectors in  $\mathbb{C}^n$  defining the extreme corners of the box, then we write the box in  $\mathbb{R}^{2n}$  as

$$[\operatorname{Re}(x_1), \operatorname{Re}(y_1)] \times [\operatorname{Im}(x_1), \operatorname{Im}(y_1)] \times \cdots \times [\operatorname{Re}(x_n), \operatorname{Re}(y_n)] \times [\operatorname{Im}(x_n), \operatorname{Im}(y_n)],$$

where all sides are of equal length

$$|\operatorname{Re}(x_k) - \operatorname{Re}(y_k)| = |\operatorname{Im}(x_k) - \operatorname{Im}(y_k)| = \text{constant}, 1 \leq k \leq n.$$

**Definition 2.2.1.** Let  $V = \mathcal{N}_\infty(0, R')$ , for some  $R' > 0$ . We denote a collection of boxes  $B_k \subset V$ , of (minimum) side length  $\epsilon$  by  $\mathcal{V}_\epsilon = \{B_k : 1 \leq k \leq M\}$ , and we denote the subset of  $V$  consisting of the union of the boxes by  $\mathcal{B} = \mathcal{B}(\mathcal{V}_\epsilon) = \cup\{B_k : B_k \in \mathcal{V}_\epsilon\}$ . If  $\mathcal{B}(\mathcal{V}_\epsilon)$  contains a set  $\mathcal{S}$ , we say  $\mathcal{V}_\epsilon$  is a *box cover* of  $\mathcal{S}$ .

We will often discuss one subset of  $\mathcal{V}_\epsilon$  at a time, and since the ordering is unimportant we will avoid double subscripts and simply use  $\{B_0, B_1, \dots, B_\ell\}$ .

Throughout this section, let  $f$  be a complex polynomial diffeomorphism of  $\mathbb{C}^2$  (or map of  $\mathbb{C}$ ), with  $d(f) > 1$ .

**Definition 2.2.2.** Let  $\mathcal{V}_\epsilon$  be a box cover of  $\mathcal{R}$  for  $f$ . If  $\delta$  satisfies  $0 < \delta < \epsilon$ , then the *box-chain graph* of  $\mathcal{V}_\epsilon$ ,  $\Upsilon = \Upsilon_\delta$ , is the directed graph with vertex set  $\mathcal{V}_\Upsilon = \mathcal{V}_\epsilon$ , and edge set

$$\mathcal{E}_\Upsilon = \mathcal{E} = \{B_k \rightarrow B_j : B_j \cap \mathcal{N}_\infty(f(B_k), \delta) \neq \emptyset\}.$$

Then we let  $\mathcal{B}_\Upsilon = \mathcal{B}(\mathcal{V}_\epsilon)$ .

From a box-chain graph we cull a *box-chain recurrent graph*,  $\Gamma$ .

**Definition 2.2.3.** Let  $\mathcal{V}_\epsilon$  be a box cover of  $\mathcal{R}$  for  $f$ , and let  $\Upsilon_\delta$  be the box-chain graph for  $\mathcal{V}_\epsilon$ . The *box-chain recurrent graph*,  $\Gamma = \Gamma_\delta$ , (of  $\Upsilon_\delta$ ) is the (maximal) subgraph of  $\Upsilon_\delta$  with vertices all of the boxes which are in cycles of  $\Upsilon_\delta$ , and an edge set including precisely the edges in  $\Upsilon_\delta$  connecting the chosen vertices. The *box-chain recurrent set* is  $\mathcal{B}_\Gamma$ .

Note a box-chain recurrent graph is also a box-chain graph for the boxes in its vertex set. Thus when the distinction is unimportant, we often just say box-chain graph.

Also note that a smaller  $\delta$  yields a smaller box-chain recurrent set. However, we need this positive factor  $\delta$  to prove Corollary 2.2.5, which is important in guaranteeing that that box-hyperbolicity implies a standard definition of hyperbolicity.

We first need a lemma on the size of the image of the boxes.

**Lemma 2.2.4.** *Let  $\mathcal{V}_\epsilon$  be a box cover of  $\mathcal{R}$  for  $f$ . Let  $\Upsilon_\delta$  be a box-chain graph of  $\mathcal{V}_\epsilon$ . Then there exists  $r > 0$  such that for  $\epsilon' = r + \epsilon + \delta$ , and for any  $B_k \in \mathcal{V}$ , we have:*

1. *the side length of the box  $\text{Hull}(f(B_k))$  is less than or equal to  $r$ , and*
2. *if  $B_k \rightarrow B_j \in \mathcal{E}_\Upsilon$ , then for any  $x_k \in B_k$  and any  $x_j \in B_j$ ,  $\|f(x_k) - x_j\|_\infty < \epsilon'$ .*

For  $f = H_{a,c}$ , we may take  $r = \epsilon^2 + \epsilon(2R' + |a|_\infty)$ , where  $R'$  is as in Proposition 2.1.4. For  $f = P_c$ , set  $a = 0$  in the above.

*Proof.* The second item follows immediately from the first item, and the fact that there is an edge from  $B_k$  to  $B_j$  precisely when  $B_j \cap \mathcal{N}_\infty(\text{Hull}(f(B_k)), \delta) \neq \emptyset$ .

We prove the first item using the linearization of  $f$  to approximate it.

We assume  $f$  is a generalized Hénon mapping,  $f(x, y) = (p(x) - ay, x)$ ,  $p$  monic of degree  $d > 1$ . Let  $B \in \mathcal{V}$  and  $(z, w) \in B$ . The linearization of  $f$  at  $(z, w)$  is

$$\begin{aligned} L_z \begin{bmatrix} x \\ y \end{bmatrix} &= f \begin{bmatrix} z \\ w \end{bmatrix} + D_z f \begin{bmatrix} x - z \\ y - w \end{bmatrix} \\ &= \begin{bmatrix} p(z) - aw \\ z \end{bmatrix} + \begin{bmatrix} p'(z) & -a \\ 1 & 0 \end{bmatrix} \begin{bmatrix} x - z \\ y - w \end{bmatrix} \\ &= \begin{bmatrix} p(z) - p'(z)(x - z) - ay \\ x \end{bmatrix}. \end{aligned}$$

Note  $L_z(z, \cdot) = f(z, \cdot)$ . Next, we compute

$$\begin{aligned} \left\| f \begin{bmatrix} x \\ y \end{bmatrix} - L_z \begin{bmatrix} x \\ y \end{bmatrix} \right\|_\infty &= \left\| \begin{bmatrix} p(x) - ay \\ x \end{bmatrix} - \begin{bmatrix} p(z) - p'(z)(x - z) - ay \\ x \end{bmatrix} \right\|_\infty \\ &= \left\| \begin{bmatrix} p(x) - p(z) - p'(z)(x - z) \\ 0 \end{bmatrix} \right\|_\infty \\ &\leq \sum_{k=2}^d \frac{|p^{(k)}(z)|}{k!} |x - z|^k. \end{aligned}$$

If  $(x, y)$  is also in  $B$ , then  $|x - z|_\infty \leq \epsilon$ . Since  $p$  is a polynomial, and  $z \in V = \mathcal{N}_\infty(0, R')$ , there exist  $T_k > 0$ , for  $2 \leq k \leq d$ , such that

$$\sum_{k=2}^d \frac{|p^{(k)}(z)|}{k!} |x - z|^k \leq \sum_{k=2}^d T_k \epsilon^k.$$

Now we need to bound

$$\begin{aligned} \left\| L_z \begin{bmatrix} x \\ y \end{bmatrix} - L_z \begin{bmatrix} z \\ w \end{bmatrix} \right\|_\infty &= \left\| \begin{bmatrix} p'(z)(x-z) - a(y-w) \\ x-z \end{bmatrix} \right\|_\infty \\ &= \max\{|x-z|_\infty, |p'(z)(x-z) - a(y-w)|_\infty\}. \end{aligned}$$

If  $(x, y)$  is in  $B$ , then we also know  $|x-z|_\infty \leq \epsilon$ , and  $|y-w|_\infty \leq \epsilon$ , and since  $p$  is monic of degree  $d$ , and  $(z, w) \in V = \mathcal{N}_\infty(0, R')$ , we have:

$$\begin{aligned} |p'(z)(x-z) - a(y-w)|_\infty &\leq |dz^{d-1}|_\infty |x-z|_\infty + |a|_\infty |y-w|_\infty \\ &\leq d(R')^{d-1}\epsilon + |a|_\infty \epsilon. \end{aligned}$$

By Proposition 2.1.4, we have  $R' > 1$ , hence the maximum needed above is the latter value.

Finally, we put the above pieces together to compute, for any  $(x, y), (z, w)$  in  $B$ ,

$$\begin{aligned} \left\| f \begin{bmatrix} x \\ y \end{bmatrix} - f \begin{bmatrix} z \\ w \end{bmatrix} \right\|_\infty &= \left\| f \begin{bmatrix} x \\ y \end{bmatrix} - L_z \begin{bmatrix} z \\ w \end{bmatrix} \right\|_\infty \\ &\leq \left\| f \begin{bmatrix} x \\ y \end{bmatrix} - L_z \begin{bmatrix} x \\ y \end{bmatrix} \right\|_\infty + \left\| L_z \begin{bmatrix} x \\ y \end{bmatrix} - L_z \begin{bmatrix} z \\ w \end{bmatrix} \right\|_\infty \\ &\leq \sum_{k=2}^d T_k \epsilon^k + \epsilon(d(R')^{d-1} + |a|_\infty). \end{aligned}$$

Hence, for  $r = \sum_{k=2}^d T_k \epsilon^k + \epsilon(d(R')^{d-1} + |a|_\infty)$ , we have that the diameter of the set  $f(B_k)$  in the metric  $\|\cdot\|_\infty$  is less than or equal to  $r$ , hence the side length of  $\text{Hull}(f(B_k))$  is less than or equal to  $r$ .

Note  $r = r(f, \epsilon)$ . If  $f = f_m \circ \cdots \circ f_1$ , then  $r_1 = r(f_1, \epsilon), r_2 = r(f_2, r_1), \dots, r_m = r(f_m, r_{m-1})$ . Set  $r = r_m$ .  $\square$

**Corollary 2.2.5.** *Let  $\mathcal{V}_\epsilon$  be a box cover of  $\mathcal{R}$  for  $f$ . Let  $\Upsilon_\delta$  be a box-chain graph of  $\mathcal{V}_\epsilon$ . If  $\eta > 0$  is sufficiently small and if  $x \in \mathcal{N}_\infty(B_k, \eta)$  and  $f(x) \in \mathcal{N}_\infty(B_j, \eta)$ , then there is an edge from  $B_k$  to  $B_j$  in  $\Upsilon$ , i.e.,  $B_k \rightarrow B_j \in \mathcal{E}_\Upsilon$ .*

For  $f = H_{a,c}$ , we need  $\eta > 0$  small enough that

$$\eta < \frac{1}{2} \left( -(2(R') + |a|_\infty + 1) + \sqrt{(2(R') + |a|_\infty + 1)^2 + 4\delta} \right),$$

where  $R'$  is as in Proposition 2.1.4. For  $f = P_c$ , set  $a = 0$  in the above.

*Proof.* Again we give the proof for  $f(x, y) = (p(x) - ay, x)$ ,  $p$  monic of degree  $d > 1$ . Let  $(x, y) \in \mathcal{N}_\infty(B_k, \eta)$  and  $f(x, y) \in \mathcal{N}_\infty(B_j, \eta)$ . Let  $(z, w)$  be a point in  $B_k$  which realizes this minimum distance (since  $B_k$  is closed), i.e.,

$$\left\| \begin{bmatrix} x \\ y \end{bmatrix} - \begin{bmatrix} z \\ w \end{bmatrix} \right\|_\infty < \eta.$$

Then in order to guarantee that  $B_k \rightarrow B_j \in \mathcal{E}_\Upsilon$ , we just need

$$\left\| f \begin{bmatrix} x \\ y \end{bmatrix} - f \begin{bmatrix} z \\ w \end{bmatrix} \right\|_\infty < \delta - \eta.$$

But examining the proof of Lemma 2.2.4, since  $(z, w) \in B_k$ , we see that we have

$$\left\| f \begin{bmatrix} x \\ y \end{bmatrix} - f \begin{bmatrix} z \\ w \end{bmatrix} \right\|_\infty \leq \sum_{k=2}^d T_k \eta^k + \epsilon(d(R')^{d-1} + |a|_\infty).$$

Thus, we just need  $\eta$  to satisfy

$$\sum_{k=2}^d T_k \eta^k + \eta(d(R')^{d-1} + |a|_\infty + 1) - \delta < 0.$$

Let  $q(\eta) = \sum_{k=2}^d T_k \eta^k + \eta(d(R')^{d-1} + |a|_\infty + 1) - \delta$ . We simply require  $\eta$  to be less than the smallest positive root. Note for  $H_{a,c}$ , this yields

$$\eta < \frac{1}{2} \left( -(2R' + |a|_\infty + 1) + \sqrt{(2R' + |a|_\infty + 1)^2 + 4\delta} \right).$$

If  $f = f_m \circ \cdots \circ f_1$ , we may take  $\eta = \min\{\eta_1, \dots, \eta_m\}$ .  $\square$

Finally, we are ready to show that the box-chain recurrent set  $\mathcal{B}_\Gamma$  is a good cover of the chain recurrent set, in the following sense.

**Theorem 2.2.6.** *Let  $\mathcal{V}_\epsilon$  be a box cover of  $\mathcal{R}_\eta$  for  $f$ , where  $\eta$  is as in Proposition 2.1.4 (or Corollary 2.1.5). Let  $\Upsilon_\delta$  be the box-chain graph of  $\mathcal{V}_\epsilon$ , and let  $\Gamma$  be the box-chain recurrent graph for  $\Upsilon_\delta$ . Then for  $\epsilon'$  as in Lemma 2.2.4, and  $\delta' = \min(\delta, \eta)$ , we have*

$$\mathcal{R}_{\delta'} \subset \mathcal{B}_\Gamma \subset \mathcal{R}_{\epsilon'}. \quad (2.1)$$

Note as  $\epsilon \rightarrow 0$ , both  $\epsilon'$  and  $\delta'$  tend to zero.

*Proof.* For the first inclusion,  $\mathcal{R}_{\delta'} \subset \mathcal{B}_\Gamma$ , note by choice of  $\delta'$  we have  $\mathcal{R}_{\delta'} \subset V \cap \mathcal{B}_\Upsilon = \mathcal{B}_\Upsilon$ . Suppose  $p \in \mathcal{R}_{\delta'}$ . Then there exist  $x_1 = p, x_2, \dots, x_n = p$  such that  $\|f(x_k) - x_{k+1}\|_\infty < \delta'$  for  $1 \leq k < n$ . Note that  $x_k \in \mathcal{R}_{\delta'}$ , for  $1 \leq k < n$ . Hence each  $x_k \in V \cap \mathcal{B}_\Upsilon = \mathcal{B}_\Upsilon$  as well. Then there are boxes  $B_k \in \Upsilon$  such that  $x_k \in B_k$  for  $1 \leq k < n$ . Since  $\|f(x_k) - x_{k+1}\|_\infty < \delta'$ , we have  $f(x_k) \in \mathcal{N}_\infty(B_{k+1}, \delta')$ . Since  $\delta' \leq \delta$ , there is an edge in  $\Upsilon$  from  $B_k$  to  $B_{k+1}$ .

Hence,  $p$  is in a box  $B_1$  which lies in a cycle of  $\Upsilon$ ,  $B_1 \rightarrow B_2 \rightarrow \cdots \rightarrow B_{n-1} \rightarrow B_1$ . Thus  $B_1 \in \mathcal{V}_\Gamma$ , hence  $p \in \mathcal{B}_\Gamma$ .

For the second inclusion,  $\mathcal{B}_\Gamma \subset \mathcal{R}_{\epsilon'}$ , suppose  $p \in \mathcal{B}_\Gamma$ . Thus  $p$  lies in some box  $B_1$  which lies in a cycle  $B_1 \rightarrow B_2 \rightarrow \cdots \rightarrow B_{n-1} \rightarrow B_1$  in  $\Upsilon$ . Recall  $\epsilon$  is the side length of the boxes in the cover. Let  $x_1 = x_n = p$ , and  $x_k$  be any point in  $B_k$  for  $2 \leq k \leq n-1$ . Then by Lemma 2.2.4, since  $B_1 \rightarrow B_2 \rightarrow \cdots \rightarrow B_{n-1} \rightarrow B_1$  is a cycle in  $\Upsilon$ , we have  $\|f(x_k) - x_{k+1}\|_\infty < \epsilon'$  for  $1 \leq k \leq n$ . Hence,  $p$  is  $\epsilon'$ -chain recurrent.  $\square$

From this we immediately get:

**Corollary 2.2.7.** *Let  $\mathcal{V}_\epsilon$  be a box cover of  $\mathcal{R}$  for  $f$ . Let  $\Upsilon_\delta$  be the box-chain graph of  $\mathcal{V}_\epsilon$ , and let  $\Gamma$  be the box-chain recurrent graph for  $\Upsilon_\delta$ . Then  $\mathcal{R} \subset \mathcal{B}_\Gamma \subset \mathcal{R}_{\epsilon'}$ , where  $\epsilon'$  is as in Lemma 2.2.4.*

Now we discuss how  $\Gamma$  gives an approximation to the chain-transitive components.

**Definition 2.2.8.** Given a box-chain recurrent graph  $\Gamma$ , let  $\Gamma'$  be a connected component of  $\Gamma$ , *i.e.*, a maximal edge-connected subgraph. We call  $\mathcal{B}_{\Gamma'}$  a *box-chain transitive component* (with respect to  $\Gamma$ ).

Theorem 2.2.6 and the definitions of these notions give us:

**Theorem 2.2.9.** *Let  $\Gamma$  be a box-recurrent graph satisfying the hypotheses of Theorem 2.2.6.*

1. *Let  $\mathcal{R}'_\delta$  be any  $\delta'$ -chain transitive component. Then there is a box-chain transitive component,  $\mathcal{B}_{\Gamma'}$  (with respect to  $\Gamma$ ), such that  $\mathcal{R}'_\delta \subset \mathcal{B}_{\Gamma'}$ .*
2. *Let  $\mathcal{B}_{\Gamma'}$  be any box-chain transitive component (with respect to  $\Gamma$ ). Then there is some  $\epsilon'$ -chain transitive component,  $\mathcal{R}'_{\epsilon'}$ , such that  $\mathcal{B}_{\Gamma'} \subset \mathcal{R}'_{\epsilon'}$ .*

We get immediately:

**Corollary 2.2.10.** *Let  $\Gamma$  be a box-recurrent graph satisfying the hypotheses of Corollary 2.2.7.*

1. *Let  $\mathcal{R}'$  be any chain transitive component. Then there is a box-chain transitive component,  $\mathcal{B}_{\Gamma'}$  (with respect to  $\Gamma$ ), such that  $\mathcal{R}' \subset \mathcal{B}_{\Gamma'}$ .*
2. *Let  $\mathcal{B}_{\Gamma'}$  be any box-chain transitive component (with respect to  $\Gamma$ ). Then there is some  $\epsilon'$ -chain transitive component,  $\mathcal{R}'_{\epsilon'}$ , such that  $\mathcal{B}_{\Gamma'} \subset \mathcal{R}'_{\epsilon'}$ .*

Finally, we can conclude:

**Corollary 2.2.11.** *Let  $\Gamma$  be a box-recurrent graph satisfying the hypotheses of Theorem 2.2.6, or Corollary 2.2.7.*

*Then there is a single box-chain transitive component  $\mathcal{B}_{\Gamma'}$  (with respect to  $\Gamma$ ) such that  $J \subset \mathcal{B}_{\Gamma'}$ .*

*Proof.* By Theorem 1.2.9, we know  $J$  is contained in a single chain transitive component of  $\mathcal{R}$ . By Theorem 2.2.9, or Corollary 2.2.10, each chain transitive component is contained in a single box-chain transitive component.  $\square$

*Remark.* Note that if  $\Gamma'$  is the connected component of  $\Gamma$  such that  $J \subset \mathcal{B}_{\Gamma'}$ , we can say  $\mathcal{V}' = \mathcal{V}_{\Gamma'}$  is a box cover of  $J$ , and  $\Gamma'$  is a box-chain graph of  $\mathcal{V}'$ .

We observe also that more than one  $\delta'$ -chain transitive component can be in a box-chain transitive component. Also, an  $\epsilon'$ -chain component may not actually contain any chain recurrent points, hence a box-chain transitive component may not contain any chain recurrent points. We will see examples of such components in Section 3.6.

### 2.3 Algorithm to build a box-chain recurrent graph

*Hypatia's* algorithm to build a box-chain recurrent graph satisfying Theorem 2.2.6 starts with using Proposition 2.1.4 (or Corollary 2.1.5) to compute the constant  $R > 1$ , then we choose an  $R'$  slightly larger than  $R$ , for example,  $R' = R + 0.1$ , and define  $V$  (and  $V^\pm$ ) using  $R'$ . Then we know  $\mathcal{R}_\eta \subset V$ , for  $\eta$  as in Proposition 2.1.4 (or Corollary 2.1.5).

After computing  $R'$ , *Hypatia* divides the box  $V = \mathcal{N}_\infty(0, R')$  into a grid of  $2^m \times \dots \times 2^m = (2^m)^{2n}$  equally sized boxes,  $\mathcal{V}_\epsilon = \{B_k : 0 \leq k \leq 2mn\}$ , with side length  $\epsilon = R'/2^{m-1}$ . Then for some  $\delta > 0$  (like  $\delta = \epsilon/1000$ ), it computes the box-chain graph  $\Upsilon_\delta$  for  $\mathcal{V}_\epsilon$ . To compute the edges, *Hypatia* uses interval arithmetic (described in Appendix A) to compute a box  $\text{Hull}(f(B_k))$  which contains  $f(B_k)$ . In order to find the box-chain recurrence graph  $\Gamma$ , we need a method for finding all boxes that are in cycles of  $\Upsilon$ .

**Definition 2.3.1.** A *strongly connected component*, or *s.c.c.*,  $\Gamma'$ , of a graph  $\Upsilon$ , is a subgraph with vertex set  $W$  such that given any two vertices  $v, u$  in  $W$ , there is a path of edges in  $\Upsilon$  from  $v$  to  $u$  and a path from  $u$  to  $v$ ; further,  $W$  is maximal in that if  $W' \supset W$ , then there exists a pair of vertices  $u, w \in W'$  such that there is no path from  $u$  to  $w$  in  $\Upsilon$ . The edges of the s.c.c. are all those in  $\Upsilon$  between the vertices of  $\Gamma'$ .

Thus, all boxes which are in cycles in  $\Upsilon$  will be in an s.c.c. of  $\Upsilon$ . Hence,  $\Gamma$  is the union of the s.c.c.'s of  $\Upsilon$ . *Hypatia* employs an algorithm described in [20] to decompose a graph  $\Upsilon$  into its s.c.c.'s.

Definition 2.3.1 gives us immediately that:

**Lemma 2.3.2.** *The s.c.c.'s of a box-chain graph,  $\Upsilon$ , are precisely the connected components of the box-chain recurrent graph  $\Gamma$  (of  $\Upsilon$ ).*

Thus, if *Hypatia* employs this basic algorithm above, then all of the (strongest) results of the previous section apply to *Hypatia's* graphs, for example,  $\mathcal{B}_\Gamma$  satisfies  $\mathcal{R}_{\delta'} \subset \mathcal{B}_\Gamma \subset \mathcal{R}_{\epsilon'}$ , for some  $\delta', \epsilon' > 0$ .

Before implementing the algorithm to find a box-chain recurrent set, we can make various additions which improve the performance by getting to a small  $\Gamma$  more quickly and using less memory.

#### Subdivision

Rather than defining a  $(2^{13})^{2n}$  grid on  $V$  full of very tiny boxes, we go through a refinement process to get smaller boxes from larger ones. That is, first define a coarse, say  $(2^3)^{2n}$ , grid on  $V$ . Compute the box-chain graph for this grid on  $V$ , then the s.c.c.'s of it. Call this level one. Now we can ignore all the boxes which did not make it to an s.c.c. and put a, say  $(2^2)^{2n}$ , grid on just the boxes in the level one s.c.c.'s, and then compute a new transition graph and its s.c.c.'s to form level

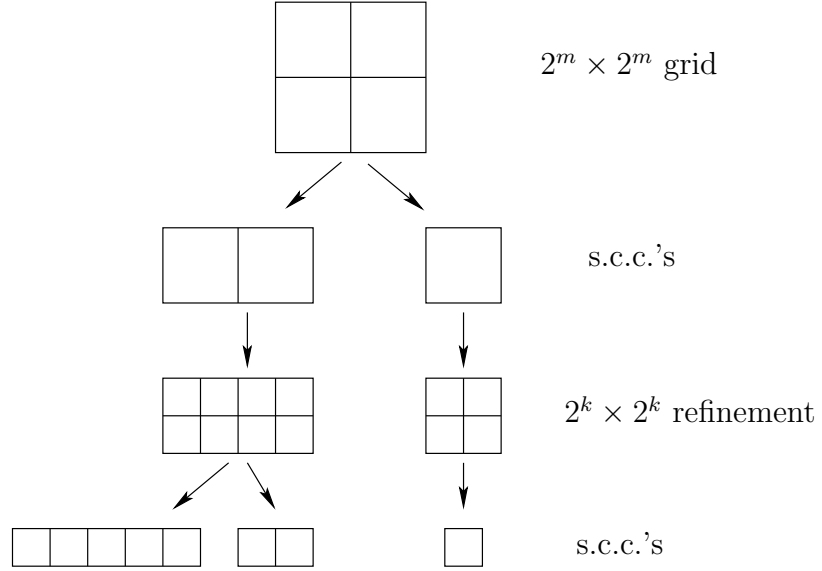


Figure 2.1: Subdivision of box cover

two. Now we have the same s.c.c. boxes as we would have had if we had just put a  $(2^5)^{2n}$  grid on  $V$ , but we have saved time and memory by eliminating some larger boxes in level one before getting down to the desired box size. See Figure 2.1 for an illustration of a couple of levels of grids and s.c.c.'s.

Note that Theorem 2.2.6 and 2.2.9 still apply to the box-chain recurrent graph computed with subdivision, since at any level the collection of boxes  $\mathcal{V}_\epsilon$  satisfies the hypotheses required.

Not only does this subdivision method help to find a good box-chain recurrent set composed of small boxes more efficiently, but the tree structure given by the nested boxes is useful for quickly computing things such as which boxes intersect a given set (like the image of another box). This allows us to store the s.c.c.'s as an array of vertices with adjacency lists of edge information, with no need to arrange the vertices in any particular order in the array.

## Eliminating boxes with iteration: the $V$ -check

A very useful technique to eliminate quite a bit of the work of computing the new box-chain graph at each level is to immediately eliminate boxes whose images lie outside of  $V$ . Note by Proposition 2.1.4 and Corollary 2.1.5 that if a box  $B_k$  has its entire image outside of  $V$ , then none of the points in the box are in  $\mathcal{R}$ . But then if *any* iterate of  $B_k$  is all outside of  $V$ , then  $B_k \cap \mathcal{R} = \emptyset$ . We use this fact to eliminate some boxes before creating edges from or to them. That is, given a set of s.c.c.'s, with a new  $(2^m)^{2n}$  grid of boxes in each old box, for each new box  $B_k$  compute (using interval arithmetic, described in Appendix A), up to say 100,

forward images  $B_k^1 = \text{Hull}(f(B_k))$ ,  $B_k^2 = \text{Hull}(f(B_k^1))$ , etc. If any of the images  $B_k^n$  lies entirely outside  $V$ , then the box  $B_k$  does not contain any points of  $\mathcal{R}$ , and so can be deleted from the grid. After each new box has been checked, compute the edges only for the remaining boxes, and then the s.c.c.'s for that graph.

For the Hénon family, we can also take advantage of invertibility. That is, it follows from Lemma 2.1.2 that if an image of a box under  $H^{-1}$  lies outside of  $V$ , then it is not in  $\mathcal{R}$ . Thus we can check forward and backward images of boxes.

Since a box-chain recurrent set found in this way still contains  $\mathcal{R}$ , we have the slightly weaker results of Corollary 2.2.7 and 2.2.10 in this case. Note we still have Lemma 2.2.4 and Corollary 2.2.5.

The main computational limitation of *Hypatia* is in memory usage. Not having to store edges corresponding to boxes which are eliminated with the “ $V$ -check” is a big memory gain. In many instances, this check eliminates half or even three-fourths or more of the new boxes.

## Selective subdivision

We can concentrate our efforts on the boxes which are most preventing a successful hyperbolicity test by allowing boxes of different sizes. Since *Hypatia*'s hyperbolicity test treats all the points in each box the same, it is necessary to have the behavior in each box varying by at most a small amount. Thus, we would like to refine down to a certain reasonable box size, then somehow select only a small fraction of the boxes to be subdivided further.

Before even attempting to prove hyperbolicity, we need the s.c.c.'s to separate the Julia set from the sinks. That is, we need small enough boxes so that the box-chain transitive component containing the Julia set is separate from each of the box-chain transitive components for the attracting periodic orbits. So, it would be helpful to have methods for more efficiently separating  $J$  from the sinks. We discuss this issue further in Chapter 4 and Chapter 5.

Next, in an s.c.c. covering  $J$  and not the sinks there are two fundamentally different ways in which a box could be obstructing a hyperbolicity test. One way is that it could be a bit too close to the attracting periodic cycle, and we would need to subdivide it to eliminate the part which is not hyperbolic. The other kind of box would contain “mostly” points of  $\mathcal{R}$ , but cover a region of  $\mathcal{R}$  in which the behavior of the points in the box is varying widely. We have tried many ways of detecting which of these kinds of boxes most need to be subdivided. We discuss specific tests we used for selective subdividing when we describe the hyperbolicity testing in Chapters 3 and 4.

# Chapter 3

## Hyperbolicity in one complex dimension

### 3.1 Introduction: box-expansion

In this chapter, we describe the algorithm for proving hyperbolicity in one complex dimension. Recall in Definition 1.3.1, we defined hyperbolicity for a polynomial map  $f: \mathbb{C} \rightarrow \mathbb{C}$  as uniform expansion over a neighborhood of  $J$  with respect to a riemannian norm. The one dimensional algorithm to test expansion of a map could prove a useful tool for the study of expansive maps of high degree or in higher dimensions. In addition, some of the key elements of the two dimensional algorithm for diffeomorphisms can be dealt with in isolation in this simpler setting. In particular, in two dimensions we will build an approximate unstable and an approximate stable line field, and use this one dimensional algorithm to attempt to build a metric which is contracted on the stable directions, and another metric which is expanded on the unstable directions. These metrics will then determine the cones that we will use to verify the cone check for hyperbolicity (Theorem 1.3.4).

Throughout this chapter, let  $f: \mathbb{C} \rightarrow \mathbb{C}$  denote a polynomial map of degree  $d > 1$ , with Julia set,  $J$ , let  $\mathcal{V} = \{B_k\}$  be a box cover of  $J$ , and let  $\Gamma'$  be a strongly connected box-chain graph for  $\mathcal{V}$ . Note by Corollary 2.2.11 and Proposition 2.1.4, we have the existence of such a  $\Gamma'$ .

*Hypatia* attempts to construct a piecewise constant metric (not a continuous one) under which a differentiable map  $f$  expands by a given  $L$  on the set  $J$ .

**Definition 3.1.1.** Call  $f$  *box-expansive* (with respect to  $\Gamma'$ ) if there exist constants  $\{c_k\}$  and an  $L > 1$  such that  $f$  is expanding on  $B_k \in \mathcal{V}$  by  $L$ , in the norm  $|\cdot|_k = c_k |\cdot|$ . That is, if for all  $k, j$ , such that  $B_k \rightarrow B_j$  is an edge in  $\Gamma'$ , and for all  $x$  in  $B_k$ , and for all  $\mathbf{v}$  in  $T_x\mathbb{C}$ , we have  $|D_x f(\mathbf{v})|_j \geq L |\mathbf{v}|_k$ .

If  $f$  is box-expansive with respect to some  $\Gamma'$ , we say  $\Gamma'$  and  $\mathcal{V}$  are box-expansive. We also sometimes say  $f$  is box-expansive on  $\mathcal{V}$ , or simply  $f$  is box-expansive.

It is important to remember that showing box-expansion by  $L = 1$  may be instructive, but it is not enough to prove hyperbolicity.

In Section 3.3, we prove Theorem 3.3.3, showing that box-expansion implies the standard definition of expansion. Thus, if *Hypatia* successfully defines a metric showing  $f$  is box-expansive by some  $L > 1$ , then  $f$  is proven hyperbolic.

We give *Hypatia's* algorithm for testing box-expansion by attempting to build metric constants,  $\{c_k\}$ , for a given  $L$  in Section 3.2. There we also give a characterization of box-expansion independent of the algorithm used to set the constants, in Theorem 3.2.4.

In Section 3.4 we discuss how to find a good  $L$  to input into *Hypatia's* algorithm. We describe methods to add to this algorithm in order to improve the metric

in Section 3.5. We list the results of running *Hypatia* on several examples in Section 3.6.

### 3.2 Algorithm to build a metric showing box-expansion

**Step 1:** *Hypatia* first builds a minimum spanning tree for  $\Gamma'$ , and sets the constants using the edges in the tree. A connected spanning tree for the directed graph  $\Gamma'$  can always be built because it is strongly connected. The spanning tree in such a case is called an *arborescence* ([20]). Such a tree has a root vertex,  $u = B_0$ , such that there are paths from  $u$  to all other vertices in the graph, and each vertex has only one incoming edge. Now set this first constant  $c_0$  to be 1, so the metric is just euclidean on the root vertex. Then *Hypatia* traverses the rest of the tree and assigns constants to each vertex which depend on the previous constant as follows. We are trying to construct a metric which  $f$  expands by  $L$ . Thus if  $c_k$  has already been chosen, and there is an edge from  $B_k$  to  $B_j$ , we want to define  $c_j$  so that the map  $f$  is expanding by  $L$  on points of  $B_k$  which map to  $B_j$ . Thus we need that for every  $z$  in  $B_k$ , and every  $\mathbf{v}$  in  $T_zM$ ,

$$c_j |D_z f(\mathbf{v})| = c_j |D_z f| |\mathbf{v}| = \frac{c_j}{c_k} |D_z f| |\mathbf{v}| \geq L |\mathbf{v}|.$$

Hence define  $c_j = c_k L / \min_{z \in B_k} |D_z f|$ .

**Notation:** Let  $\lambda_k = \min_{z \in B_k} |D_z f|$ . So we have  $c_j = c_k L / \lambda_k$ .

Since  $D_z f = 2z$  for  $P_c(z) = z^2 + c$ , the minimum multiplier  $\lambda_k$  in a box is easily calculated.

**Step 2:** Now we have a metric which  $f$  expands by  $L$ , but only on the edges in the minimum spanning tree. To build a metric expanded by  $f$  on all of  $\Gamma'$ , *Hypatia* begins at  $u$  and starts checking edges of  $\Gamma'$  not in the spanning tree. Each time an edge is examined, the metric must be adjusted. Sometimes there is an obstruction to this adjustment, which means it is not possible to build such a metric. The way to adjust the metric is simple. If checking an edge from  $B_k$  to  $B_j$ , redefine

$$c_j = \max\{c_j, c_k L / \lambda_k\}.$$

Then  $f$  expands on the new edge. However, if  $c_j$  is increased, then all the vertices reachable from  $B_j$  may also have to be re-defined to keep the metric expanding by  $L$ . In summary, *Hypatia* adds an edge to the spanning tree from  $v$  to  $w$ , then redefines the metric constant at  $w$ , then traverses every edge reachable from  $w$  that is either in the spanning tree or has been previously checked, re-defining metric constants in turn. If *Hypatia* finds a vertex  $y$  with a constant which is already big enough, it does not search the edges emanating from  $y$ . Thus, the only obstruction to the re-defining is: what happens if *Hypatia* travels away from  $w$  and comes back through some node  $x$  and sees  $v$ ? This means every constant on the path from  $v$  to  $w$  and back to  $v$  has been increased (because we stopped the search if it was not). Thus the constant at  $v$  cannot be increased again (an infinite loop of increasing

would occur). Thus, this is a dynamical obstruction. So, *Hypatia* can only check if  $c_v$  is already big enough compared to  $c_x$ . If so, the metric is fine and *Hypatia* keeps going.

Hence, if *Hypatia* checks all the edges of  $\Gamma'$  and is successful at building a metric with the specified properties, then  $f$  is box-expansive, and thus by Theorem 3.3.3 it is hyperbolic. If *Hypatia* finds an obstruction, then  $f$  still may be hyperbolic, but either  $L$  is too large, or the boxes  $B_k$  are too large.

Appendix B contains a pseudo-code description of the complete algorithm for building a metric to achieve box-expansion by a given  $L$ , **fExpands**, listed as Algorithm B.0.1.

Now that we have explained the algorithm in detail, we consider the implications of success or failure.

**Lemma 3.2.1.** *Let  $B_0, \dots, B_{n-1}, B_n = B_0$  be an  $n$ -cycle of boxes in  $\Gamma'$ , such that consistent metric constants  $\{c_0, \dots, c_{n-1}, c_n = c_0\}$  can be chosen to show  $f$  box-expands by  $L > 1$  along the cycle. Then the multiplier of any pseudo orbit in the cycle is greater than or equal to  $L^n$ .*

*Proof.* Let  $x_k \in B_k$  be any points in the boxes. Then by hypothesis, we know

$$c_{k+1} |f'(x_k)| \geq c_{k+1} \lambda_k \geq L c_k, \quad k \in \{0, \dots, n-1\}.$$

Thus,

$$|f'(x_0) \cdots f'(x_{n-1})| \geq L \frac{c_0}{c_1} L \frac{c_1}{c_2} \cdots L \frac{c_{n-1}}{c_n = c_0}.$$

Cross cancellation and simplifying leaves only

$$|f'(x_0) \cdots f'(x_{n-1})| \geq L^n.$$

□

Conversely:

**Definition 3.2.2.** Given  $\lambda_k = \min\{|D_z f| : z \in B_k\}$ , the *box cycle multiplier* of a cycle of boxes  $B_0, \dots, B_n = B_0$  is the product  $\lambda_0 \cdots \lambda_{n-1}$ .

**Proposition 3.2.3.** *The Hypatia algorithm either shows that  $f$  is box-expansive by  $L$  (with respect to  $\Gamma'$ ), or it finds an  $n$ -cycle of boxes along which the box cycle multiplier is less than  $L^n$ .*

*Proof.* Consider what it means for *Hypatia* to not be able to show expansion using this algorithm. The only obstruction to this algorithm working is if in checking an edge  $(u, v)$ , *Hypatia* finds a cycle of boxes  $u = B_0, v = B_1, \dots, B_{n-1}, B_n = B_0$ , such that, holding  $c_0$  fixed, to get each edge expanded by  $L$  the metric constants must be increased along every edge in the cycle. That is,  $c_{k+1} = L c_k / \lambda_k$  for  $0 \leq k \leq n-2$ , and we have the failure  $c_0 < L c_{n-1} / \lambda_{n-1}$ . But then

$$c_0 < \frac{L c_{n-1}}{\lambda_{n-1}} = \frac{L^2 c_{n-2}}{\lambda_{n-1} \lambda_{n-2}} = \cdots = \frac{L^n c_0}{\lambda_{n-1} \lambda_{n-2} \cdots \lambda_0}.$$

Hence,  $\lambda_{n-1} \lambda_{n-2} \cdots \lambda_0 < L^n$ .

□

These results combine to give a characterization of box-expansion, independent of any algorithm used to find the metric constants.

**Theorem 3.2.4.**  *$f$  is box-expansive (with respect to  $\Gamma'$ ) by  $L$  iff for every  $n$ -cycle in the graph, the product of the multipliers along any pseudo orbit in the cycle is at least  $L^n$ .*

*Proof.* The forward implication is Lemma 3.2.1. We show the contrapositive of the reverse implication. Proposition 3.2.3 shows that if  $f$  is not box-expansive, *Hypatia* will not show that  $f$  is box-expansive, but rather will find an  $n$ -cycle of boxes  $B_0, \dots, B_n = B_0$  with box cycle multiplier less than  $L^n$ . Since  $B_k$  is compact,  $\lambda_k$  is realized by some point  $x_k$ . Thus the pseudo orbit  $\{x_0, \dots, x_{n-1}, x_0\}$  will have multiplier less than  $L^n$ .  $\square$

### 3.3 Box-expansion implies continuous expansion

In this section, we show box-expansion implies the standard definition of expansion, by using a partition of unity to smooth out the piecewise constant norm given by the collection of  $|\cdot|_k$ .

**Lemma 3.3.1.** *Let  $f$  be box-expansive by  $L > 1$  (with respect to  $\Gamma'$ ). Then there exists a  $\tau > 0$  such that if  $B_k, B_j \in \mathcal{V}'$ , and  $z \in \mathcal{B}' \cap \mathcal{N}_\infty(B_k, \tau)$  with  $f(z) \in \mathcal{N}_\infty(B_j, \tau)$ , then for any  $\mathbf{v} \in T_z\mathbb{C}$ ,  $c_j |D_z f(\mathbf{v})| \geq Lc_k |\mathbf{v}|$ .*

*Proof.* Among other requirements given below, let  $\tau > 0$  be smaller than  $\eta$  from Corollary 2.2.5. Then for  $z$  satisfying the hypotheses, there is an edge from  $B_k$  to  $B_j$  in  $\Gamma'$ , i.e.,  $B_k \rightarrow B_j \in \mathcal{E}'$ .

Note since we are working in one dimension,  $D_x f = f'(x)$ , hence box-expansion gives for  $x \in B_k$ ,  $c_j |f'(x)| |\mathbf{v}| \geq Lc_k |\mathbf{v}|$ , thus simply  $c_j |f'(x)| \geq Lc_k$ .

Since  $\mathcal{B}'$  is compact,  $\mathcal{V}'$  is finite, and  $f'(x)$  is continuous, there is a  $d \geq 0$  such that:

1.  $d = \min\{c_j |f'(x)| - Lc_k : x \in B_k, B_k \rightarrow B_j \in \mathcal{E}'\}$ ,
2. if  $\tau < \eta$  is sufficiently small, then for any  $j$ ,  $|x - z| < \tau$  implies that  $c_j |f'(x) - f'(z)| < d$ .

Now  $z$  is not necessarily in  $B_k$ , but  $z \in \mathcal{B}'$ , so suppose  $z \in B_m$  and  $x \in B_m \cap B_k$  such that  $|x - z| < \tau$ . Then  $c_j |f'(x) - f'(z)| < d$ ; further, there is an edge  $B_k \rightarrow B_j$ , hence  $x$  satisfies  $c_j |f'(x)| - Lc_k \geq d$ . But then combining these two gives  $c_j |f'(z)| \geq Lc_k$ . Thus  $c_j |D_z f(\mathbf{v})| \geq Lc_k |\mathbf{v}|$ .  $\square$

**Definition 3.3.2.** Let  $f$  be box-expansive (with respect to  $\Gamma'$ ). Let  $\tau > 0$  be as given by Lemma 3.3.1. Define a partition of unity on  $\mathcal{B}'$  by choosing continuous functions  $\rho_k : \mathbb{C} \rightarrow [0, 1]$ , for each box  $B_k \in \mathcal{V}'$ , such that  $\text{supp}(\rho_k) \subset \mathcal{N}_\infty(B_k, \tau)$

and  $\sum_k \rho_k(x) = 1$ , for any  $x \in \mathcal{B}'$ . Then we can define a *continuous* norm,  $|\cdot|_\rho$ , on  $T_{\mathcal{B}'\mathbb{C}}$  by

$$|\mathbf{v}|_\rho = \sum_k \rho_k(x) |\mathbf{v}|_k = |\mathbf{v}| \sum_k \rho_k(x) c_k.$$

Now we prove Theorem 3.3.3, by showing that if  $f$  is box-expansive, then  $f$  expands the norm  $|\cdot|_\rho$ .

**Theorem 3.3.3.** *Suppose  $f$  is box-expansive by  $L > 1$  (with respect to  $\Gamma'$ ). Then there exists a continuous norm  $|\cdot|_\rho$  on  $T_{\mathcal{B}'\mathbb{C}}$  which  $f$  expands by  $L$ , i.e., for all  $x \in \mathcal{B}'$ , and all  $\mathbf{v}$  in  $T_x\mathbb{C}$ ,*

$$|D_x f(\mathbf{v})|_\rho \geq L |\mathbf{v}|_\rho.$$

*Proof.* Let  $|\cdot|_\rho, \tau$  be as in Definition 3.3.2.

Thus  $\tau$  is small enough that if  $x \in \text{supp}(\rho_k)$ , then for any  $j$  such that  $f(x) \in \text{supp}(\rho_j)$ , we have  $c_j |D_x f(\mathbf{v})| \geq L c_k |\mathbf{v}|$ , for any  $\mathbf{v} \in T_x\mathbb{C}$ .

Then if we set

$$c_x = \max\{c_k : x \in \text{supp}(\rho_k)\}, \quad \text{and} \quad c_{f,x} = \min\{c_j : f(x) \in \text{supp}(\rho_j)\},$$

we know  $c_{f,x} |D_x f(\mathbf{v})| \geq L c_x |\mathbf{v}|$ , for any  $\mathbf{v} \in T_x\mathbb{C}$ .

Now we need only use the fact that  $\sum_k \rho_k(x) = \sum_j \rho_j(f(x)) = 1$  to get the result, for:

$$\begin{aligned} |D_x f(\mathbf{v})|_\rho &= |D_x f(\mathbf{v})| \sum_j \rho_j(f(x)) c_j \geq |D_x f(\mathbf{v})| c_{f,x} \\ &\geq L c_x |\mathbf{v}| \geq L |\mathbf{v}| \sum_k \rho_k(x) c_k = L |\mathbf{v}|_\rho. \end{aligned}$$

□

Thus if *Hypatia* verifies that a map is box-expansive on a cover of  $J$ , then the map is expanding on  $J$ , thus hyperbolic.

### 3.4 Finding a good expansion amount

One weakness of *Hypatia's* metric-building algorithm is that the amount of expansion to test,  $L$ , must be inputted in advance. In addition, an  $L$  more appropriate for a particular box cover yields a metric closer to euclidean.

The method for testing hyperbolicity of a diffeomorphism of  $\mathbb{C}^2$  is based on the one dimensional method. There we will be defining a cone field based on two sets of metric constants, one set for stable/contraction and the other for unstable/expansion. If the constants are small the cones may be extremely thin, and it would be difficult for the computer to verify that the map preserves the cone field, since it must check that a cone is mapped inside another cone.

Thus if we can develop methods to significantly improve the metric in one dimension, then in two dimensions we will be more likely to verify the diffeomorphism is hyperbolic, because the cone field will be more numerically robust.

In running *Hypatia* it is easy to find behavior like the following. Suppose for some  $c$ , *Hypatia* can build a metric with  $L = 1.2$ , but the resulting metric constants range between  $4.3 \times 10^{-18}$  and 0.6. Depending on the value of  $c$ , trying something like  $L = 1.5$  could improve the metric constants to be in the range 0.068 to 0.55.

Why do we see this behavior? Consider the example:

**Example 3.4.1.** Suppose there is a path of boxes  $B_0, \dots, B_n$  such that (for simplicity) all minimum multipliers  $\lambda_k$  are approximately the same value  $\lambda$ . Then suppose we ask *Hypatia* to show box-expansion by some  $L < \lambda$ . It defines the metric in the boxes of this cycle so that  $c_{k+1} \geq Lc_k/\lambda$ , for  $0 \leq k \leq n-1$ . Thus we get

$$c_1 = \frac{c_0 L}{\lambda}, c_2 = \frac{c_1 L}{\lambda} = \frac{c_0 L^2}{\lambda^2}, \dots, c_n = \frac{c_0 L^n}{\lambda^n}.$$

But since  $L < \lambda$ , large  $n$  leads to  $L^n \ll \lambda^n$ , hence  $c_n \ll c_0$ . Thus, if we try to show expansion by a  $L$  which is “too small”, then the metric constants plummet to small values.

In this section we show Proposition 3.4.3, which is an alternate version of Theorem 3.2.4 giving a theoretical characterization of the largest  $L$  for which a map is box-expansive. However we also show this is infeasible to compute. Then we give an efficient method for finding an approximation to the optimal  $L$ .

### 3.4.1 An optimal, yet impractical solution

**Definition 3.4.2.** If  $B_0, \dots, B_{n-1}, B_n = B_0$  is an  $n$ -cycle of boxes, then the *average (box) cycle multiplier* is  $(\lambda_0 \cdots \lambda_{n-1})^{1/n}$ .

A cycle in a graph is called *simple* if it is composed of distinct vertices.

**Proposition 3.4.3.** Let  $\mathcal{L}$  be the minimum average cycle multiplier over all simple cycles in the graph  $\Gamma'$ . If  $\mathcal{L} > 1$ , then  $f$  is box-expansive on  $\Gamma'$  by  $\mathcal{L}$ , but not by any  $L > \mathcal{L}$ .

*Proof.* Suppose to the contrary that  $f$  is not box-expansive on  $\Gamma'$  by  $\mathcal{L}$ . Then by Lemma 3.2.1, there is an  $n$ -cycle  $B_0, \dots, B_{n-1}, B_n = B_0$  whose box multiplier is less than  $\mathcal{L}^n$ . But then this cycle’s average multiplier is less than  $\mathcal{L}$ . This contradicts minimality of  $\mathcal{L}$ .

Further, suppose  $f$  is box-expansive by some  $L$ . Now, the cycle multiplier of the  $n$ -cycle with the minimum average multiplier  $\mathcal{L}$  is  $\mathcal{L}^n$ . Then by Proposition 3.2.3, since  $f$  box-expands by  $L$  we can conclude  $\mathcal{L}^n \geq L^n$ . But then  $\mathcal{L} \geq L$ .  $\square$

Thus, if we could simply compute the average cycle multiplier for each simple cycle, and note whether it is larger than 1, we could conclude the map was hyperbolic.

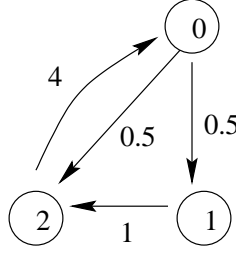


Figure 3.1: Graph illustrating Example 3.4.5

We might posit that we could efficiently compute the minimum average cycle multiplier by considering best paths, as we would if simply trying to compute the smallest cycle multiplier. Unfortunately, it seems necessary to compute the average cycle multiplier along **all** of the simple cycles in order to find the minimum.

**Definition 3.4.4.** If  $B_0, \dots, B_n$  is a path in the graph  $\Gamma'$ , then the *path multiplier* is the product  $\lambda_0 \cdots \lambda_{n-1}$ , and the *average path multiplier* is the  $n$ -th root of the path multiplier.

Thus we ask: If  $P_{k,j}$  is the path from  $B_k$  to  $B_j$  with the smallest average path multiplier of all paths from  $B_k$  to  $B_j$ , does the cycle containing a path from  $B_k$  to  $B_j$  with the smallest average multiplier contain the path  $P_{k,j}$ ? If this were true, we could use it as a shortcut to compute the minimum average cycle multiplier. However, the “average” prevents this shortcut from working.

**Example 3.4.5.** Consider the graph with three vertices  $\{0, 1, 2\}$ , and with the four edges  $\{(0, 1), (1, 2), (0, 2), (2, 1)\}$ , shown in Figure 3.1. It has two cycles:  $0 \rightarrow 1 \rightarrow 2 \rightarrow 0$  and  $0 \rightarrow 2 \rightarrow 0$ . Suppose the vertex multipliers are:  $\lambda_0 = 0.5, \lambda_1 = 1, \lambda_2 = 4$  (as shown).

Comparing paths from vertex 0 to vertex 2, we see  $\lambda_0 = 1/2 < (\lambda_0 \lambda_1)^{1/2} = 1/\sqrt{2}$ . So the smallest average path multiplier is along the path  $0 \rightarrow 2$ . However, comparing average cycle multipliers we get  $(\lambda_0 \lambda_2)^{1/2} = \sqrt{2} > (\lambda_0 \lambda_1 \lambda_2)^{1/3} = 2^{1/3}$ . Thus the smallest average cycle multiplier is along the cycle  $0 \rightarrow 1 \rightarrow 2 \rightarrow 0$ . Thus we must compute the average cycle multiplier along every simple cycle, and not take shortcuts with paths.

*Remark.* A simple combinatorial argument shows that the number of simple cycles in a graph (even a sparse graph) is exponential in  $N$ , the number of vertices in the graph. Example 3.4.5 suggests that an algorithm to compute the smallest average cycle multiplier in a graph will have to compute the average cycle multiplier for each simple cycle separately.

To suggest the difficulty of running an exponential-time algorithm, consider an example of a sparse graph with bound on out-degree  $d = 5$ , and  $N = 10^5$  vertices (which is a size *Hypatia* must work with for even the most simple maps). Thus the

graph has  $5^{(10^5)} \approx 10^{25}$  cycles. Suppose the computer can perform a billion ( $10^9$ ) operations per second (this is reasonable for present-day computers). Then if we could examine each cycle in just one operation, it would take:  $\frac{10^{25}}{10^9 \times 60 \times 60 \times 24 \times 365} \approx 300,000$  years!

### 3.4.2 An approximate, efficient solution

In order to determine a good value for  $L$ , we need a good starting guess. We have a lower bound of 1 for  $L$ .

For a polynomial map  $f$ , the *Lyapunov exponent*  $\lambda$  measures the rate of growth of tangent vectors to  $J$  under iteration. A description of the one-variable case is given in [59].

**Theorem 3.4.6** ([15, 49]). *For a polynomial map  $f$  of  $\mathbb{C}$  of degree  $d > 1$ ,  $\lambda \geq \log d$ , with equality iff  $J$  is connected.*

This theorem implies that for degree 2 maps with connected Julia sets,  $L = 2$  is an upper bound.

One straightforward way to obtain good values for  $L$  in some preset number of steps  $M$  is a basic **Bisection** method. Keep track of  $\text{lo}L$ , the most recent working  $L$ , and  $\text{hi}L$ , the most recent failing  $L$ . Then lower  $L$  halfway to  $\text{lo}L$  when box-expansion fails, and raise it halfway to  $\text{hi}L$  when it succeeds. Start with  $\text{lo}L = 1$  and  $\text{hi}L = 2$ . shows that  $L = 2$  is the upper bound for expansion on the unstable directions).

The bisection process is described in detail in pseudo-code in Appendix B, as Algorithm B.0.2.

An alternative to straight bisection is to utilize the information that *Hypatia* already discovers in a test for box-expansion. Indeed, if box-expansion fails for some  $L$ , then we realized in Proposition 3.4.3 that it is due to a cycle with average multiplier  $L'$  less than  $L$ . But we can easily adapt the algorithm **fExpands** to compute and return the average multiplier of this bad cycle,  $L'$ . Then if  $L' \leq 1$ , we know the map is not box-expansive on  $\Gamma'$  and we can stop. Otherwise, on the next pass instead of lowering by some arbitrary amount we may simply test by this new average multiplier  $L'$ . Better yet, we can test by the minimum of  $L'$  and  $L$  minus some preset step size  $\delta$ , in order to prevent increasingly small steps down. Appendix B contains the pseudo-code for this improved algorithm, **CheckCycles**, and a slightly modified **fExpands**, both listed under Algorithm B.0.3. In case of failure to show expansion, **fExpands** stores the vertices in the bad cycle and computes the average cycle multiplier.

Thus we can use this to quickly find within  $\delta$  of the largest  $L$  for which  $f$  is box-expansive. Indeed, we showed in Section 3.4.1 that finding the exact largest  $L$  for which  $f$  is box-expansive on a given graph seems to be an exponential-time problem. However here we find that we can get to within a preset approximation of the best  $L$  in a reasonable number of steps, as we did with the bisection method.

**Proposition 3.4.7.** *Let  $\mathcal{L}$  be the minimum average multiplier over all simple cycles in the graph  $\Gamma'$ . If  $2 \geq \mathcal{L} > 1 + \delta$ , then the method **CheckCycles** shows box-expansion by some  $L$  within  $\delta$  of  $\mathcal{L}$ , in (probably a lot fewer than)  $1/\delta$  trials of **fExpands**.*

*Proof.* Since we are looking for an expansion amount in the interval  $[1, 2]$ , and decrease by at least  $\delta$  at each step, we perform at most  $1/\delta$  attempts. Suppose one of these attempts is successful. That is, suppose  $\Gamma'$  fails to box-expand by some  $L_0 \leq 2$ , and thus outputs an average cycle multiplier of  $L_1 < L_0$ . Since  $\mathcal{L}$  is the minimum,  $\mathcal{L} \leq L_1$ . Suppose *Hypatia* verifies successfully box-expansion by  $L = \min\{L_1, L_0 - \delta\}$ . Then by Lemma 3.2.1 we have  $\mathcal{L} \geq L$ . Thus we have:

$$L_0 > L_1 \geq \mathcal{L} \geq L = \min\{L_1, L_0 - \delta\}.$$

Thus, either we were very lucky and  $\mathcal{L} = L_1$  and we have shown box-expansion by exactly that amount, or  $L_0 > L_1 > \mathcal{L} \geq L_0 - \delta$  and we have shown expansion by  $L_1$  within  $\delta$  of  $\mathcal{L}$ .  $\square$

*Remark.* In actually running *Hypatia*, we of course cannot compute exactly the average multiplier of a cycle, due to round-off error. We use interval arithmetic (described in Appendix A) to “round down”, and set

$$L_1 = \text{Inf}([\lambda_0, \lambda_0] \cdots [\lambda_{n-1}, \lambda_{n-1}])^{1/n}.$$

So, we use a number just slightly less than the average cycle multiplier to try and show box-expansion.

Another note on the actual implementation, due to the recursive nature it is easy for a bad choice of  $L$  to lead to constants which are so large or small that the machine cannot distinguish them from 0 or  $\infty$ . Checks must be put in place in the algorithms to flag such occurrences.

### 3.5 Building a better metric

In Section 3.4 we showed how to optimally (but perhaps in exponential time) determine the best expansion amount, and how to approximately (and in bounded time) determine a good expansion amount. That is the limit of what we can do to improve the metric using only one expansion constant  $L$ .

However, suppose the minimum average cycle multiplier in the graph  $\Gamma'$  is  $\mathcal{L}$ , but there is some other separate cycle in the graph with average cycle multiplier  $\mathcal{L}' \gg \mathcal{L}$ . Then using the basic algorithm, we would set all the constants based on some  $L$  close to  $\mathcal{L}$ . So just as in Example 3.4.1, we get constants plummeting to small values along the cycle with the large average multiplier. Ignoring any interaction between the two cycles for the moment, we could have defined better metric constants by using the better expansion,  $\mathcal{L}'$ , along the appropriate cycle.

In this section we explore optimal (yet impractical) and approximate (and reasonable) ways to build better metric constants by carefully determining an appropriate expansion amount for each edge, rather than setting all the metric constants based on the same  $L$ .

### 3.5.1 An optimal, yet very impractical solution

Our search for an optimal metric begins by realizing that for a cycle with the average multiplier  $\mathcal{L}$ , there is only one way to set the metric constants (up to scaling) to get expansion on each edge by precisely  $\mathcal{L}$ .

**Lemma 3.5.1.** *Suppose  $B_0, \dots, B_n = B_0$  is a cycle in the graph  $\Gamma'$  with average cycle multiplier  $\mathcal{L}$ . Then for a given  $c_0$ , setting  $c_k = \mathcal{L}c_{k-1}/\lambda_{k-1}$ ,  $1 \leq k \leq n-1$ , gives expansion by  $\mathcal{L}$  on every edge in the cycle.*

*Proof.* The constants were set to force expansion by  $\mathcal{L}$  on edges  $0 \rightarrow 1, \dots, n-1 \rightarrow n-2$ . But then we automatically get expansion by precisely  $\mathcal{L}$  on edge  $n-1 \rightarrow n=0$ , since

$$\frac{\mathcal{L}c_{n-1}}{\lambda_{n-1}} = \frac{(\mathcal{L})^2c_{n-2}}{\lambda_{n-1}\lambda_{n-2}} = \dots = \frac{(\mathcal{L})^nc_0}{\lambda_{n-1}\cdots\lambda_0} = c_0,$$

by definition of average cycle multiplier  $\mathcal{L} = (\lambda_{n-1}\cdots\lambda_0)^{1/n}$ .  $\square$

Thus if we want to set metric constants to optimize the expansion along the edges, we see that we must start with the cycle in the graph with the smallest average cycle multiplier,  $\mathcal{L}$ . Once the metric is set along the vertices of this cycle, to proceed our basic approach is to find a path in the graph which begins and ends on the cycle, called a “handle”, and define the metric on the vertices in the handle.

Realize that this handle forms a new cycle, using part of the first cycle. This new cycle has a larger average multiplier  $\mathcal{L}'$ . If we were to use the previous algorithm, and set the metric on the new boxes in the handle using  $\mathcal{L}$ , then the metric is set to get expansion by  $\mathcal{L}$  across every edge in this new cycle, except for the last one. On that last edge, with this metric the expansion is going to be large, because it absorbs the extra expansion not used on the other handle edges. To fix this, we would like to set the metric on the handle to get a uniform expansion. The key to understanding how to set the metric on a handle is the following.

**Definition 3.5.2.** If  $B_0, \dots, B_n$  is a path in the graph  $\Gamma'$ , and the metric constants  $c_0$  and  $c_n$  are set, then the *relative path multiplier* is  $(\lambda_0\cdots\lambda_{n-1}c_n/c_0)^{1/n}$ .

This definition makes sense because if the metric is set all along the path  $B_0, \dots, B_n$ , then the multiplier along the path is

$$\lambda_0 \frac{c_0}{c_1} \lambda_1 \frac{c_1}{c_2} \cdots \lambda_{n-1} \frac{c_{n-1}}{c_n} = \lambda_0 \cdots \lambda_{n-1} \frac{c_n}{c_0}.$$

Thus we see immediately that the relative path multiplier is exactly what is needed to define a metric along a path with constant expansion, and we get, parallel to Lemma 3.5.1:

**Lemma 3.5.3.** *Suppose  $B_0, \dots, B_n$  is a path in the graph  $\Gamma'$ , and the metric constants  $c_0$  and  $c_n$  have been determined. Let  $L'$  be the corresponding relative path multiplier. Then  $c_1, \dots, c_{n-1}$  defined by  $c_k = L'c_{k-1}/\lambda_{k-1}, 1 \leq k \leq n-1$  yield a metric under which the map expands by  $L'$  along every edge in the path.*

*Proof.* The constants were defined to force expansion by  $L'$  on the edges  $B_0 \rightarrow B_1, \dots, B_{n-2} \rightarrow B_{n-1}$ . We need only check edge  $B_{n-1} \rightarrow B_n$ . But we see that

$$\frac{L'c_{n-1}}{\lambda_{n-1}} = \frac{(L')^2c_{n-2}}{\lambda_{n-1}\lambda_{n-2}} = \dots = \frac{(L')^nc_0}{\lambda_{n-1}\dots\lambda_0} = c_n,$$

since by definition of the relative path multiplier,  $L' = (\lambda_0 \dots \lambda_{n-1}c_n/c_0)^{1/n}$ .  $\square$

In order to build an “optimal” metric, at each step, we want to set the metric so that the expansion on each edge is the maximum possible, given the metric set so far. The following inductive algorithm is a way to achieve this type of goal. However, since it requires performing a task similar to finding the minimum average cycle multiplier in a graph several times, it is perhaps an exponential algorithm. We first demonstrate that this ideal algorithm is desirable, then later use it to develop an approximate and feasible algorithm. We do not write the following in pseudo-code since we are uninterested in coding this, but instead in a style more conducive to theoretical study.

**Algorithm 3.5.4. BestMetric( $\Gamma'$ ):**

**Step 1:** Find the simple cycle in the graph  $\Gamma'$  with the smallest average cycle multiplier  $\mathcal{L}$ . Define  $L_1 = \mathcal{L}$ . Pick an arbitrary box in the cycle, and set its metric constant to 1. Define the rest of the metric on the cycle to achieve each edge expansion exactly  $L_1$  (as in Lemma 3.5.1). Let  $V_1$  be the set of boxes in this first cycle.

**Step  $N \geq 2$ :** The input is a subset of boxes  $V_{N-1}$  which have metric constants set on them. If  $V_{N-1}$  does not contain all of the vertices of  $\Gamma'$ , find the handle with least relative path multiplier, with respect to  $V_{N-1}$ . That is, find the handle  $\mathcal{H}_N = (B_0 \rightarrow B_1 \rightarrow \dots \rightarrow B_k)$  such that  $B_0, B_k \in V_{N-1}$  but  $B_1, \dots, B_{k-1} \notin V_{N-1}$ , with the smallest relative path multiplier. Note one cannot just consider simple handles to get everything. Set  $L_N$  equal to this smallest relative path multiplier. Since  $c_0$  is defined, set  $c_j = L_Nc_{j-1}/\lambda_{j-1}, 1 \leq j \leq k-1$ . Define  $V_N = V_{N-1} \cup \{B_0, \dots, B_k\}$ .

We show this process successfully builds a metric which is expanding on every edge in the graph by at least the original minimum average cycle multiplier, precisely because of the careful order in which the constants were set.

**Proposition 3.5.5.** *Given a graph  $\Gamma'$  with smallest average cycle multiplier  $\mathcal{L}$ , the algorithm **BestMetric** builds a metric under which the map is expanding on every edge by at least  $\mathcal{L}$ . Specifically, the algorithm builds, in some number  $M$  steps, a metric in which the map expands each edge by one of  $\mathcal{L} = L_1 \leq L_2 \leq \dots \leq L_M$ .*

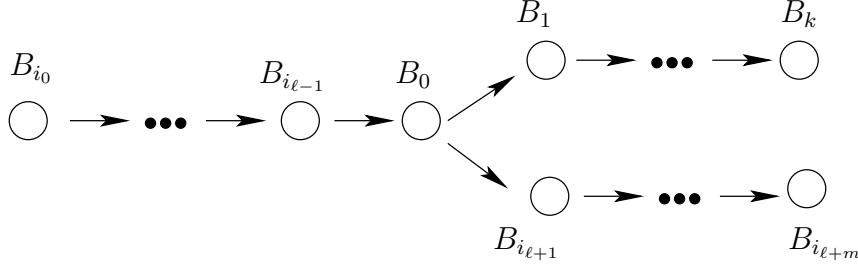


Figure 3.2: Diagram illustrating proof of Proposition 3.5.5

*Proof.* The proof is by induction. Lemma 3.5.1 shows that we can define the metric constants on the cycle in Step 1. Now suppose we have successfully performed Step  $N - 1$  and we are working on Step  $N$ . We find the handle  $\mathcal{H}_N = (B_0 \rightarrow B_1 \rightarrow \cdots \rightarrow B_k)$  such that  $B_0, B_k \in V_{N-1}$  but  $B_1, \dots, B_{k-1} \notin V_{N-1}$ , with the smallest relative path multiplier  $L_N = (\lambda_0 \cdots \lambda_{k-1} c_k / c_0)^{1/k}$ . We need to show  $L_N \geq L_{N-1}$ . We have a few cases here, depending on whether  $B_0$  and/or  $B_k$  are in  $V_{N-2}$ . (In case  $N = 2$ , consider  $V_{N-2} = \emptyset$ ).

**Case 1:** The easy case is when both  $B_0$  and  $B_k$  are in  $V_{N-2}$ . Then both  $c_0$  and  $c_k$  were defined at the start of Step  $N - 1$ , so in that step  $\mathcal{H}_N$  was an existing handle, and since it was not the minimum,  $L_{N-1} \leq L_N$ .

**Other Cases:** If one or both of  $B_0$  and  $B_k$  were not in  $V_{N-2}$ , then since  $B_0$  and  $B_k$  are in  $V_{N-1}$ , on Step  $N - 1$  the handle  $\mathcal{H}_N$  was not a separate handle, but part of some handle  $\mathcal{H}'$  which overlapped  $\mathcal{H}_{N-1}$ . Notationally, there are three cases: (1)  $B_0, B_k \notin V_{N-2}$ , (2)  $B_0 \in V_{N-2}, B_k \notin V_{N-2}$ , and (3)  $B_0 \notin V_{N-2}, B_k \in V_{N-2}$ . However they are all based on the same ideas, so we just demonstrate (3).

Suppose  $B_0 \notin V_{N-2}$  and  $B_k \in V_{N-2}$ . Then  $\mathcal{H}_{N-1} = (B_{i_0} \rightarrow \cdots \rightarrow B_{i_{\ell-1}} \rightarrow B_{i_\ell} = B_0 \rightarrow B_{i_{\ell+1}} \rightarrow \cdots \rightarrow B_{i_{\ell+m}})$ , where the only box shared by  $\mathcal{H}_N$  and  $\mathcal{H}_{N-1}$  is  $B_0$ , and  $\mathcal{H}' = (B_{i_0} \rightarrow \cdots \rightarrow B_{i_\ell} = B_0 \rightarrow B_1 \rightarrow \cdots \rightarrow B_k)$  is formed by the first part of  $\mathcal{H}_{N-1}$  attached to  $\mathcal{H}_N$ . See Figure 3.2.

Let  $L'$  be the relative path multiplier of  $\mathcal{H}'$  from Step  $N - 1$ . Then  $L' \geq L_{N-1}$ .

Now during Step  $N - 1$ , we defined the metric constants  $c_{i_1}, \dots, c_{i_{\ell-1}}, c_0$  based on  $L_{N-1}$ . Hence,

$$c_0 = \frac{L_{N-1} c_{i_{\ell-1}}}{\lambda_{i_{\ell-1}}} = \cdots = \frac{(L_{N-1})^\ell c_{i_0}}{\lambda_{i_0} \cdots \lambda_{i_{\ell-1}}}.$$

But then by definition of relative path multiplier, we have

$$(L_N)^k = \lambda_0 \cdots \lambda_k \frac{c_k}{c_0} = \lambda_0 \cdots \lambda_k c_k \frac{\lambda_{i_0} \cdots \lambda_{i_{\ell-1}}}{(L_{N-1})^\ell c_{i_0}} = \frac{(L')^{\ell+k}}{(L_{N-1})^\ell} \geq (L_{N-1})^k.$$

Hence,  $L_N \geq L_{N-1}$ .

Thus by induction, we can successfully define a metric in some number of steps  $M$ , in which the map expands each edge by one of  $\mathcal{L} = L_1 \leq L_2 \leq \cdots \leq L_M$ .  $\square$

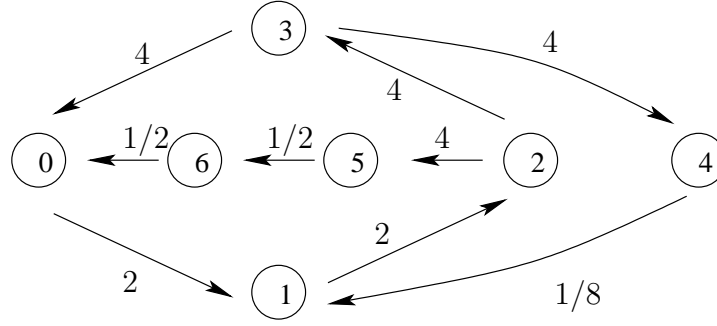


Figure 3.3: Graph, with box multipliers, for Examples 3.5.6, 3.5.7, and 3.5.8

Below is an example of setting the metric constants using **BestMetric**.

**Example 3.5.6.** Consider the graph shown in Figure 3.3, with six vertices  $V = \{0, 1, 2, 3, 4, 5, 6\}$ , and edges

$$E = \{(0, 1), (1, 2), (2, 3), (2, 5), (3, 0), (3, 4), (4, 1), (5, 6), (6, 0)\}.$$

Suppose the vertex multipliers are (as shown):  $\lambda_0 = 2, \lambda_1 = 2, \lambda_2 = 4, \lambda_3 = 4, \lambda_4 = 1/8, \lambda_5 = 1/2, \lambda_6 = 1/2$ .

There are three cycles, with average cycle multipliers,

$$\begin{aligned} \mathcal{L} &= (\lambda_0 \lambda_1 \lambda_2 \lambda_5 \lambda_6)^{1/5} = 2^{2/5}, \\ \mathcal{L}' &= (\lambda_1 \lambda_2 \lambda_3 \lambda_4)^{1/4} = 2^{1/2}, \text{ and} \\ \mathcal{L}'' &= (\lambda_0 \lambda_1 \lambda_2 \lambda_3)^{1/4} = 2^{3/2}. \end{aligned}$$

Since  $\mathcal{L} < \mathcal{L}' \ll \mathcal{L}''$ , we expect that the optimal solution would prescribe setting the constants first on the weak cycle  $0 \rightarrow 1 \rightarrow 2 \rightarrow 5 \rightarrow 6 \rightarrow 0$ , then the handle  $2 \rightarrow 3 \rightarrow 4 \rightarrow 1$ , and finally the handle  $3 \rightarrow 0$ .

We set  $c_0 = 1, c_1 = \mathcal{L}c_0/\lambda_0 = 2^{-3/5}, c_2 = \mathcal{L}c_1/\lambda_1 = 2^{-6/5}, c_5 = \mathcal{L}c_2/\lambda_2 = 2^{-14/5}, c_6 = \mathcal{L}c_5/\lambda_5 = 2^{-7/5}$ , using the weakest cycle first.

Now there are two handles to choose from. The handle  $2 \rightarrow 3 \rightarrow 4 \rightarrow 1$  has relative path multiplier  $(\lambda_2 \lambda_3 \lambda_4 c_1 / c_2)^{1/3} = 2^{8/15}$ , and the handle  $2 \rightarrow 3 \rightarrow 0$  has relative path multiplier  $(\lambda_2 \lambda_3 c_0 / c_2) = 2^{13/5}$ . So the handle with the smallest relative path multiplier. is the former. Set  $P' = 2^{8/15}$ , and  $c_3 = P'c_2/\lambda_2 = 2^{-8/3}$  and  $c_4 = P'c_3/\lambda_3 = 2^{-62/15}$ .

Last we find handle  $3 \rightarrow 0$  has relative path multiplier  $P'' = (\lambda_3 c_0 / c_3) = 2^{14/3}$ . See Figure 3.4.

Thus we have built a metric with edge expansions of  $\mathcal{L} \approx 1.32, P' \approx 1.45$ , and  $P'' \approx 25.4$ .

This algorithm may well be exponential time, for the basic reason that the algorithm just to find the cycle with the minimum average multiplier seems it should take exponential time. Each attempt to find the handle with the next largest relative multiplier is similarly difficult.

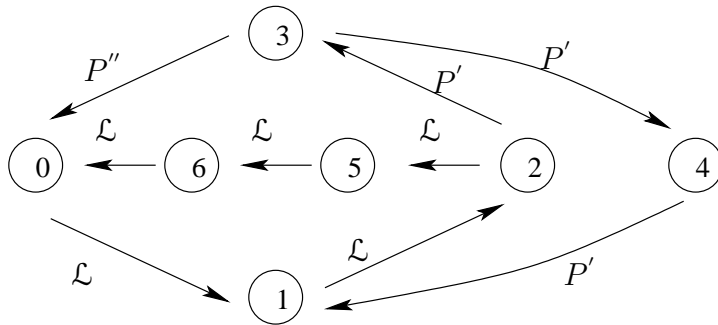


Figure 3.4: Graph with optimal edge expansion.

### 3.5.2 An approximate, realistic solution

Since setting optimal metric constants is computationally not feasible, we wish to find an algorithm which is an approximation.

A first idea would be to try setting constants along a random cycle and its handles in a random order, then when an obstruction is found (*i.e.*, a handle with relative path multiplier less than one, or maybe less than the original cycle multiplier), start over with a new cycle containing that weak path. However the following example illustrates that, even if the weakest cycle is selected first, with no way to order the handles a solution cannot easily be found.

**Example 3.5.7.** Consider the graph of Example 3.5.8, shown in Figure 3.3. Suppose we are lucky and detect first the weakest cycle,  $0 \rightarrow 1 \rightarrow 2 \rightarrow 5 \rightarrow 6 \rightarrow 0$ , with  $\mathcal{L} = 2^{2/5}$ , and as in Example 3.5.6 set  $c_0 = 1, c_1 = \mathcal{L}c_0/\lambda_0 = 2^{-3/5}, c_2 = \mathcal{L}c_1/\lambda_1 = 2^{-6/5}, c_5 = \mathcal{L}c_2/\lambda_2 = 2^{-14/5}c_2 = \mathcal{L}c_5/\lambda_5 = 2^{-7/5}$ .

But, suppose we next detect the wrong handle:  $2 \rightarrow 3 \rightarrow 0$ . Then the relative path multiplier is  $L'' = (\lambda_2\lambda_3c_0/c_2)^{1/2} = 2^{13/5}$ . So we set  $c_3 = L''c_2/\lambda_2 = 2^{-3/5}$ .

Then lastly we detect the handle  $3 \rightarrow 4 \rightarrow 1$ . The relative path multiplier is then  $L' = (\lambda_3\lambda_4c_1/c_3)^{1/2} = 2^{-1/2} < 1$ . Unfortunately, we have a relative path multiplier less than one. See Figure 3.5.

Our strategy is that we should try to start over with a cycle involving this bad path, say  $1 \rightarrow 2 \rightarrow 3 \rightarrow 4 \rightarrow 1$ , and set  $c_1 = 1, c_2 = \mathcal{L}'c_1/\lambda_1 = 2^{-1/2}, c_3 = \mathcal{L}'c_2/\lambda_2 = 2^{-2}, c_4 = \mathcal{L}'c_3/\lambda_3 = 2^{-7/2}$ .

But suppose we are very unlucky again and detect the handle  $3 \rightarrow 0 \rightarrow 1$  first. It has a relative path multiplier of  $M'' = (\lambda_3\lambda_0c_1/c_3)^{1/2} = 2^{5/2}$ . So we set  $c_0 = M''c_3/\lambda_3 = 2^{-3/2}$ .

Then lastly we detect the handle  $2 \rightarrow 5 \rightarrow 6 \rightarrow 0$ . The relative path multiplier is then  $M' = (\lambda_2\lambda_5\lambda_6c_0/c_2)^{1/3} = 2^{-1/3} < 1$ . See Figure 3.6.

But if we take a cycle containing this bad handle, that is cycle  $0 \rightarrow 1 \rightarrow 2 \rightarrow 0$ , and we are back where we started at the beginning of the example.

Thus we cannot just go about setting constants on cycles and handles in a

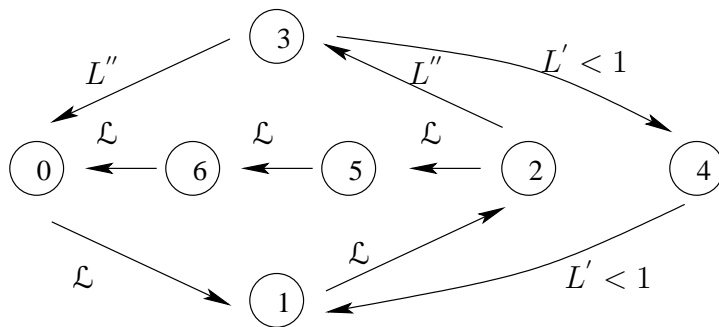


Figure 3.5: Graph with badly guessed edge expansion.

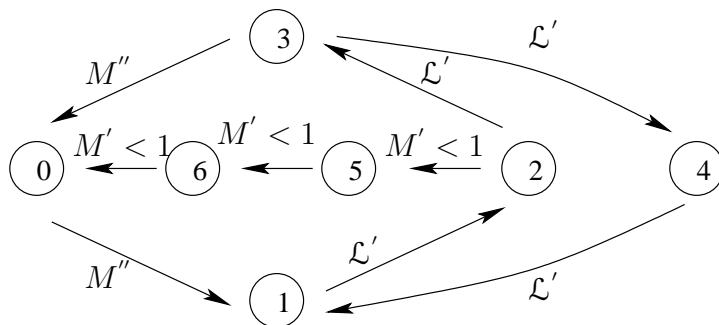


Figure 3.6: Graph illustrating another way of badly guessing edge expansion.

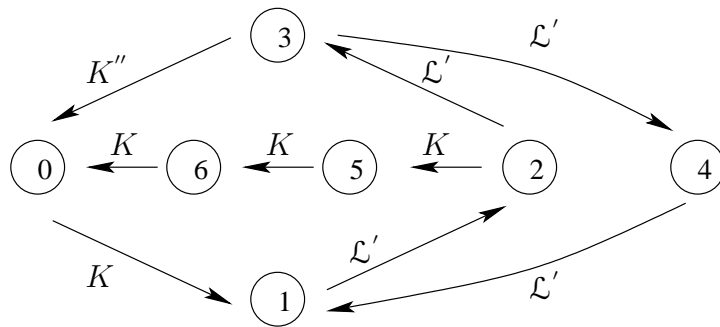


Figure 3.7: Graph illustrating a good way of guessing edge expansion.

random order. But really this failed because the cycle multiplier of one of the cycles was much larger than the other two, forcing one handle to have much larger average multiplier than the other. In fact, the example below shows that for this particular graph, if we had set the constants on the weaker two cycles in either order, and then set the constants on the stronger cycle, we could have successfully defined a metric.

**Example 3.5.8.** Consider again the graph of Figure 3.3, with the same box multipliers, and cycles of multipliers  $\mathcal{L} < \mathcal{L}' \ll \mathcal{L}''$ . Suppose we start with the cycle of multiplier  $\mathcal{L}' = 2^{1/2}$ , cycle  $1 \rightarrow 2 \rightarrow 3 \rightarrow 4 \rightarrow 1$ , and set  $c_1 = 1, c_2 = \mathcal{L}'c_1/\lambda_1 = 2^{-1/2}, c_3 = \mathcal{L}'c_2/\lambda_2 = 2^{-2}, c_4 = \mathcal{L}'c_3/\lambda_3 = 2^{-7/2}$ .

Then suppose we next detect the handle  $2 \rightarrow 5 \rightarrow 6 \rightarrow 0 \rightarrow 1$ , with relative path multiplier  $K = (\lambda_2\lambda_5\lambda_6\lambda_0c_1/c_2)^{1/4} = 2^{3/8}$ , and set  $c_5 = Kc_2/\lambda_2 = 2^{-17/8}, c_6 = Kc_5/\lambda_5 = 2^{-3/4}, c_0 = Kc_6/\lambda_6 = 2^{1/8}$ .

Then we would lastly detect the handle  $3 \rightarrow 0$ , and find its relative path multiplier is  $K'' = (\lambda_3c_0/c_3) = 2^{33/8} > 1$ . See Figure 3.7.

Thus we have a metric with edge expansions of  $\mathcal{L}' \approx 1.4, K \approx 1.297$ , and  $K'' \approx 17.5$ . Note this minimum expansion is smaller than that of Example 3.5.6, in which the cycles and paths were set in the optimal order.

This last example suggests that if we define the metric on cycles and handles in approximately the right order, then we are likely to be successful. We next describe an algorithm **BetterMetric** to do just that. Again we take advantage of the fact that when the basic algorithm **fExpands** fails to show box-expansion by some  $L'$ , it produces a cycle, *badcycle* with average multiplier  $L$  less than  $L'$ . In this way we can detect cycles with average multipliers less than a given amount.

We first run the algorithm **CheckCycles**, which repeatedly calls *fExpands* to find approximately the largest  $L$  for which the map is box-expansive for  $\Gamma'$ , and a cycle *badcycle* of boxes with average multiplier less than  $L + \delta$  (where  $\delta$  was some preset minimum step size). We know then that  $L$  is close to the maximum expansion amount we could hope to use along that cycle. So, we mark the edges  $(u, v)$  along *badcycle* with the expansion amount  $L_0 = L$ . Then run a slightly

modified **fExpands** with  $L_1 = L + \delta$ , trying to build a metric in which the map box-expands by  $L_1$  on every edge in the graph *except* the marked edges, and using  $L_0$  as an expansion amount on those edges. If this fails, it produces another cycle (possibly attached to the first) with average multiplier less than  $L_1$ . So, mark the edges on that cycle with  $L_0$  and repeat. Each time start from scratch building a metric, using  $L_0$  on edges marked with  $L_0$ , and  $L_1$  on the rest. Eventually, we have successfully built a metric using expansion by  $L_0$  on some edges, and  $L_1$  on the rest (or in the extreme case, if  $L_1$  is really too large, we may have marked  $L_0$  on all the edges, but this is unlikely).<sup>1</sup>

Next, try to build a metric expanding by  $L_2 = L_1 + \delta$  on edges not marked, and by  $L_0$  on marked edges. If this fails, we know since the previous step worked that it produces a cycle with average multiplier between  $L_2$  and  $L_1$ . So, mark the edges in that cycle, which are not already marked with  $L_0$ , with expansion amount  $L_1$  (so it may be marking a cycle or a handle).

Continue as above, with some cycles marked from the first round with  $L_0$ , adding more cycles which need to be marked with  $L_1$ , until a metric is successfully built with a combination of  $L_0, L_1, L_2$ . Repeat this process with  $L$ 's increasing by  $\delta$  for some preset number of steps, or until all the edges are marked with a maximum expansion amount. In the end, a metric is built with edge expansions by  $L, L + \delta, L + 2\delta, \dots, L + m\delta$ . Our intuition suggests that such a metric is closer to euclidean than a metric using only one  $L$ , and in fact we demonstrate evidence of this collected by running this algorithm on  $z^2 + c$  in Section 3.6.

The detailed pseudo-code for the algorithm **BetterMetric** is in Appendix B, as Algorithm B.0.4.

## Selective subdivision

Another use of this algorithm, besides improving the metric on the given graph, is to determine another selective subdivision procedure (in addition to those already described in Section 2.3). After **BetterMetric** is run, the boxes involved in edges with edgeL set at  $L_0$  can be chosen to be subdivided. These are the boxes involved in the weakest cycles, and so subdividing them should help improve the expansion amounts. The results of this on some examples are discussed in Section 3.6 and Section 4.4.3.

## 3.6 Examples of running *Hypatia* for polynomial maps

In this section, we give data and pictures on the results of running *Hypatia* on some examples for  $P_c(z) = z^2 + c$  and  $P_{c,a}(z) = z^3 - 3a^2z + c$ , using first just

---

<sup>1</sup>Actually, we often want the step size for  $L$ -increases smaller than the step size used in **CheckCycles** for  $L$ -decreases, so we modify the algorithm to not use the very first bad cycle.



Figure 3.8: A box cover of  $\mathcal{R}$  ( $= J$  and period 2 sink) for  $P_c$ ,  $c = -1$ , for a  $2^7 \times 2^7$  grid. Different s.c.c.'s are in different shades of gray. Note the s.c.c.'s, skirting the inner edge of the cover of  $J$ . These will disappear when the box size is decreased.  $P_c$  is box-expansive on the cover of  $J$ .

the basic algorithm for box-expansion. We also describe one example of using the improvement to build a better metric, for  $z^2 - 1$ .

### Examples for $z^2 + c$

All of these examples have  $|c| < 2$ , so we used as the initial box  $V = \mathcal{N}_\infty(0, 2.1)$ . Also, we used the method **CheckCycles**, of Section 3.4.2, to try to show box-expansion in each case.

### Connected, Star-like Julia Sets

**Example 3.6.1.** The quadratic polynomial for  $c = -1$  is called the basilica. This map has a period 2 attracting cycle  $0 \leftrightarrow -1$ . Shown in Figure 3.6 is a box cover  $\mathcal{V}'$  of the chain recurrent set, composed of selected boxes from a  $2^7 \times 2^7$  grid in  $V$ . Each s.c.c. of the graph  $\Gamma$  is shown in a different color (shade of gray). The s.c.c. covering the Julia set is a graph with 1,800 boxes and 14,000 edges (*i.e.*,  $B = 1,800, E = 14,000$ ). This cover is box-expansive (by 1.14067). The computation took only 8 MB of RAM and less than a minute of CPU time, which is very manageable given that our equipment had 4 GB of RAM.

**Example 3.6.2.** A map with a period 3 attracting cycle is  $c = -.123 + .745i$ , approximately the classic rabbit parameters. Shown in Figure 3.9 is a cover of boxes from a  $2^9 \times 2^9$  grid. The Julia set s.c.c. has  $B = 20,000, E = 180,000$ .

We found that the rabbit is box-expansive on this s.c.c. However, we could show hyperbolicity more efficiently for this map. At the  $2^8 \times 2^8$  grid, the Julia set

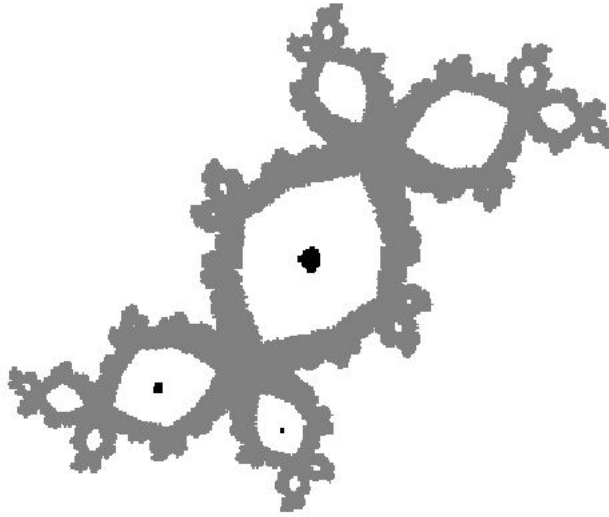


Figure 3.9: A box cover of  $\mathcal{R}$  ( $= J$  and period 3 sink) for  $P_c$ ,  $c = -.123+.745i$ , for a  $2^9 \times 2^9$  grid. Different s.c.c.'s are different shades of gray.  $P_c$  is box-expansive on the s.c.c. covering  $J$ .

s.c.c. fails to expand by  $L = 1$ , so we had *Hypatia* subdivide just the bad cycle from the  $L = 1$  check, which is only 12 vertices. Then we had a Julia set s.c.c. of size  $V = 8,000$ ,  $E = 71,000$  on which the map is also box-expansive, (by 1.00508)! Shown in Figure 3.10 is the  $2^8 \times 2^8$  cover.

**Example 3.6.3.** The map with  $c = -1.31$ , we call the double basilica, has a period 4 attracting cycle. Shown in Figure 3.11 is a cover of boxes from a  $2^{10} \times 2^{10}$  grid. The Julia set s.c.c. has  $B = 47,000$ ,  $E = 328,000$ . The double basilica is box-expansive (by 1.06758) on this cover.

All of the above basic examples in one dimension (*i.e.*, up to period 4 star-like Julia sets) finished computing their s.c.c.'s and verifying hyperbolicity in a small number of minutes, using less than 200 Megs of RAM.

**Example 3.6.4.** One of the five-eared rabbits,  $c = -.504 + .563i$ , with a period 5 attracting cycle, is shown in Figure 3.12. The box cover shown is from a  $2^{10} \times 2^{10}$  grid, and yields an s.c.c. graph with  $B = 95,000$ ,  $E = 842,000$ . The map is box-expansive (by 1.0264) on this grid. The computation used less than 200 Megs of RAM, but took about 250 minutes to verify box-expansion!

**Example 3.6.5.** A six-eared rabbit,  $c = .388 + .22i$ , naturally with a period 6 attracting cycle, is shown in Figure 3.13. The box cover shown is from a  $2^{11} \times 2^{11}$  grid, and yields an s.c.c. graph with  $B = 384,000$ ,  $E = 3,600,000$ .

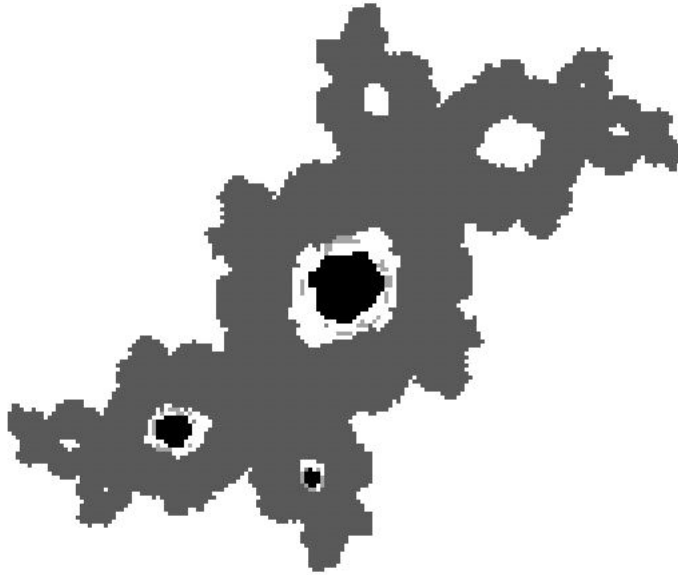


Figure 3.10: A box cover of  $\mathcal{R}$  for  $P_c, c = -.123 + .745i$ , for a  $2^8 \times 2^8$  grid. Subdivide 12 boxes and  $P_c$  is box-expansive on the resulting s.c.c. covering  $J$ .

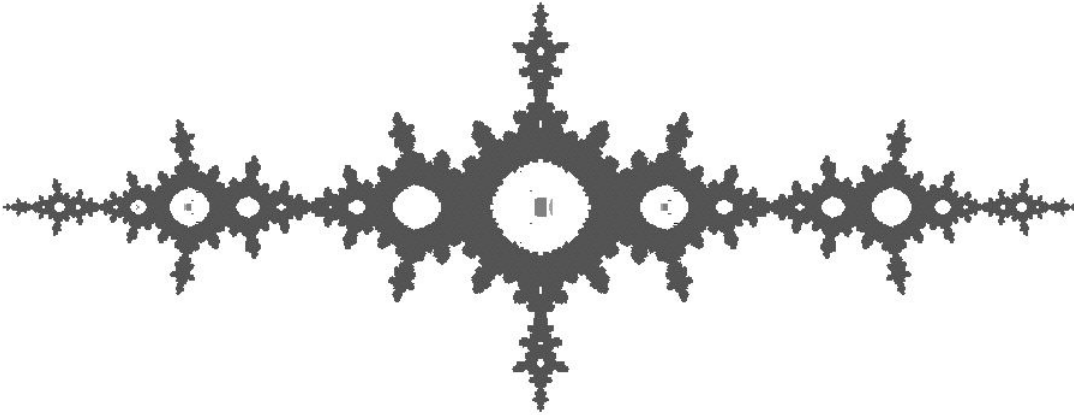


Figure 3.11: A box cover of  $\mathcal{R}$  ( $= J$  and a period 4 sink) for  $P_c, c = -1.31$ , for a  $2^{10} \times 2^{10}$  grid.  $P_c$  is box-expansive on this cover.

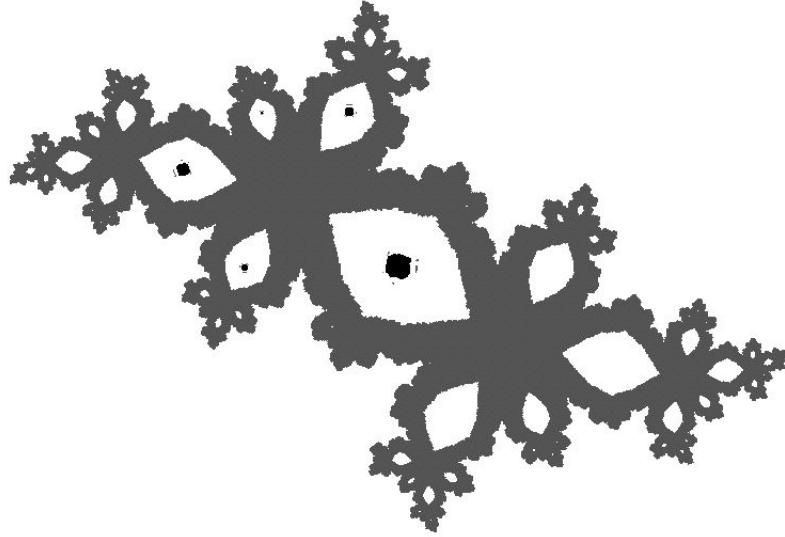


Figure 3.12: A box cover of  $\mathcal{R}$  ( $=J$  and a period 5 sink) for  $P_c$ ,  $c = -.504 + .563i$ , for a  $2^{10} \times 2^{10}$  grid.  $P_c$  is box-expansive on the cover of  $J$ .

This example suggests the limits of the basic algorithm. Uniform subdivision required a  $2^{11} \times 2^{11}$  grid in order to get separate s.c.c.'s for the Julia set and the sink, but the memory used was 1.6 GB, and we could not run the hyperbolicity testing. To get to this level took about 10 minutes.

### Connected Julia sets from baby Mandelbrot sets

**Example 3.6.6.** The aeroplane,  $c = -1.755$ , has a period 3 sink. Shown in Figure 3.14 is a box cover from a  $2^{11} \times 2^{11}$  grid, which forms an s.c.c. graph with  $B = 43,000$ ,  $E = 260,000$ . The map is box-expansive on this cover (by 1.05069). The computation took less than 200 MB of RAM and 6.5 minutes.

**Example 3.6.7.** The map with  $c = -.1588 + 1.033i$  has a period 4 sink. A box cover from a  $2^{13} \times 2^{13}$  grid is shown in Figure 3.15. The s.c.c. covering the Julia set is size  $B = 687,000$ ,  $E = 6,000,000$ .

This is another map which suggests the limits of the basic algorithm. Uniform subdivision required a  $2^{13} \times 2^{13}$  grid to resolve the sink from the Julia set, but this took 1.7 GB of RAM, leaving insufficient memory for a hyperbolicity test. The CPU time to get to this level is 13 minutes.

### Cantor Julia sets

The following examples, with Julia sets homeomorphic to the cantor set, were also computed using less than 200 MB of RAM in just a few minutes.



Figure 3.13: A box cover of  $J$  for  $P_c$ ,  $c = .388 + .22i$ , for a  $2^{11} \times 2^{11}$  grid. Insufficient memory for hyperbolicity test to be completed.

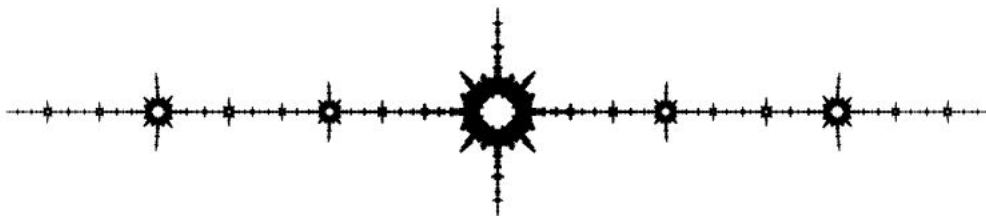


Figure 3.14: A box cover of  $J$  for  $P_c$ ,  $c = -1.755$ , for a  $2^{11} \times 2^{11}$  grid.  $P_c$  is box-expansive on this cover of  $J$ .

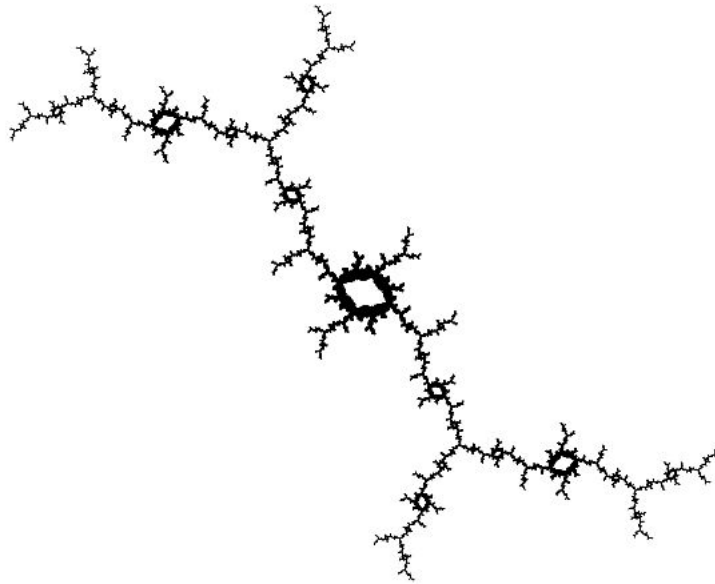


Figure 3.15: A box cover of  $J$  for  $P_c$ ,  $c = -.1588 + 1.033i$ , for a  $2^{13} \times 2^{13}$  grid. Insufficient memory for a hyperbolicity test.

**Example 3.6.8.** The map  $c = -.75 + .3i$  has a Cantor set for its Julia set, and is relatively close to the basilica. The box cover from a  $2^{10} \times 2^{10}$  grid, shown in Figure 3.6, yields a Julia set s.c.c. with  $B = 94,000$ ,  $E = 771,000$ . This cover is box-expansive (by 1.05303).

**Example 3.6.9.** A Cantor Julia set near the cusp of the Mandelbrot set is  $c = .3$ . Shown in Figure 3.6 is a box cover from a  $2^8 \times 2^8$  of size  $B = 16,000$ ,  $E = 150,000$ .

This is another example in which we used selective subdivision to show hyperbolicity quickly. The box cover from the  $2^8 \times 2^8$  grid fails to be box-expansive by  $L = 1$  due to a bad cycle of length 1! We had the program subdivide just that box, and again the resulting s.c.c. failed for  $L = 1$  due to a length 1 bad cycle. But, upon subdividing that one box, we found that the resulting s.c.c. is box-expansive (by 1.00469)!

Table 3.1 summarizes the information in these examples.



Figure 3.16: A box cover of  $J$ , for  $P_c$ ,  $c = -.75 + .3i$ , for a  $2^{10} \times 2^{10}$  grid.  $P_c$  is box-expansive on this cover.

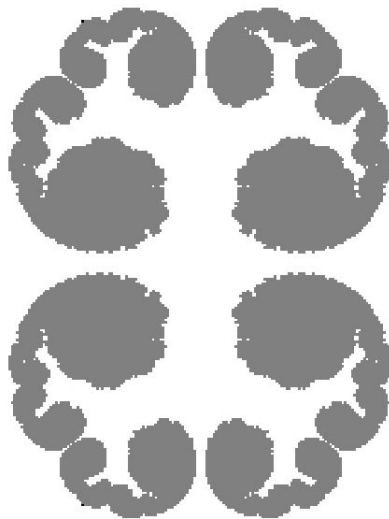


Figure 3.17: A box cover of  $J$  for  $P_c$ ,  $c = .3$ , for a (mostly)  $2^8 \times 2^8$  grid.  $P_c$  is box-expansive on this cover.

Table 3.1: Examples of running *Hypatia* for  $P_c(x) = x^2 + c$ .

Example	$c$	sink period	Figure	box size	boxes (1000s)	edges (1000s)	box- exp?	memory (MB)	time (min.)
3.6.1	-1	2	3.6	$4/2^7 = .03125$	1.8	14	Yes	< 200	< 5
3.6.2	$-.123 + .745i$	3	3.9	$4/2^9 = .008$	20	180	Yes	< 200	< 5
				3.10	$4/2^8 = .0156$ and $4/2^9$	8	71	Yes	< 200
3.6.3	-1.31	4	3.11	$4/2^{10} = .004$	47	328	Yes	< 200	< 5
3.6.4	$-.504 + .563i$	5	3.12	$4/2^{10}$	95	842	Yes	< 200	250
3.6.5	$.388 + .22i$	6	3.13	$4/2^{11} = .002$	384	3,600	N/A	1,600	10
3.6.6	-1.755	3	3.14	$4/2^{11}$	43	260	Yes	< 200	6.5
3.6.7	$-.1588 + 1.033i$	4	3.15	$4/2^{13} = .005$	687	6,000	N/A	1,700	13
3.6.8	$-.75 + .3i$	N/A	3.6	$4/2^{10}$	94	771	Yes	< 200	< 5
3.6.9	.3	N/A	3.6	$4/2^8$	16	150	No	< 200	< 5
				$4/2^8$ and $4/2^9$	16	150	Yes	< 200	< 5

## BetterMetric example

Now we will examine the effect of running the algorithm **BetterMetric** (described in Section 3.5.2) on the basilica ( $c = -1$ , Example 3.6.1). As mentioned previously, the box cover for the  $2^7 \times 2^7$  grid (of Figure 3.6), of size  $B = 1,784$ ,  $E = 13,856$ , is box-expansive for  $L_0 = 1.14067$  (found using **CheckCycles**, see Section 3.4.2). The associated metric has metric constants,  $c_k$ , with minimum 0.019, average 0.049, and maximum 1. To get a better idea of this metric, we had *Hypatia* create a picture of the box cover, with shading of each box according to the metric constant for that box. Figure 3.18 shows the ranges of constants for each shade, and Figure 3.19 shows the metric on this  $2^7 \times 2^7$  box cover formed using  $L_0$ . Red boxes have very small metric constants (less than 0.1), while blue boxes have better metric constants (larger than 0.1).

With the goal of raising the metric constants to get a metric closer to euclidean, we tested the algorithm **BetterMetric** on this example. Figure 3.20 shows the result of our efforts described below. Starting with the cover from the  $2^7 \times 2^7$  grid, we ran **BetterMetric** to try and set expansion by  $L_1 = L_0 + 0.05 = 1.19067$  on some edges. It succeeded in building an improved metric after calling **BetterfExpands** 77 times, using  $L_0$  on 275 edges involving 155 boxes, resulting in a metric of minimum 0.024, average 0.072, and maximum 1.

Instead of trying a larger  $L$  value, we had *Hypatia* subdivide only the 155 boxes in the weakest ( $L_0$ ) cycles. The resulting s.c.c., of size  $B = 1847$ ,  $E = 14,157$ , is box-expansive by  $L_2 = 1.18067$  (found with **CheckCycles**), with metric minimum 0.023, average 0.06, and maximum 1. We again used **BetterMetric** to try and set expansion by  $L_3 = L_2 + 0.05 = 1.23067$  on some edges. It succeeded in building an improved metric after calling **BetterfExpands** 71 times, using  $L_2$  on 368 edges involving 267 boxes. The metric constants had minimum 0.03, average 0.094, and maximum 1.

Finally, we repeated the above procedure, subdividing only the 267 boxes in weakest ( $L_2$ ) cycles above, resulting in an s.c.c. of size  $B = 2,284$ ,  $E = 17,146$ . This s.c.c. is box-expansive by  $L_4 = 1.22358$  (found with **CheckCycles**), with metric minimum 0.029, average 0.075, and maximum 1. We again used **BetterMetric** to try and set expansion by  $L_5 = L_4 + 0.05 = 1.27358$  on some edges. It succeeded in building an improved metric after calling **BetterfExpands** 193 times, using  $L_4$  on 1676 edges involving 822 boxes. The metric constants had minimum 0.037, average 0.111, and maximum 1.

Once we managed to raise the average metric constant above 0.1, we were satisfied with the results and quit the run. Figure 3.20 shows the result of the above procedure. Comparing to Figure 3.19, we can see where the boxes lie that were subdivided: precisely those closest to the immediate basin of attraction of the sink (*i.e.*, near the points 0 and  $-1$ ).

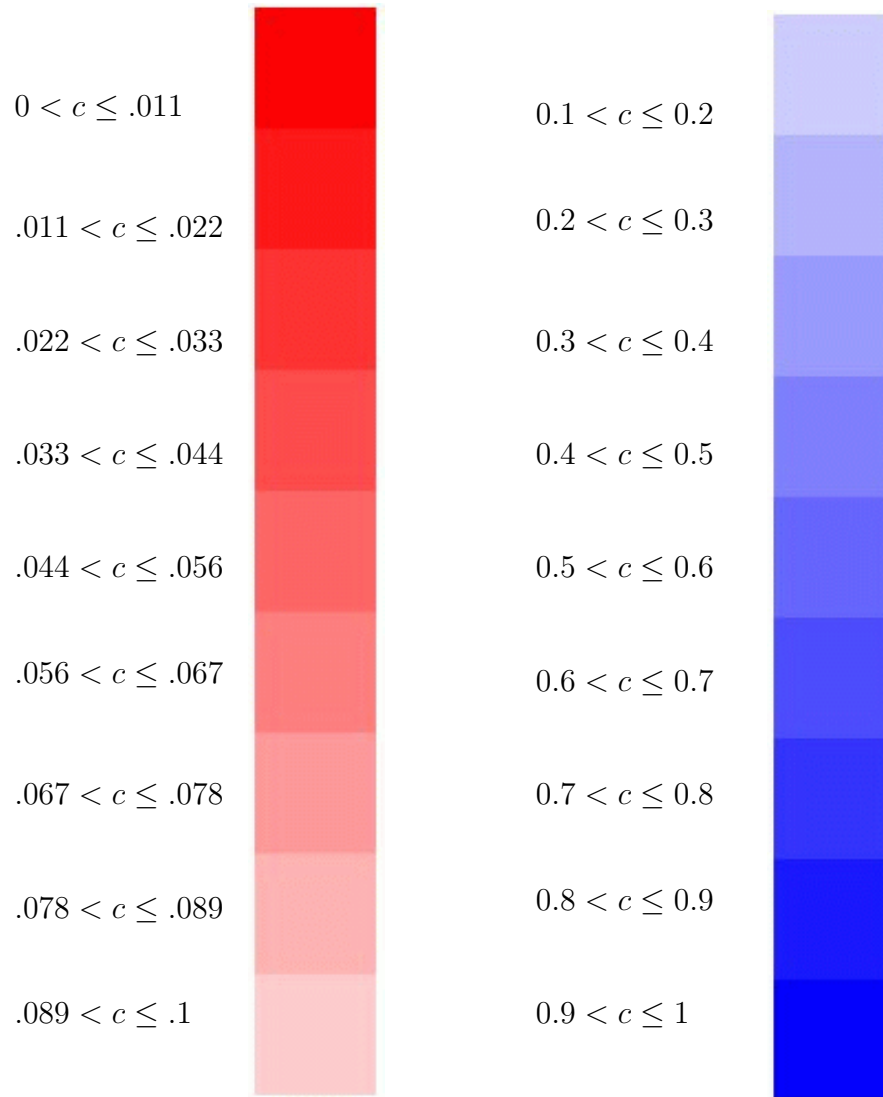


Figure 3.18: A legend for the metric constant shading in Figures 3.19 and 3.20. Red is assigned to undesirable constants, with dark red the worst, and blue is better constants, with dark blue the best.

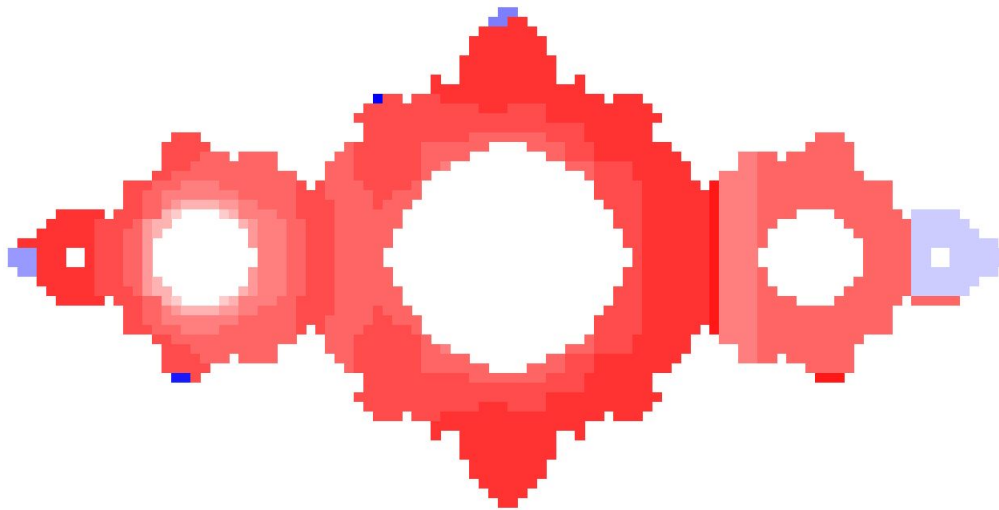


Figure 3.19: Shading illustrates the first box-expanded metric found for  $P_c, c = -1$ , from a  $2^7 \times 2^7$  grid. Red regions have very small metric constants, while blue regions are more reasonable.

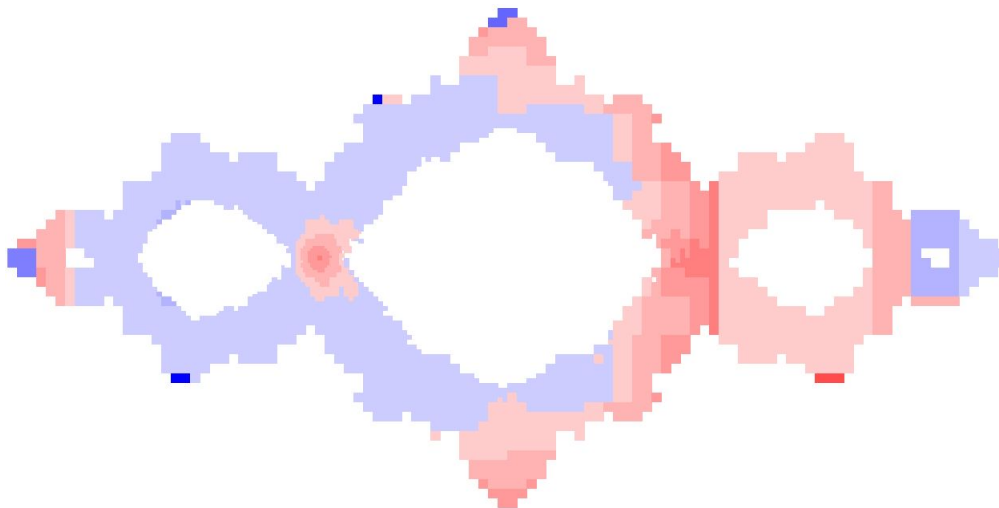


Figure 3.20: Shading illustrates an improved box-expanded metric, using **BetterMetric** and selective subdivision of a  $2^7 \times 2^7$  grid. Note the increase in the desirable blue regions, and decrease and lightening of red regions of small metric constants. Note also the asymmetry. This is not dynamically significant, but an artifact of the tree construction for assigning metric constants.

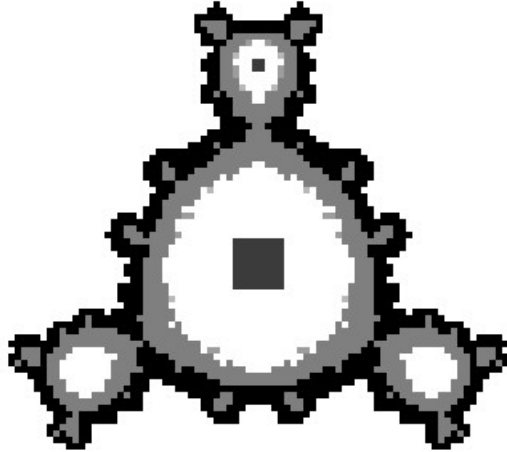


Figure 3.21: A box cover of  $J$  for  $P_{c,a}$ ,  $c = i$ ,  $a = 0.1i$  for a  $2^7 \times 2^7$  grid on  $V$ .  $P_{c,a}$  is box-expansive on this cover. Compare to Figure 3.6.

### Examples for $z^3 - 3z^2 + c$

*Hypatia* is easy to adapt to study the cubic polynomial family,  $P_{c,a}(z) = z^3 - 3z^2 + c$ . For example, one can easily check that  $R = 2$  suffices for  $|c| \leq 2$  and  $|a| \leq (2/3)^{1/2}$ . Then use  $V = \mathcal{N}_\infty(0, 2.1)$ . This family of maps has two critical points, in this parametrization at  $\pm a$ . When  $a = 0$ , there is a clear correspondence between  $z^2 + c$  and  $z^3 + c$ . Below, we examine analogs of the basilica, the rabbit, and the double basilica.

**Example 3.6.10.** The cubic polynomial  $P_{c,a}$ ,  $c = i$ ,  $a = 0.1i$  is a small perturbation of the analog of the quadratic polynomial  $z^2 - 1$ , the “basilica”, of Example 3.6.1. This cubic also has a period 2 attracting cycle. Shown in Figure 3.21 is a box cover of the chain recurrent set, of boxes from a  $2^7 \times 2^7$  grid. Each s.c.c. of the graph  $\Gamma$  is in a different shade of gray. The s.c.c. covering the Julia set is a graph with 1600 boxes and 21,000 edges ( $B = 1,600$ ,  $E = 21,000$ ).  $P_{c,a}$  is box-expansive on this cover.

**Example 3.6.11.** The cubic  $P_{c,a}$ ,  $c = .75i$ ,  $a = 0.5i$  also appears to have an attracting cycle of period two, but looks significantly different than the basilica. This seems to be an analog of the alternate period two Hénon diffeomorphism of Example 1.3.19. Shown in Figure 3.22 is a box cover from a  $2^9 \times 2^9$  grid on  $V$ . The Julia set s.c.c. is size  $B = 19,000$ ,  $E = 360,000$ .  $P_{c,a}$  is box-expansive on this cover.

**Example 3.6.12.** The cubic  $P_{c,a}$ ,  $c = -.19 + 1.1i$ ,  $a = 0.1i$  is a perturbation of a direct analog of the double basilica (Example 3.6.3). This map has a period four

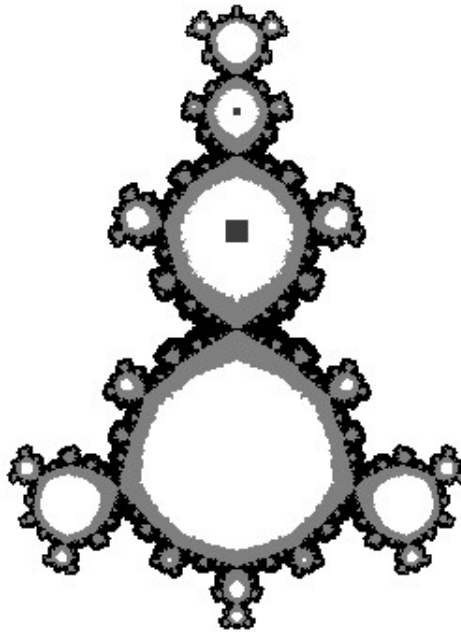


Figure 3.22: A box cover of  $J$  for  $P_{c,a}$ ,  $c = .75i$ ,  $a = 0.5i$  for a  $2^9 \times 2^9$  grid on  $V$ .  $P_{c,a}$  is box-expansive on this cover.

attracting cycle. Shown in Figure 3.23 is a box cover from a  $2^{10} \times 2^{10}$  grid on  $V$ . The map is not box-expansive by  $L = 1$  on this cover. However, subdividing only one cycle of length four which has multiplier less than one yields a cover on which the map is box expansive. The Julia set s.c.c. is size  $B = 60,000$ ,  $E = 780,000$ .

**Example 3.6.13.** A direct analog of the rabbit (Example 3.6.2) is the cubic  $P_{c,a}$ ,  $c = -.54 + .54i$ ,  $a = 0.1i$ . This map has an attracting cycle of period three. Shown in Figure 3.24 is a box cover from a  $2^9 \times 2^9$  grid on  $V$ . The Julia set s.c.c. is size  $B = 19,000$ ,  $E = 255,000$ .  $P_{c,a}$  is box-expansive on this cover.

**Example 3.6.14.** A seemingly rabbit-like cubic is  $P_{c,a}$ ,  $c = -.44 - .525i$ ,  $a = .3i$ . This map has an attracting period three cycle. Shown in Figure 3.25 is the box cover for a  $2^{10} \times 2^{10}$  grid on  $V$ . The sink has separated from  $J$ , however the cover is not hyperbolic because it contains one of the critical points,  $a = .3i$ . We then subdivided only the boxes whose midpoints were heuristically in  $K$ , to get the box cover shown in Figure 3.26. This box cover is box-expansive by the map, and the Julia set s.c.c. is size  $B = 160,000$ ,  $E = 250,000$ .

**Example 3.6.15.** A rabbit-like cubic which is clearly not conjugate to the previous cubic rabbit is  $P_{c,a}$ ,  $c = -.38125 + .40625i$ ,  $a = 0.5i$ . This does have an attracting

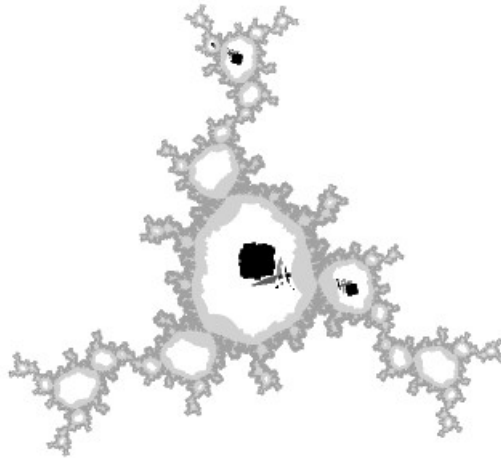


Figure 3.23: A box cover of  $J$  for  $P_{c,a}$ ,  $c = -.19 + 1.1i$ ,  $a = 0.1i$  for a  $2^{10} \times 2^{10}$  grid on  $V$ . Subdivide 4 boxes, and then  $P_{c,a}$  is box-expansive on this cover.

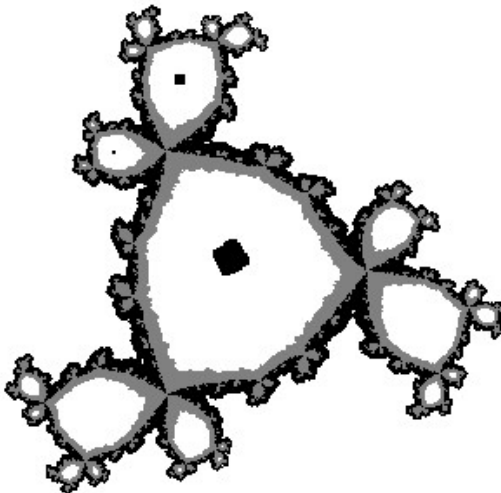


Figure 3.24: A box cover of  $J$  for  $P_{c,a}$ ,  $c = -.54 + .54i$ ,  $a = 0.1i$  for a  $2^9 \times 2^9$  grid on  $V$ .  $P_{c,a}$  is box-expansive on this cover.

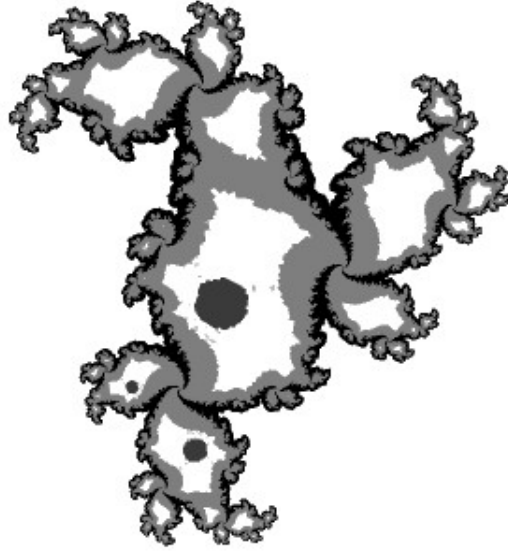


Figure 3.25: A box cover of  $J$  for  $P_{c,a}$ ,  $c = -.44 - .525i$ ,  $a = .3i$  for a  $2^{10} \times 2^{10}$  grid on  $V$ . This cover contains a critical point, so the map is not box-expansive on it.

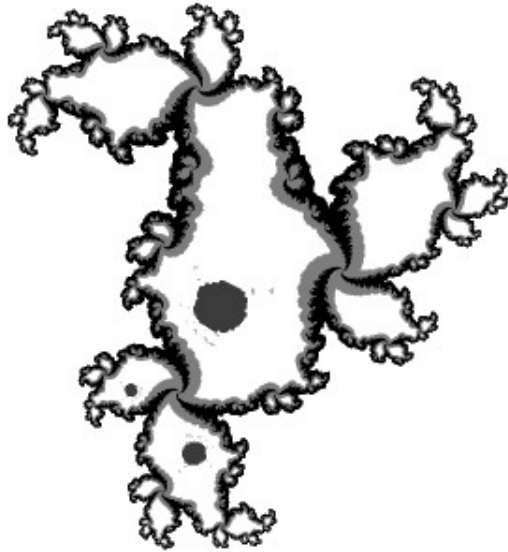


Figure 3.26: A box cover of  $J$  for  $P_{c,a}$ ,  $c = -.44 - .525i$ ,  $a = .3i$  for boxes of side length  $4/2^{10}$  and  $4/2^{11}$ .  $P_{c,a}$  is box-expansive on this cover.



Figure 3.27: A box cover of  $J$  for  $P_{c,a}$ ,  $c = -.38125 + .40625i$ ,  $a = 0.5i$  for a boxes of side length  $4/2^9$  and  $4/2^{10}$ .  $P_{c,a}$  is box-expansive on this cover.

cycle of period three, however the Julia set is disconnected. The quickest and least memory-intensive method for separating the Julia set from the sink is to first subdivide all boxes uniformly to obtain a  $2^9 \times 2^9$  grid, and then subdivide only the boxes whose midpoints seemed to be in  $K$ . Shown in Figure 3.27 is a box cover of this hybrid grid on  $V$ . The Julia set s.c.c. is size  $B = 45,000$ ,  $E = 867,000$ .  $P_{c,a}$  is box-expansive on this cover.

Table 3.2 summarizes the data for these cubic examples.

Table 3.2: Examples of running *Hypatia* for  $P_{c,a}(z) = z^2 - 3a^2z + c$ .

Example	$c$	$a$	sink period	Figure	box size	# boxes (1,000s)	# edges (1,000s)	box- exp?
3.6.10	$i$	$0.1i$	2	3.21	$4/2^7 = .03125$	1.6	21	Yes
3.6.11	$.75i$	$0.5i$	2	3.22	$4/2^9 = .008$	19	360	Yes
3.6.12	$-.19 + 1.1i$	$0.1i$	4	3.23	$4/2^{10} = .004$ , some $4/2^{11} = .002$	60	780	Yes
3.6.13	$-.54 + .54i$	$0.1i$	3	3.24	$4/2^9$	19	255	Yes
3.6.14	$-.44 - .525i$	$.3i$	3	3.25	$4/2^{10}$	92	142	No
				3.26	$4/2^{10}$ and $4/2^{11}$	160	250	Yes
3.6.15	$-.38125 + .40625i$	$0.5i$	3	3.27	$4/2^9$ and $4/2^{10}$	45	867	Yes

# Chapter 4

## Hyperbolicity in two complex dimensions

### 4.1 Introduction: box-hyperbolicity

In this chapter, let  $f : \mathbb{C}^2 \rightarrow \mathbb{C}^2$  be a polynomial diffeomorphism with  $d(f) > 1$ , and with Julia set  $J$ . Let  $\mathcal{V}'$  be a box cover of  $J$ , with  $\mathcal{B}' = \mathcal{B}(\mathcal{V}')$ , and  $\Gamma'$  a box-chain graph of  $\mathcal{V}'$  that is strongly connected. Note by Corollary 2.2.11 and Proposition 2.1.4 we always have the existence of such a  $\Gamma'$ .

*Hypatia* uses (in spirit) the Newhouse cone field condition (Theorem 1.3.4) to test for hyperbolicity.

**Definition 4.1.1.** Let  $\mathcal{C}_k^u$  be an “unstable” cone field which is constant on each box,  $B_k$ . Let the complements be the “stable” cones, *i.e.*,  $\mathcal{C}_k^s = \mathbb{C}^2 \setminus \mathcal{C}_k^u$ . Then the cone field determines (up to scaling) an indefinite Hermitian form,  $Q_k : \mathbb{C}^2 \rightarrow \mathbb{R}$ , such that  $\mathcal{C}_k^u = \{\mathbf{w} : Q_k(\mathbf{w}) \geq 0\}$ , hence  $\mathcal{C}_k^s = \{\mathbf{v} : Q_k(\mathbf{v}) < 0\}$ .

Call  $f$  *box-hyperbolic* (with respect to  $\Gamma'$  and  $\{Q_k\}$ ) if there exists a choice of scaling for each  $Q_k$  so that  $Df$  ( $Df^{-1}$ ) preserves and expands the unstable (stable) cones with respect to  $\{Q_k\}$ , *i.e.*, if for every edge  $B_k \rightarrow B_j$  in  $\Gamma'$  and every  $z \in B_k$ :

1. If  $\mathbf{w} \in \mathcal{C}_k^u$ , then  $D_z f(\mathbf{w}) \in \mathcal{C}_j^u$  and  $Q_j(D_z f(\mathbf{w})) > Q_k(\mathbf{w})$ ;
2. If  $\mathbf{v} \in \mathcal{C}_j^s$ , then  $[D_z f]^{-1}(\mathbf{v}) \in \mathcal{C}_k^s$  and  $-Q_k([D_z f]^{-1}(\mathbf{v})) > -Q_j(\mathbf{v})$ .

If  $f$  is box-hyperbolic with respect to some  $\Gamma'$  and some choice of  $\{Q_k\}$ , we will say  $\Gamma'$  and  $\mathcal{V}'$  are box-hyperbolic. We also sometimes say  $f$  is box-hyperbolic on  $\mathcal{V}'$ , or simply  $f$  is box-hyperbolic.

Condition 2 in its most natural form would be stated in terms of the matrix  $[D_{fz} f^{-1}]$ . But by the chain rule, for a diffeomorphism  $f$ , this is equal to  $[D_z f]^{-1}$ . For ease of notation we use the latter.

The function  $|Q_k(\cdot)|^{1/2}$  is not quite a norm on  $\mathbb{C}^2$ , since for example it is zero on the boundary of the cones. However, in Section 4.3.2, we prove Theorem 4.3.10, showing that box-hyperbolicity does imply the standard definition of hyperbolicity.

We explain *Hypatia*'s algorithm for testing box-hyperbolicity in detail in Section 4.2. First we give a sketch. *Hypatia* starts by finding an approximately invariant splitting, that is a pair of “unstable” and “stable” vectors,  $\mathbf{u}_k, \mathbf{s}_k$ , in each box,  $B_k$  in the cover  $\mathcal{V}'$  of  $J$ , such that  $\mathbf{u}_k(\mathbf{s}_k)$  must be contained in any unstable (stable) box-constant cone field that is preserved by  $Df$  (Propositions 4.2.1 and 4.2.2). Since the splitting is only approximate, it must define cones and use them to check for box-hyperbolicity. It defines cones using the  $\mathbf{u}_k, \mathbf{s}_k$  as axes. To determine the width of the cones and appropriate scaling constants for the Hermitian forms, it attempts to build an “unstable” metric which is uniformly expanded by  $Df$  on

the set of unstable directions,  $\{\mathbf{Cu}_k\}$ , and a “stable” metric which is uniformly expanded by  $Df^{-1}$  on the set of stable directions,  $\{\mathbf{Cs}_k\}$ . If successful, it then uses the directions and their metrics to define the cones and Hermitian forms. Finally, it checks whether the diffeomorphism preserves the cone field, and whether with respect to the Hermitian forms,  $Df(Df^{-1})$  is expanding on the unstable (stable) cones.

Just as in one dimension, *Hypatia* either proves  $H_{a,c}$  is hyperbolic, or provides several types of information regarding which parts of the cover were obstructions to a successful test. We give examples of results running *Hypatia* in Section 4.4, describing the various information *Hypatia* gathers during the run.

## 4.2 Algorithm to show box-hyperbolicity

Below we describe in detail the steps which *Hypatia* follows in order to test box-hyperbolicity.

### 4.2.1 Defining stable and unstable directions

The first step is to guess reasonable unstable and stable directions,  $\mathbf{u}_k$  and  $\mathbf{s}_k$ , in each box  $B_k \in \mathcal{V}$ . To do so, we use a saddle periodic point,  $p$ . Recall if  $p$  is a saddle periodic point of period  $m$ , then the eigenvalues  $\lambda, \mu$  of  $D_p f^m$  satisfy  $|\lambda| > 1 > |\mu|$  (or vice-versa). The large (small) eigenvalue is called the unstable (stable) eigenvalue.

For  $f = H$ , the diffeomorphism  $(x, y) \rightarrow (x^2 + c - ay, x)$  has two fixed points. Note first that fixed points of  $H$  must be on the diagonal, *i.e.*,  $x = y$ . Then the fixed points are given by:

$$x_{\pm} = \frac{1}{2} \left( (1 + a) \pm \sqrt{(1 + a)^2 + 4c} \right).$$

Proposition 1.2.15 stated that except when  $|a| = 1$  or on the locus  $4c = (1 + a)^2$ , a saddle fixed point always exists for  $H$ . The eigenvalues of  $D_x H$  for the fixed point  $(x, x)$  are:

$$\lambda, \mu = x \pm \sqrt{x^2 - a}.$$

Choose a saddle periodic point,  $p$ , of period  $m$ . There is some box, call it  $B_0$ , which contains  $p$ . Compute the eigenvalues and eigenvectors of  $D_p f^m$ . Let  $\mathbf{u}_0$  be the eigenvector of unit length (*i.e.*, corresponding to the unstable eigenvalue, and  $\mathbf{s}_0$  be the eigenvector of unit length corresponding to the stable eigenvalue. Thus we have natural directions in the box  $B_0$ .

*Hypatia* next finds a spanning tree of  $\Gamma'$  using  $B_0$  as the root vertex. Since  $\Gamma'$  is strongly connected, a connected spanning tree called an *arborescence* ([20]) can be built using any vertex  $B_0$  as a root, so that there is one path in the tree from  $B_0$  to any other vertex in the graph, and each vertex has only one incoming edge. Now the root vertex  $B_0$  has an unstable direction  $\mathbf{u}_0$ . Define the rest of the

unstable direction by pushing the images of  $\mathbf{u}_0$  under  $Df$  across the tree. That is, if  $B_k \rightarrow B_j$  is an edge in the tree, and  $\mathbf{u}_k$  is defined, then define

$$\mathbf{u}_j = D_{z_k} f(\mathbf{u}_k) / \|D_{z_k} f(\mathbf{u}_k)\|,$$

where  $z_k$  is the center point of box  $B_k$ . Note we normalized so that all the unstable direction have norm one.

Thus the directions  $\{\mathbb{C}\mathbf{u}_k\}$  are an approximation to an  $f$ -invariant unstable line field. Since we want  $Df$  to preserve and expand the unstable cones, it makes sense that successive images of  $\mathbf{u}_0$  under  $Df$  would do the best job of finding the preserved unstable line field. We see directly from the choice of  $\mathbf{u}_k$  that these directions satisfy the following:

**Proposition 4.2.1.** *Let  $\mathbf{u}_k$  be as above, i.e., if  $\mathcal{S}$  is an arborescence of  $\Gamma'$ , with root vertex  $B_0$ , then*

$$\begin{aligned} \mathbf{u}_0 &= \text{the unstable eigenvector of a saddle periodic point,} \\ \mathbf{u}_j &= D_{z_k} f(\mathbf{u}_k) / \|D_{z_k} f(\mathbf{u}_k)\|, \text{ if edge } B_k \rightarrow B_j \text{ is in } \mathcal{S}. \end{aligned}$$

Let  $\mathcal{C}_k^u$  be any box-constant cone field preserved by  $D_z f$ , for each  $z \in B_k$ . Then for each  $B_k$ , we must have  $\mathbf{u}_k \subset \mathcal{C}_k^u$ .

Note that for edges  $B_k \rightarrow B_m$  not in the spanning tree,  $Df$  does not map  $\mathbf{u}_k$  to  $\mathbf{u}_m$ . It is helpful in establishing invariance of the cone field if  $Df(\mathbf{u}_k)$  is close to  $\mathbf{u}_m$ , and  $D_z f$  does not vary greatly as  $z$  varies within one box. Thus the variation of  $Df(\mathbf{u}_k)$  among boxes whose images hit the same box, as well as within each box, is an indication of the likelihood of proving hyperbolicity with the box cover.

We define the stable directions similarly, keeping in mind that we want stable cones expanded and preserved by  $Df^{-1}$ . So we first compute the backward edges of  $\Gamma'$ , i.e., those in the transpose of the graph. We build a spanning tree of  $(\Gamma')^T$  with  $B_0$  as root vertex. Then, compute successive images of  $\mathbf{s}_0$  under  $Df^{-1}$  along the tree edges to define all of the  $\mathbf{s}_k$ . In this way we get an good approximation to a stable line field, approximately preserved by  $Df^{-1}$ . Again, the variation in  $Df^{-1}(\mathbf{s}_k)$  within a box, and among boxes whose inverse image hit the same box, is also an indicator of how likely it is that  $f$  is box-hyperbolic on the cover. Note there is a result corresponding to Proposition 4.2.1 for the stable directions as well:

**Proposition 4.2.2.** *Let  $\mathbf{s}_k$  be as above, i.e., if  $\mathcal{S}$  is an arborescence of  $\Gamma'$ , with root vertex  $B_0$ , then*

$$\begin{aligned} \mathbf{s}_0 &= \text{the stable eigenvector of a saddle periodic point,} \\ \mathbf{s}_k &= D_{z_k} f^{-1}(\mathbf{s}_j) / \|D_{z_k} f^{-1}(\mathbf{s}_j)\|, \text{ if edge } B_k \rightarrow B_j \text{ is in } \mathcal{S}. \end{aligned}$$

Let  $\{\mathcal{C}_k^s\}$  be any box-constant cone field which is preserved by  $D_z f^{-1}$ , for each  $z \in B_k$ . Then for each  $B_k$ , we must have  $\mathbf{s}_k \subset \mathcal{C}_k^s$ .

*Remark.* Propositions 4.2.1 and 4.2.2 imply that in order a computer program to be able to check whether a box constant cone field is preserved by  $Df$ , it is helpful to have an angle between each pair  $\mathbf{u}_k, \mathbf{s}_k$  which is not very small.

### 4.2.2 Defining a metric on the directions

Consider the “unstable” directions  $\{\mathbb{C}\mathbf{u}_k\}$ . As we discussed above,  $Df$  does not quite preserve the directions, so we take that into account. Let  $P_{\mathbf{s}}^{\mathbf{u}}$  be the projection onto  $\mathbb{C}\mathbf{u}$  with  $\mathbb{C}\mathbf{s}$  as its Null space. Given the vectors  $\mathbf{u} = (u_1, u_2)$  and  $\mathbf{s} = (s_1, s_2)$  in  $\mathbb{C}^2$ , the projection can easily be calculated, to get:

$$P_{\mathbf{s}}^{\mathbf{u}} \begin{bmatrix} v_1 \\ v_2 \end{bmatrix} = \frac{v_1 s_2 - v_2 s_1}{u_1 s_2 - u_2 s_1} \begin{bmatrix} u_1 \\ u_2 \end{bmatrix}.$$

Let  $\Phi_{k,j}^{\mathbf{u}} = P_{\mathbf{s}_j}^{\mathbf{u}} \circ D_{z_k} f$  denote the projection composed with  $Df$ , so that  $\Phi_{k,j}^{\mathbf{u}}$  does map  $\mathbb{C}\mathbf{u}_k$  to  $\mathbb{C}\mathbf{u}_j$ , and if the unstable directions are a good approximation to an unstable line field, then  $\Phi^u$  is close to  $Df$  on these unstable directions.

*Hypatia* uses the same algorithm as in one dimension to try to build a metric defined by constants  $\{c_k^u\}$  under which  $\Phi^u$  is box-expansive by some amount  $L > 1$ . We will call the  $c_k^u$  unstable metric constants. Define  $c_0^u = 1$  in box  $B_0$ , and on an edge  $B_k \rightarrow B_j$ , the constants must satisfy

$$c_j^u \geq \frac{L c_k^u}{\|\Phi_{k,j}^u(\mathbf{u}_k)\|}.$$

Since  $\Phi^u$  is linear, and  $\{\mathbf{u}_k\}$  has norm one, if such constants can be built (using the methods described in Chapter 3) then  $\Phi^u$  is box-expansive by  $L$  on  $\{\mathbb{C}\mathbf{u}_k\}$ . This is of course not always possible, but the intuition is that it should be possible if the box cover is sufficiently small in the right places.

One way to define stable metric constants is to use the method analogous to that for the unstable metric constants. That is, define  $\Phi_{k,j}^s = P_{\mathbf{u}_j}^{\mathbf{s}_k} \circ D_{z_k} f$ , and try to build constants  $\{c_k^s\}$  so that

$$c_j^s \leq \frac{c_k^s M}{\|\Phi_{k,j}^s(\mathbf{s}_k)\|},$$

for some  $M < 1$ . The the stable directions are definitely contracted by  $\Phi^s$ .

Using this method, the stable and unstable metric constants in each box are defined completely independently. We are going to use  $c_k^u$  and  $c_k^s$  in a box to define the width of the cone, and if these constants are not of comparable size, then the cone could be very thin and could cause difficulties in showing that  $Df$  preserves the cone field. As we discussed in Section 3.4, the largest successful value for  $L$  will define metric constants  $c_k^u$  closest to euclidean, while an  $L$  that is too small can define  $c_k^u$  several orders of magnitude smaller than one. The same applies to  $M$ , though here we want the smallest  $M$  possible. Extremely small metric constants give cones which are not robust. In fact, experience with *Hypatia* shows these problems do arise. Thus finding appropriate values of  $L$  and  $M$  is crucial.

We use methods discussed in Chapter 3 to find good values for  $L$  and  $M$ . We know that we want  $0 < M < 1$  and  $1 < L$ . As in one dimension, Lyapunov exponents give us some intuition. For a polynomial automorphism of  $\mathbb{C}^2$ , there are

two Lyapunov exponents,  $\lambda^\pm$ , which measure expansion and contraction of tangent vectors.

**Theorem 4.2.3 ([9]).** *Let  $f$  be a polynomial automorphism of  $\mathbb{C}^2$  with  $d = d(f) > 1$ . Then  $\lambda^+ \geq \log d$ ,  $\lambda^- \leq -\log d$ , and*

$$\lambda^+ + \lambda^- = \log(\text{Det}Df). \quad (4.1)$$

Note that for Hénon diffeomorphisms,  $|\text{Det}(Df)| = |a|$ . Thus  $\lambda^+ + \lambda^- = \log(a)$ . Since  $\lambda^+ \geq \log d$ , we have the inequality:  $\lambda^- \leq \log(a) - \log d$ . In the case  $|a| < 1$ , we have  $\log(a) < 0$ , hence the inequality for  $\lambda^-$  is stronger than the inequality for  $\lambda^+$ . Thus in general we expect stronger contraction than expansion of tangent vectors under Hénon diffeomorphisms.

Equation 4.1 implies that a good rule of thumb for choosing  $L$  and  $M$  is  $LM = |a|$ , thus find a good  $M$  and then try  $L = |a|/M$ , or vice-versa.

## Defining stable metric in terms of unstable metric

We describe here an alternate method for defining the stable metric constant in a box in terms of the unstable metric constant and some linear algebra involving the stable and unstable directions, which could provide a more robust cone field. Both methods are implemented in *Hypatia* currently, and we will compare them on various examples in Section 4.4.

For this alternate method, we use the intuition that for a box-hyperbolic cover, there is small variation in the various  $Df(\mathbf{u}_k)$  such that  $B_k$  has an edge to a fixed box  $B_j$ . So  $\Phi$  is close to  $Df$ . If we make the assumption that  $\Phi = Df$ , then we can compute  $c_k^s$  in terms of  $c_k^u$ , the directions  $\mathbf{u}_k, \mathbf{s}_k$ , and  $\text{Det}(Df)$ .

**Assumption:** Suppose for the following calculations that  $\Phi = Df$ , *i.e.*,  $Df$  preserves the stable and unstable directions. Then we have that for some complex constants  $\alpha, \beta$ ,

$$\begin{aligned} Df(\mathbf{u}_k) &= \alpha \mathbf{u}_j, & \text{hence } \|Df(\mathbf{u}_k)\| &= |\alpha|, & \text{and} \\ Df(\mathbf{s}_k) &= \beta \mathbf{s}_j, & \text{hence } \|Df(\mathbf{s}_k)\| &= |\beta|. \end{aligned}$$

Consider an edge in the graph  $B_k \rightarrow B_j$ , and suppose we have unstable metric constants  $c_k^u, c_j^u$  defined to give box-expansion by  $L > 1$ . Then we have

$$c_j^u |\alpha| > L c_k^u, \quad \text{hence } \frac{1}{|\alpha|} < \frac{1}{L} \frac{c_j^u}{c_k^u}.$$

We want  $c_k^s, c_j^s$  such that

$$c_j^s |\beta| < \frac{|a|}{L} c_k^s, \quad \text{hence } |\beta| < \frac{|a|}{L} \frac{c_k^s}{c_j^s},$$

showing contraction by  $M = |a|/L < 1$ , assuming  $|a| \leq 1$  (which can be achieved by possibly switching  $H$  with  $H^{-1}$ ).

Now we can use the determinant of  $Df$  to relate all of these quantities. First, we get

$$|\det[Df(\mathbf{u}_k) \ Df(\mathbf{s}_k)]| = |\det[\alpha \mathbf{u}_j \ \beta \mathbf{s}_j]| = |\alpha| |\beta| |\det[\mathbf{u}_j \ \mathbf{s}_j]|$$

But for the complex Hénon family  $H(x, y) = (x^2 + c - ay, x)$ , note that  $\det(Df) = a$ . Thus we also get

$$|\det[Df(\mathbf{u}_k) \ Df(\mathbf{s}_k)]| = |\det(Df)| |\det[\mathbf{u}_k \ \mathbf{s}_k]| = |a| |\det[\mathbf{u}_k \ \mathbf{s}_k]|.$$

Combining the previous two equations, we get

$$|a| |\det[\mathbf{u}_k \ \mathbf{s}_k]| = |\alpha| |\beta| |\det[\mathbf{u}_j \ \mathbf{s}_j]|, \quad \text{hence} \quad |\beta| = \frac{|a| |\det[\mathbf{u}_k \ \mathbf{s}_k]|}{|\alpha| |\det[\mathbf{u}_j \ \mathbf{s}_j]|}.$$

Finally then we relate the previous equation to the metric constants, to see that we need

$$\frac{|a| |\det[\mathbf{u}_k \ \mathbf{s}_k]|}{L |\det[\mathbf{u}_j \ \mathbf{s}_j]|} \frac{c_j^u}{c_k^u} < \frac{|a|}{L} \frac{c_k^s}{c_j^s}.$$

Thus in any box  $B_k$ , set

$$c_k^s = \frac{|\det[\mathbf{u}_k \ \mathbf{s}_k]|}{c_k^u}.$$

With stable metric constants defined in this way, since we actually do not have  $Df = \Phi$ , we are not guaranteed that  $\Phi^s$  contracts the stable directions. Hence we must check for cone preservation and expansion. However for a box-hyperbolic cover, intuition suggests that  $Df$  and  $\Phi$  should be close enough that this method should define more natural cones.

Both methods are implemented in *Hypatia* currently, and we will compare them on various examples in Section 4.4.

### 4.2.3 Defining a cone field

In each box,  $B_k$ , define unstable cones,  $\mathcal{C}_k^u$ , so that a vector  $\mathbf{w}$  is in the unstable cone if it is closer to  $\mathbf{u}_k$  than  $\mathbf{s}_k$ , relative to the unstable and stable metrics. That is,  $\mathbf{w} \in \mathcal{C}_k^u$  iff  $c_k^u \|P_{\mathbf{s}_k}^{\mathbf{u}_k}(\mathbf{w})\| \geq c_k^s \|P_{\mathbf{u}_k}^{\mathbf{s}_k}(\mathbf{w})\|$ . Then the stable cones are just the complements,  $\mathcal{C}_k^s := \mathbb{C}^2 \setminus \mathcal{C}_k^u$ .

Then we define the Hermitian form  $Q_k: \mathbb{C}^2 \rightarrow \mathbb{R}$ , by

$$Q_k(\mathbf{w}) = (c_k^u \|P_{\mathbf{s}_k}^{\mathbf{u}_k}(\mathbf{w})\|)^2 - (c_k^s \|P_{\mathbf{u}_k}^{\mathbf{s}_k}(\mathbf{w})\|)^2.$$

Thus the unstable cone,  $\mathcal{C}_k^u$  is simply the set of vectors for which  $Q_k$  is nonnegative, and the stable cone  $\mathcal{C}_k^s$ , is the set of vectors for which the form is negative.

Note that the ratio of the metric constants determines the angle width of the cones. Thus if the constants  $c_k^u$  and  $c_k^s$  are several orders of magnitude different

then the cones will be very thin, thus difficult for the computer to work with. This explains the need to find good values of  $L$  and  $M$  to give get a reasonable pair of constants in each box.

We can construct a Hermitian matrix,  $A_k$ , which encodes the information of  $Q_k$ , following standard linear algebra as in [39]. A Hermitian form  $Q$  defines a sesquilinear form  $g: \mathbb{C}^2 \times \mathbb{C}^2 \rightarrow \mathbb{R}$ , such that  $g(\mathbf{w}, \mathbf{w}) = Q(\mathbf{w})$ , where we can recover  $g$  using:

$$g(\mathbf{v}, \mathbf{w}) = \frac{1}{4}Q(\mathbf{v} + \mathbf{w}) - \frac{1}{4}Q(\mathbf{v} - \mathbf{w}) + \frac{i}{4}Q(\mathbf{v} + i\mathbf{w}) - \frac{i}{4}Q(\mathbf{v} - i\mathbf{w}).$$

A sesquilinear form  $g$  can be represented by a matrix  $A$  so that  $g(\mathbf{v}, \mathbf{w}) = \mathbf{w}^* A \mathbf{v}$ , with  $a_{m,n} = g(\mathbf{e}_n, \mathbf{e}_m)$  for an ordered basis  $\{\mathbf{e}_1, \mathbf{e}_2\}$ , like  $\{(1, 0), (0, 1)\}$ . Now  $g$  Hermitian implies that  $A$  is also Hermitian, and the range of  $Q$  is  $\mathbb{R}$ . Thus,  $Q(\mathbf{w}) = \mathbf{w}^* A \mathbf{w}$ , where  $a_{m,n} = \frac{1}{4}Q(\mathbf{e}_n + \mathbf{e}_m) - \frac{1}{4}Q(\mathbf{e}_n - \mathbf{e}_m) + \frac{i}{4}Q(\mathbf{e}_n + i\mathbf{e}_m) - \frac{i}{4}Q(\mathbf{e}_n - i\mathbf{e}_m)$ .

We easily calculate that for  $\mathbf{u} = (u_1, u_2)$ ,  $\mathbf{s} = (s_1, s_2)$ , if we set

$$b_{11} = (c^u |s_2| \|u\|)^2 - (c^s |u_2| \|s\|)^2, \quad b_{22} = (c^u |s_1| \|u\|)^2 - (c^s |u_1| \|s\|)^2,$$

$$b_{12} = \frac{1}{4} \left[ (c^u \|u\|)^2 (|s_2 - s_1|^2 - |s_2 + s_1|^2 + i |is_2 - s_1|^2 - i |is_2 + s_1|^2) \right. \\ \left. - (c^s \|s\|)^2 (|u_2 - u_1|^2 - |u_2 + u_1|^2 + i |iu_2 - u_1|^2 - i |iu_2 + u_1|^2) \right],$$

and  $b_{21} = \bar{b}_{12}$ , then  $a_{nm} = b_{nm}/|u_1 s_2 - u_2 s_1|^2$ .

## 4.3 Characterizing box-hyperbolicity

### 4.3.1 Checking box-hyperbolicity with Hermitian forms

To test box-hyperbolicity, we need to test whether  $Df$  ( $Df^{-1}$ ) expands the unstable (stable) cones, with respect to  $\{Q_k\}$ . Below we give a condition in terms of these Hermitian forms which is equivalent to box-hyperbolicity.

Let  $B_k \rightarrow B_j$  be an edge in  $\Gamma'$ . The unstable cones are preserved by  $D_z f$  if  $Q_k(\mathbf{w}) \geq 0$  implies  $Q_j(D_z f(\mathbf{w})) \geq 0$ . Note  $(Q_j \circ D_z f)$  is also a Hermitian form, given by.

$$Q_j(D_z f(\mathbf{w})) = \mathbf{w}^* ((D_z f)^* A_j (D_z f)) \mathbf{w},$$

for  $z \in B_k$ .

**Proposition 4.3.1.**  *$f$  is box-hyperbolic (with respect to  $\Gamma'$  and  $\{Q_k\}$ ) iff  $((Q_j \circ D_z f) - Q_k)$  is positive definite for every edge  $B_k \rightarrow B_j$  in  $\Gamma'$  and every  $z \in B_k$ .*

*Proof.* We begin by proving the reverse implication ( $\Leftarrow$ ). Let  $z \in B_k$  and  $B_j$  be a box such that there is an edge  $B_k \rightarrow B_j$ . Then we have  $Q_j(D_z f)(\mathbf{w}) > Q_k(\mathbf{w})$ , for all  $z \in B_k$  and all  $\mathbf{w} \in \mathbb{C}^2$ .

First consider the unstable cones. Suppose  $\mathbf{w} \in \mathcal{C}_k^u$ , so by definition  $0 < Q_k(\mathbf{w})$ . But then by hypothesis, we get

$$0 < Q_k(\mathbf{w}) < Q_j(D_z f(\mathbf{w})).$$

Thus  $D_z f(\mathbf{w}) \in \mathcal{C}_j^u$ , so the unstable cones are preserved by  $D_z f$ , and we have established Condition 1 of box-hyperbolicity.

Next we consider the stable cones. First, we show that stable cone preservation follows from unstable cone preservation, since they are complementary. Indeed, above we showed that  $Df$  preserves the unstable cones, *i.e.*,  $D_z f(\mathcal{C}_k^u) \subset \mathcal{C}_j^u$ . Hence,  $\mathcal{C}_k^u \subset [D_z f]^{-1}(\mathcal{C}_j^u)$ . But by definition,  $\mathcal{C}^s = \mathbb{C}^2 \setminus \mathcal{C}^u$ . Thus  $\mathcal{C}_k^s \supset [D_z f]^{-1}(\mathcal{C}_j^s)$  and so the stable cones are preserved by  $Df^{-1}$ .

Now let  $\mathbf{v} \in \mathcal{C}_j^s$ , so that

$$0 < -Q_j(\mathbf{v}) = -(Q_j \circ D_z f) ([D_z f]^{-1}(\mathbf{v})).$$

Then since we have stable cone preservation under  $Df^{-1}$ , we also know that

$$0 < -Q_k([D_z f]^{-1}(\mathbf{v})).$$

Combining this with the negative of the hypothesis establishes Condition 2 of box-hyperbolicity, *i.e.*,

$$-Q_k([D_z f]^{-1}(\mathbf{v})) > -Q_j(\mathbf{v}).$$

Now we prove the forward implication ( $\Rightarrow$ ). Suppose  $f$  is box-hyperbolic (with respect to  $\Gamma'$ ,  $\{Q_k\}$ ), *i.e.*, we have Conditions 1 and 2. Let  $B_k \rightarrow B_j$  be an edge in  $\Gamma'$  and  $z \in B_k$ .

We consider  $\mathbf{w}$  in each of three regions to show  $((Q_j \circ D_z f) - Q_k)$  is positive definite.

**Case 1:** Suppose  $\mathbf{w} \in \mathcal{C}_k^u$ . Then by definition  $0 < Q_k(\mathbf{w})$ .

Since box-hyperbolicity implies the unstable cones are preserved by  $Df$ , we have that  $D_z f(\mathbf{w}) \in \mathcal{C}_j^u$ , so  $0 < Q_j(D_z f(\mathbf{w}))$ .

Then Condition 1 of box-hyperbolicity gives us

$$Q_j(D_z f(\mathbf{w})) > Q_k(\mathbf{w}).$$

**Case 2:** Suppose  $\mathbf{w} \in [D_z f]^{-1}(\mathcal{C}_j^s)$ , *i.e.*,  $\mathbf{v} = D_z f(\mathbf{w}) \in \mathcal{C}_j^s$ . Then by definition  $Q_j(D_z f(\mathbf{w})) < 0$ .

Now by stable cone preservation, we know  $\mathbf{w} \in \mathcal{C}_k^s$ , hence  $Q_k(\mathbf{w}) < 0$ .

Condition 2 of box-hyperbolicity says that

$$-Q_j(\mathbf{v}) < -Q_k([D_z f]^{-1}(\mathbf{v}))$$

for all vectors  $v \in \mathcal{C}_j^s$ , hence it applies to  $\mathbf{v} = D_z f(\mathbf{w})$ . Thus we get

$$-Q_j(D_z f(\mathbf{w})) < -Q_k(\mathbf{w}),$$

and negating yields

$$Q_j(D_z f(\mathbf{w})) - Q_k(\mathbf{w}) > 0.$$

**Case 3:** For the remaining  $\mathbf{w}$ , we have  $\mathbf{w} \notin \mathcal{C}_k^u$  and  $\mathbf{w} \notin [D_z f]^{-1}(\mathcal{C}_j^s)$ . Then  $Q_k(\mathbf{w}) < 0$  and  $Q_j(D_z f(\mathbf{w})) \geq 0$ . Hence,

$$Q_j(D_z f(\mathbf{w})) \geq 0 > Q_k(\mathbf{w}).$$

Thus we easily get  $Q_j(D_z f(\mathbf{w})) - Q_k(\mathbf{w}) > 0$ .  $\square$

In implementation, *Hypatia* uses interval arithmetic (described in Appendix A) to compute  $\text{Hull}(\{D_z f: z \in B_k\})$  each time it needs an inequality which is true for  $D_z f$  for all  $z \in B_k$ . This direct use of interval arithmetic is fine in this situation, however such usage has been carefully avoided in other parts of the algorithm due to its tendency to introduce complications (see discussion of iteration of boxes, Appendix A).

### 4.3.2 Box-hyperbolicity implies hyperbolicity

In this section we prove Theorem 4.3.10, showing that if  $f$  is box-hyperbolic, then it satisfies a standard definition of hyperbolicity. Part of the proof is very similar to the one dimensional analog, Theorem 3.3.3, proved in Section 3.3, in that we use a partition of unity to smooth out a norm. But before we deal with the norm, we verify the existence of a continuous splitting preserved by the map.

**Lemma 4.3.2.** *If  $f$  is box-hyperbolic (with respect to  $\Gamma'$  and some  $\{Q_k\}$ ), then there exists a splitting of the tangent bundle  $T_z \mathbb{C}^2 = E_z^s \oplus E_z^u$ , for each  $z$  in  $J$ , which varies continuously with  $z$  in  $J$ , such that  $f$  preserves the splitting, i.e.,  $D_z f(E_z^s) = E_{fz}^s$ , and  $D_z f(E_z^u) = E_{fz}^u$ . Further, for each  $z \in B_k$ ,  $E_z^u \subsetneq \mathcal{C}_k^u$ , and  $E_z^s \subsetneq \mathcal{C}_k^s$ .*

*Proof.* Newhouse and Palis (Theorem 1.3.4) show that a diffeomorphism  $f$  is hyperbolic if there is a field of cones  $\mathcal{C}_z$  (not necessarily continuous) which is preserved and expanded by  $Df$ , such that the complements are expanded by  $Df^{-1}$ . In their proof ([55]), they first show that the existence of a cone field preserved by  $Df$  implies the existence of a continuous splitting preserved by  $f$ , with the unstable (stable) directions lying inside the unstable (stable) cones. Box-hyperbolicity gives a cone field preserved by  $Df$ . Thus we have cones  $\mathcal{C}_z = \mathcal{C}_k^u$ , if  $z$  is in box  $B_k$  (make some consistent choice of box  $B_k$  containing  $z$ , for the benefit of points on the boundaries of the closed boxes). Thus by the proof in [55], we have the existence of the continuous splitting preserved by  $Df$ .  $\square$

We will need to measure the difference between pairs of lines in  $\mathbb{C}^2$ , like  $E_z^u$  and  $E_z^s$ , or  $E_z^u$  and  $E_x^u$ . To do so, we view the set of lines through the origin in  $\mathbb{C}^2$  as the projective space  $\mathbb{C}\mathbb{P}^1 = \hat{\mathbb{C}}$ . Then the spherical metric on  $\mathbb{C}\mathbb{P}^1$  induces the following metric.

**Definition 4.3.3.** If  $\mathbf{v} = \begin{bmatrix} v_1 \\ v_2 \end{bmatrix}$ ,  $\mathbf{w} = \begin{bmatrix} w_1 \\ w_2 \end{bmatrix}$  are vectors in  $\mathbb{C}^2$ , define the distance between the directions  $\mathbb{C}\mathbf{v}, \mathbb{C}\mathbf{w}$  to be

$$\sigma(\mathbf{v}, \mathbf{w}) = \sin^{-1} \left( \frac{|v_1 w_2 - v_2 w_1|}{\|\mathbf{v}\| \|\mathbf{w}\|} \right).$$

Note that  $\sigma(\mathbf{v}, \mathbf{w}) \in [0, \pi/2]$ , and for any complex numbers  $\alpha, \beta$ ,

$$\sigma(\mathbf{v}, \mathbf{w}) = \sigma(\alpha\mathbf{v}, \beta\mathbf{w}).$$

Think of this metric as measuring the angle between the complex lines, since it is a number in  $[0, \pi/2]$ .

We prove Theorem 4.3.10 in several steps. Lemmas 4.3.4 through 4.3.6 culminate in Definition 4.3.7 and Proposition 4.3.8, which combine with Lemma 4.3.2 to give the theorem.

**Lemma 4.3.4.** *Let  $f$  be box-hyperbolic (with respect to  $\Gamma'$  and some  $\{Q_k\}$ ). Then there exist  $d_1 > 0$  and  $\delta_1 > 0$  such that if  $z \in J \cap \mathcal{N}_\infty(B_k, \delta_1)$ , then  $\sigma(E_z^u, \mathbb{C}_k^s) \geq d_1$  and  $\sigma(E_z^s, \mathbb{C}_k^u) \geq d_1$ .*

*Proof.* First, note that by compactness of  $J$  and the fact that the line fields are contained in the interior of the cones, there exists a  $d_0 > 0$  such that

$$d_0 \leq \min\{\sigma(E_z^u, \mathbb{C}_k^s) : z \in J \cap B_k\} \quad \text{and} \quad d_0 \leq \min\{\sigma(E_z^s, \mathbb{C}_k^u) : z \in J \cap B_k\}.$$

Let  $d_1 = d_0/2$ .

Next, by compactness of  $J$  and continuity of the splitting, there exists a  $\delta_1 > 0$  such that for any  $x, z \in J$  with  $\|x - z\|_\infty < \delta_1$ , we have  $\sigma(E_z^u, E_x^u) < d_1$  and  $\sigma(E_z^s, E_x^s) < d_1$ .

Now let  $z \in J \cap \mathcal{N}_\infty(B_k, \delta_1)$ . Since  $z$  is not necessarily in  $B_k$ , let  $m$  be such that  $z \in B_m$ , and  $x$  is a point satisfying  $x \in J \cap B_m \cap B_k$  and  $\|x - z\|_\infty < \delta_1$ . Then  $\sigma(E_z^u, E_x^u) < d_1$  and  $\sigma(E_z^s, E_x^s) < d_1$ . Since  $x \in B_k$  we have  $\sigma(E_x^u, \mathbb{C}_k^s) \leq d_0$  and  $\sigma(E_x^s, \mathbb{C}_k^u) \leq d_0$ . Hence,  $\sigma(E_z^u, \mathbb{C}_k^s) \geq d_0 - d_1 = d_1$ , and  $\sigma(E_z^s, \mathbb{C}_k^u) \geq d_1$ .  $\square$

**Lemma 4.3.5.** *Let  $f$  be box-hyperbolic (with respect to  $\Gamma'$  and  $\{Q_k\}$ ). If  $B_k, B_j \in \mathcal{V}'$  and  $z \in J$  satisfies  $z \in \mathcal{N}_\infty(B_k, \delta_1)$  and  $f(z) \in \mathcal{N}_\infty(B_j, \delta_1)$ , then  $\sigma(E_{fz}^u, \mathbb{C}_j^s) \geq d_1$  and  $\sigma(E_{fz}^s, \mathbb{C}_j^u) \geq d_1$ .*

*Proof.* This lemma follows directly from Lemma 4.3.4 applied to  $f(z)$  instead of  $z$ .  $\square$

**Lemma 4.3.6.** *Let  $f$  be box-hyperbolic (with respect to  $\Gamma'$  and  $\{Q_k\}$ ).*

*Then there is a  $\tau > 0$  such that for any  $B_k, B_j \in \mathcal{V}'$  and any  $z \in J$  such that  $z \in \mathcal{N}_\infty(B_k, \tau)$  and  $f(z) \in \mathcal{N}_\infty(B_j, \tau)$ , we have*

1. if  $\mathbf{w} \in E_z^u$ , then  $Q_j(D_z f(\mathbf{w})) > Q_k(\mathbf{w})$ ;
2. if  $\mathbf{v} \in E_{fz}^s$ , then  $-Q_k([D_z f]^{-1}(\mathbf{v})) > -Q_j(\mathbf{v})$ .

*Proof.* Among additional requirements given below, let  $\tau$  be less than  $\eta$  from Corollary 2.2.5. Then for any  $z \in J$  such that  $z \in \mathcal{N}_\infty(B_k, \tau)$  and  $f(z) \in \mathcal{N}_\infty(B_j, \tau)$ , there is an edge in  $\Gamma'$  from  $B_k$  to  $B_j$ , *i.e.*,  $B_k \rightarrow B_j \in \mathcal{E}'$ .

Note that since  $J$  is compact, and by Lemmas 4.3.4 and 4.3.5, there exists  $d_2 \geq 0$  such that:

$$d_2 \leq \min\{Q_j(D_x f(\mathbf{u}_x)) - Q_k(\mathbf{u}_x) : x \in B_k, B_k \rightarrow B_j \in \mathcal{E}', \mathbf{u}_x \in E_x^u, \|\mathbf{u}_x\| = 1\}.$$

Let  $\epsilon = d_2/3$ . By continuity of  $D_x f$  and the splitting, there is a  $\tau < \eta$  small enough that for any  $x, z \in J$  with  $\|x - z\| < \tau$ ,  $z \in \mathcal{N}_\infty(B_k, \tau)$ , and  $f(z) \in \mathcal{N}_\infty(B_j, \tau)$ , we have

$$\begin{aligned} |Q_k(\mathbf{u}_z) - Q_k(\mathbf{u}_x)| &< \epsilon, \\ |Q_j(D_x f(\mathbf{u}_x)) - Q_j(D_x f(\mathbf{u}_z))| &< \epsilon, \text{ and} \\ |Q_j(D_x f(\mathbf{u}_z)) - Q_j(D_z f(\mathbf{u}_z))| &< \epsilon. \end{aligned}$$

Then  $Q_j(D_z f(\mathbf{u}_z)) - Q_k(\mathbf{u}_z) \geq d_2 - 3\epsilon > 0$ .

Now since  $Q(\mathbf{w})$  is a Hermitian form,  $Q(\alpha\mathbf{w}) = |\alpha|^2 Q(\mathbf{w})$  for any  $\alpha \in \mathbb{C}$ . Thus by linearity of  $Df$ , the above result for  $\mathbf{u}_z$  implies the same result for any  $\mathbf{w} \subset E_z^u$ . Hence we have Condition 1.

The proof of 2. is analogous. Let  $d_3 > 0$  satisfy:

$$d_3 \leq \min\{Q_j(\mathbf{s}_{fz}) - Q_k(D_z f^{-1}(\mathbf{s}_{fz})) : x \in B_k, B_k \rightarrow B_j \in \mathcal{E}', \mathbf{s}_{fz} \in E_{fz}^s, \|\mathbf{s}_{fz}\| = 1\}.$$

Let  $\epsilon' = d_3/3$ . Then further restrict  $\tau$  so that for any  $x, z \in J$  with  $\|x - z\| < \tau$ ,  $z \in \mathcal{N}_\infty(B_k, \tau)$ , and  $f(z) \in \mathcal{N}_\infty(B_j, \tau)$ , we have

$$\begin{aligned} |Q_j(\mathbf{s}_{fz}) - Q_j(\mathbf{s}_{fx})| &< \epsilon', \\ |Q_k(D_x f^{-1}(\mathbf{s}_{fx})) - Q_k(D_x f^{-1}(\mathbf{s}_{fz}))| &< \epsilon', \text{ and} \\ |Q_k(D_x f^{-1}(\mathbf{s}_{fz})) - Q_k(D_z f^{-1}(\mathbf{s}_{fz}))| &< \epsilon'. \end{aligned}$$

Thus 2. follows from  $Q_j(\mathbf{s}_{fz}) - Q_k(D_z f^{-1}(\mathbf{s}_{fz})) \geq d_3 - 3\epsilon' > 0$ .  $\square$

Now we use a partition of unity to smooth  $Q_k$  on the invariant line fields.

**Definition 4.3.7.** Let  $f$  be box-hyperbolic (with respect to  $\Gamma'$  and  $\{Q_k\}$ ). Let  $\tau > 0$  be as given in Lemma 4.3.6. Define a partition of unity on  $\mathcal{B}'$  by choosing continuous functions  $\rho_k : \mathbb{C}^2 \rightarrow [0, 1]$  for each box  $B_k \in \mathcal{V}'$ , such that  $\text{supp}(\rho_k) \subset \mathcal{N}_\infty(B_k, \tau)$  and  $\sum_k \rho_k(z) = 1$ , for any  $z \in \mathcal{B}'$ .

Let  $z \in J$ . Then we define  $Q_z : E_z^u \cup E_z^s \rightarrow \mathbb{R}$  by

$$Q_z(\mathbf{w}) = \sum_k \rho_k(z) Q_k(\mathbf{w}).$$

Note that  $Q_z(\mathbf{w})$  is a continuous function of  $\mathbf{w}$  since  $Q_k$  is continuous within each box  $B_k$ , and further a continuous function of  $z$  due to the partition of unity.

**Proposition 4.3.8.** *Let  $f$  be box-hyperbolic (with respect to  $\Gamma'$  and  $\{Q_k\}$ ). Let  $\{Q_z\}$  be given by Definition 4.3.7. Then for any  $z \in J$  we have:*

1. *if  $\mathbf{w} \in E_z^u$ , then  $Q_{fz}(D_z f(\mathbf{w})) > Q_z(\mathbf{w})$ ;*
2. *if  $\mathbf{v} \in E_{fz}^s$ , then  $-Q_z([D_z f]^{-1}(\mathbf{v})) > -Q_{fz}(\mathbf{v})$ .*

*Proof.* Let  $\mathbf{u}_z \in E_z^u$  be such that  $\|\mathbf{u}_z\| = 1$ . If we set

$$\begin{aligned} q_{f,z}^u &= \min\{Q_j(D_z f(\mathbf{u}_z)): f(z) \in \text{supp}(\rho_j)\}, \text{ and} \\ q_z^u &= \max\{Q_k(\mathbf{u}_z): z \in \text{supp}(\rho_k)\}, \end{aligned}$$

then by Lemma 4.3.6 we know that  $q_{f,z}^u > q_z^u$ . Thus we need only use that the partition functions sum to one to get

$$\begin{aligned} Q_{fz}(D_z f(\mathbf{u}_z)) &= \sum_j \rho_j(f(z)) Q_j(D_z f(\mathbf{u}_z)) \geq \sum_j \rho_j(f(z)) q_{f,z}^u = q_{f,z}^u \\ &> q_z^u = \sum_k \rho_k(z) q_z^u \geq \sum_k \rho_k(z) Q_k(\mathbf{u}_z) = Q_z(\mathbf{u}_z). \end{aligned}$$

Hence 1. follows since  $Df$  is linear, and for any  $\alpha \in \mathbb{C}$ ,  $Q(\alpha \mathbf{w}) = |\alpha|^2 Q(\mathbf{w})$ .

Establishing 2 is analogous. Let  $\mathbf{s}_{fz} \in E_{fz}^s$  be such that  $\|\mathbf{s}_{fz}\| = 1$ . If we set

$$\begin{aligned} -q_z^s &= \min\{-Q_k([D_z f]^{-1}(\mathbf{s}_{fz})): z \in \text{supp}(\rho_k)\}, \text{ and} \\ -q_{f,z}^s &= \max\{-Q_j(\mathbf{s}_{fz}): f(z) \in \text{supp}(\rho_j)\}, \end{aligned}$$

then by Lemma 4.3.6 we know that  $-q_z^s > -q_{f,z}^s$ . Thus we need only use that the partition functions sum to one to get

$$\begin{aligned} -Q_z([D_z f]^{-1}(\mathbf{s}_{fz})) &= -\sum_k \rho_k(z) Q_k([D_z f]^{-1}(\mathbf{s}_{fz})) \geq -\sum_k \rho_k(z) q_z^s = -q_z^s \\ &> -q_{f,z}^s = -\sum_j \rho_j(f(z)) q_{f,z}^s \geq -\sum_j \rho_j(f(z)) Q_j(\mathbf{s}_{fz}) = -Q_{fz}(\mathbf{v}). \end{aligned}$$

□

**Definition 4.3.9.** Let  $f$  be box-hyperbolic (with respect to  $\Gamma'$  and  $\{Q_k\}$ ). Let  $z \in J$ . We define the norm  $\|\cdot\|_\rho$  on  $T_z \mathbb{C}^2$  using  $Q_z$  and the spaces  $E_z^u, E_z^s$  as a basis, *i.e.*, for  $\mathbf{w} \in T_z \mathbb{C}^2$ ,

$$\|\mathbf{w}\|_\rho = \max \left( |Q_z(P_{s_z}^{u_z}(\mathbf{w}))|^{1/2}, |Q_z(P_{u_z}^{s_z}(\mathbf{w}))|^{1/2} \right),$$

where  $P_{b_z}^{a_z}$  denotes the projection onto  $E_z^a$  with  $E_z^b$  as its Null space.

Finally, we can show that a box-hyperbolic map  $f$  is hyperbolic with respect to the norm  $\|\cdot\|_\rho$  on  $T_J \mathbb{C}^2$ .

**Theorem 4.3.10.** *Let  $f$  be box-hyperbolic (with respect to  $\Gamma'$  and some  $\{Q_k\}$ ). Then  $f$  is hyperbolic over  $J$ , i.e., there exists a splitting of the tangent bundle  $T_z\mathbb{C}^2 = E_z^s \oplus E_z^u$ , for each  $z$  in  $J$ , which varies continuously with  $z$  in  $J$ , a constant  $\lambda > 1$ , and a (continuous) riemannian norm  $\|\cdot\|_\rho$  such that:*

1.  $f$  preserves the splitting, i.e.,  $D_z f(E_z^s) = E_{fz}^s$ , and  $D_z f(E_z^u) = E_{fz}^u$ , and
2.  $Df(Df^{-1})$  expands on  $E_z^s(E_z^s)$  uniformly, i.e.,
  - (a) if  $\mathbf{w} \in E_z^u$  then  $\|D_z f(\mathbf{w})\|_\rho \geq \lambda \|\mathbf{w}\|_\rho$ , and
  - (b) if  $\mathbf{w} \in E_z^s$  then  $\|D_z f^{-1}(\mathbf{w})\|_\rho \geq \lambda \|\mathbf{w}\|_\rho$ .

*Proof.* We have 1. by Lemma 4.3.2. Let  $\|\cdot\|_\rho$  be given by Definition 4.3.9. Let  $z \in J$ . We show that 2. follows easily from Proposition 4.3.8.

First suppose  $\mathbf{w} \in E_z^u$ . Then  $D_z f(\mathbf{w}) \in E_{fz}^u$ . Hence  $\|\mathbf{w}\|_\rho^2 = Q_z(\mathbf{w})$  and  $\|D_z f(\mathbf{w})\|_\rho^2 = Q_{fz}(D_z f(\mathbf{w}))$ . Thus Condition 1. of Proposition 4.3.8 implies that  $\|D_z f(\mathbf{w})\|_\rho > \|\mathbf{w}\|_\rho$ .

Now consider  $\mathbf{w} \in E_z^s$ . Then  $D_z f(\mathbf{w}) \in E_{fz}^s$ . Hence  $\|\mathbf{w}\|_\rho^2 = -Q_z(\mathbf{w})$  and  $\|D_z f(\mathbf{w})\|_\rho^2 = -Q_{fz}(D_z f(\mathbf{w}))$ . Then Condition 2. of Proposition 4.3.8 applied to  $\mathbf{v} = (D_z f^{-1}(\mathbf{w}))$  implies  $\|D_z f^{-1}(\mathbf{w})\|_\rho > \|\mathbf{w}\|_\rho$ .

Finally, by compactness of  $J$  the strict inequalities imply the existence of some constant  $\lambda > 1$ , proving 2.  $\square$

## 4.4 Examples of running *Hypatia* for Hénon diffeomorphisms

The procedure used in two dimensions is much more complicated than in one, and consequently offers more options to the user as it runs. We describe a generic sample run first, then immediately following we present the detailed data for the examples.

### 4.4.1 A generic run of *Hypatia* for a Hénon diffeomorphism

The early steps of *Hypatia* involve refining to obtain a good box cover of  $J$ . Given values of  $a, c$ , it first computes an  $R'$  so that  $V = \mathcal{N}_\infty(0, R')$  contains some  $\eta$ -chain recurrent set, as given by Proposition 2.1.4. Then the user inputs  $n$  to put a  $(2^n)^4$  grid on  $V$ , for example  $n = 3$ . *Hypatia* will form the grid of boxes. Then it performs the “ $V$ -check” of computing some forward/backward images of each box, and eliminating any boxes which map entirely outside of  $V$ . Next it creates the box-chain graph  $\Upsilon$ , with vertices the remaining boxes and an edge from  $B_k$  to  $B_j$  if a certain neighborhood of  $H_{a,c}(B_k)$  intersects  $B_j$ . It decomposes the transition graph into its strongly connected components (s.c.c.’s), which are the subset of vertices and edges such that for each pair of vertices  $u, v$ , there is a path from  $u$  to  $v$  and from  $v$  to  $u$ . The union of these components is the box-chain recurrent

graph,  $\Gamma$ , which is a cover of  $\mathcal{R}$ . One of these graph components,  $\Gamma'$ , is a box cover  $\mathcal{V}'$  for  $J$ , and yields the chain-transitive component containing  $J$ .

In a typical run, the above procedure will be repeated a few times. That is, input an  $n$  (like  $n = 1$ ) so that *Hypatia* will put a  $(2^n)^4$  grid on each of the boxes in  $\Gamma'$ , eliminate some of these new boxes with the “ $V$ -check”, form the box-chain graph  $\Upsilon$ , and finally decompose  $\Upsilon$  into its s.c.c.’s to find a new box-chain recurrent graph  $\Gamma'$  representing  $J$ . Before checking hyperbolicity, this procedure should be repeated until it is evident that the Julia set s.c.c. is separate from the s.c.c. for the sink.

Uniform subdivision is not the quickest way to separate the Julia set from the sink. Note that if  $p$  is in a sink basin, then for some  $m$ , the eigenvalues of  $D_{H^m(p)}H \circ \cdots \circ D_p H$  will have modulus less than one. Thus in order to expedite this separation, we implement:

**Option B:** Subdivide box  $B_j$  if both eigenvalues of the matrix  $D_{z_m}H \circ D_{z_{m-1}}H \circ \cdots \circ D_{z_0}H$  are less than one, where  $z_0$  is the center point of the box,  $z_j = H^j(z_0)$ , and for example,  $m = 3$ .

To visualize the boxes in  $\Gamma'$  at any given step, you may ask *Hypatia* to draw a picture of the cover. It uses the same method as *FractalAsm*, discussed in Section 1.2, to draw in the plane a parametrization of an unstable manifold. In *Hypatia*’s case, to determine the coloration of a pixel it checks whether the pixel intersects some boxes of  $\Gamma$ . There are a couple of options for the user here as well. One can choose for example just to color the boxes which hit  $\Gamma'$  and leave the rest white, or to assign different colors to each s.c.c. and color boxes accordingly. Since the picture is a parametrization of a one complex dimensional manifold which does not line up with the axes in  $\mathbb{C}^2$ , a pixel may hit more than one box, and in more than one s.c.c. If the pixel hits more than one s.c.c., it is colored black or gray. One more option allows the user to slightly lighten the pixels which are heuristically found to be in  $K^+$ . That is, the center point of the pixel is iterated some large number of times, like 100, and if after that it is still inside  $V$ , it is guessed to be in  $K^+$ . In this way one can check visually how close the cover is to  $J$ . Figures 4.1, 4.2, 4.3 and 4.4 are examples of covers of  $J$  with each s.c.c. colored differently (shades of gray), and an approximation to  $K^+$  lightened.

Once one is satisfied with the cover of  $J$  (for example, if there is a sink, and it seems the sink s.c.c. is separate from the Julia set s.c.c.), it is time to begin box-hyperbolicity testing. Here also there are options. The first step is always to set the unstable/stable directions,  $\{\mathbf{u}_k/\mathbf{s}_k\}$ , in each box  $B_k$ . Recall (from Section 4.2.1) that these are some forward/backward image under  $DH$  of the unstable/stable eigenvector of  $D_p H$  for the saddle fixed point,  $p$ . Before we ask *Hypatia* to try and define a metric on the unstable/stable directions, we may ask it to take some measurements on these directions, to get an idea of whether it might be possible for *Hypatia* to prove box-hyperbolicity using these directions.

In order to measure the difference between directions, i.e., complex lines in  $\mathbb{C}^2$ , we use the spherical metric of Definition 4.3.3.

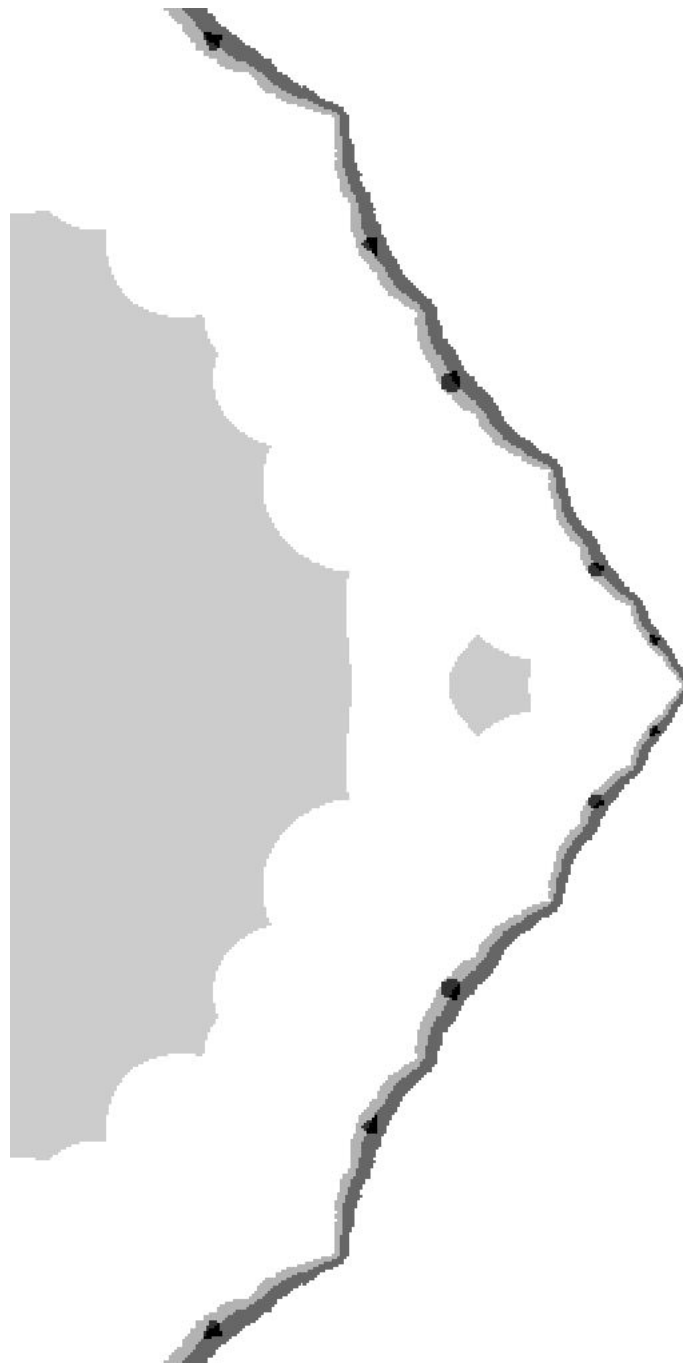


Figure 4.1: A box cover of  $\mathcal{R}$  ( $= J$  and a fixed sink) for  $H_{a,c}$ ,  $c = -.3$ ,  $a = .1$ , for a  $(2^7)^4$  grid on  $V$ . The lighter band on the cover of  $J$  is approximately  $K^+$ . The darkest spots in the cover of  $J$  show another s.c.c.  $H$  is box-hyperbolic on this cover of  $J$ .

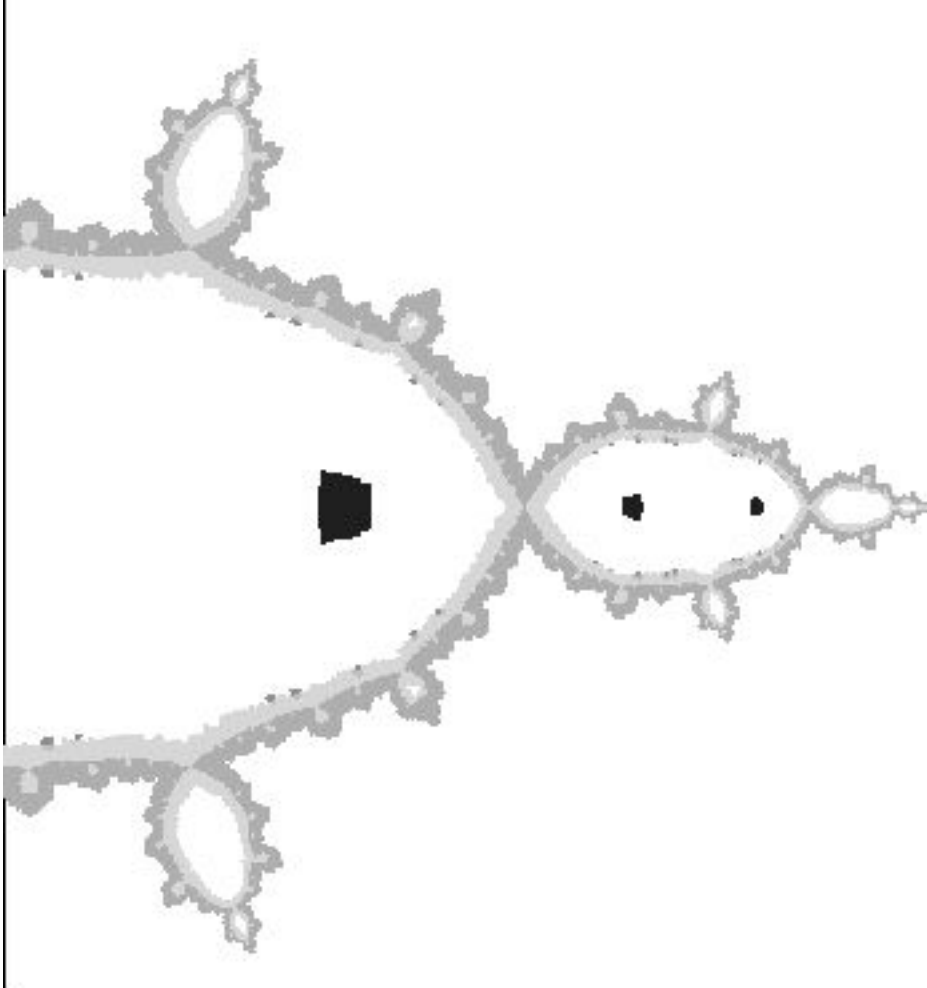


Figure 4.2: A box cover of  $\mathcal{R}$  ( $= J$  and a period 2 sink) for  $H_{a,c}, c = -1.05, a = .05$ , for boxes of side length  $2R/2^7$  and  $2R/2^8$ . Two-tone shading on the cover of  $J$  illustrates approximately where  $J$  lies. Note the s.c.c.'s skirting the inner edge of the cover of  $J$ , which would not be present for smaller box size. *Hypatia* could not verify box-hyperbolicity of  $H$  on this cover of  $J$ .

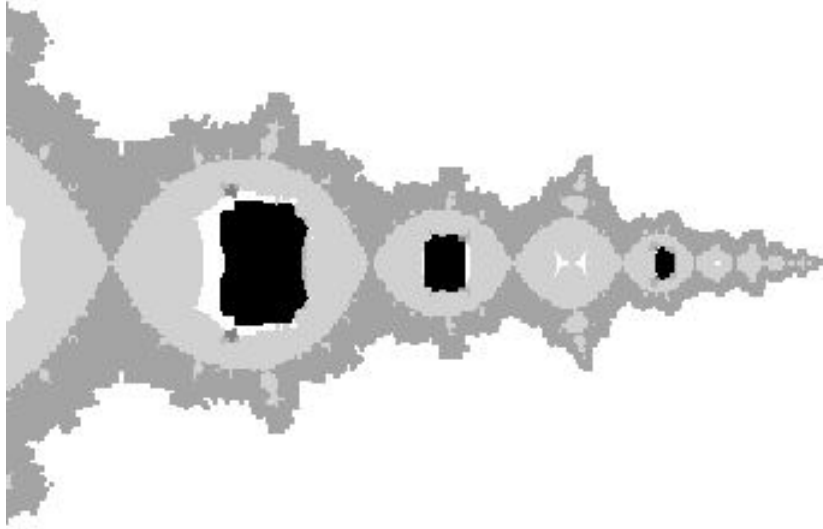


Figure 4.3: A box cover of  $\mathcal{R}$  ( $= J$  and a period 2 sink) for  $H_{a,c}$ ,  $c = -1.1875$ ,  $a = .15$ , for boxes of side length  $2R/2^6$  and  $2R/2^7$ . Two-tone shading on the cover approximately illustrates  $J$ . This is the simplest cover which has separation of  $J$  from the sink.  $H$  is not box-hyperbolic on this cover.

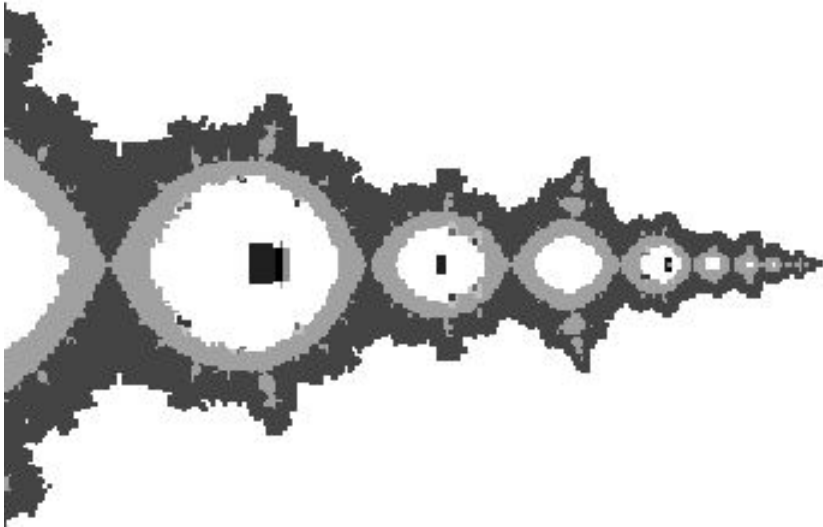


Figure 4.4: This box cover is a partial refinement of Figure 4.3.  $H$  is not box-hyperbolic on this cover of  $J$ .

To examine how suitable the directions  $\{\mathbf{u}_k, \mathbf{s}_k\}$  are in each box, we use:

**Definition 4.4.1.** For each box  $B_k$  in  $\mathcal{V}$ , let

$$\begin{aligned} \text{Udiam}[k] &= \text{diam}_\sigma\{D_{z_j}H(\mathbf{u}_j): \text{there is an edge } B_j \rightarrow B_k\}, \text{ and} \\ \text{Sdiam}[k] &= \text{diam}_\sigma\{[D_{z_j}H]^{-1}(\mathbf{s}_j): \text{there is an edge } B_k \rightarrow B_j\}, \end{aligned}$$

where  $z_j$  is the center point of box  $B_j$ .

We do not measure the variation within one box, *i.e.*, between  $D_zH$  and  $D_{z_j}H$  for different  $z$  in box  $B_j$ , since it seems that would be much smaller than among images from different boxes.

Propositions 4.2.1 and 4.2.2 suggest that a clear separation between  $\text{Udiam}[k]$  and  $\text{Sdiam}[k]$  is needed in order for a computer program to verify cone preservation under  $DH$ , thus we must have

$$\sigma(\mathbf{u}_k, \mathbf{s}_k) - (\text{Udiam}[k] + \text{Sdiam}[k]) > 0$$

in each box  $B_k$  in order for it to be possible for *Hypatia* to prove box-hyperbolicity using these directions. Figures 4.5 and 4.6 illustrate examples of covers for which  $J$  is separate from the sinks, but the directions are unsatisfactory since there are boxes  $B_k$  such that  $\sigma(\mathbf{u}_k, \mathbf{s}_k) - (\text{Udiam}[k] + \text{Sdiam}[k]) < 0$ . Boxes with this value negative are colored black, otherwise shades of gray, with the lightest gray the most positive. A precise legend for the shading is given in Figure 4.7.

After seemingly satisfactory directions are found, the next step of *Hypatia* is to attempt to build a metric with respect to which  $DH$  is expanding (contracting) by  $L$  ( $M$ ) on the unstable (stable) directions. There are two options on how to set the metric constants (as mentioned in Section 4.2.2). We recommend the first option in the case of a diffeomorphism conjugate to the inverse limit of a polynomial map with connected Julia set. In this case, the Jacobian determinant  $a$  is small and strong contraction is expected. In this case, first find a good  $M$  using simple bisection. This tend to runs fairly quickly in such cases. Then try inputting  $L = |a|/M$ , and test whether the unstable directions are box-expansive by this  $L$ . If so, *Hypatia* will test for cone preservation and expansion (as described in Section 4.3.1). Thus, here we are setting the stable and unstable metric constants in each box independent of one another. We use this method successfully in Examples 4.4.2 and 4.4.3.

An alternative, which seems could be appropriate for more general Hénon diffeomorphisms, is to first find a good  $L$  with bisection or **CheckCycles**, and then define stable metric constants in terms of the unstable metric constants and the determinant of  $DH$  (as described in Section 4.2.2). Then it seems the first likely way to increase the chance of proving box-hyperbolicity is to find the best working  $L$  to a high precision.

After successfully building a metric on the unstable/stable directions, *Hypatia* tests for cone preservation and expansion using Proposition 4.3.1 and the Hermitian

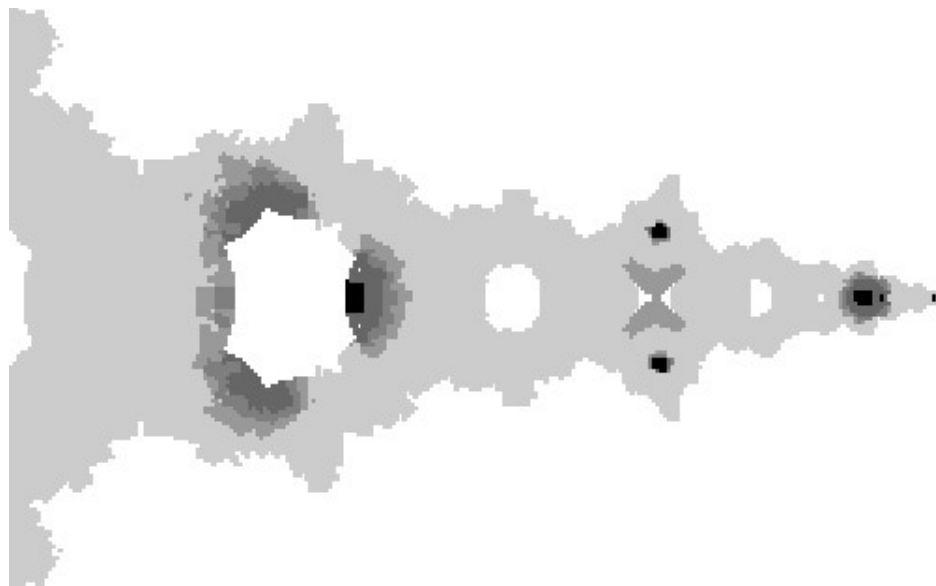


Figure 4.5: A box cover of  $J$  for  $H_{a,c}, c = -1.1875, a = .15$ , boxes of side length  $2R/2^6, 2R/2^7$ . Black boxes are definite obstacles to cone definition. Dark gray boxes could prevent cone definition.

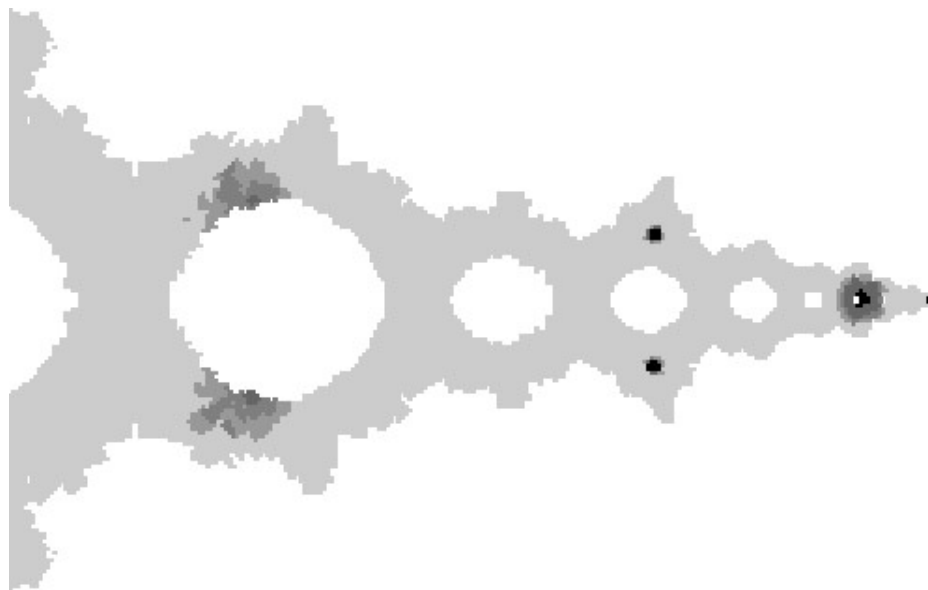


Figure 4.6: A refinement of Figure 4.5. The black and dark gray regions are smaller; however, these spots still exist, preventing reasonable cones.

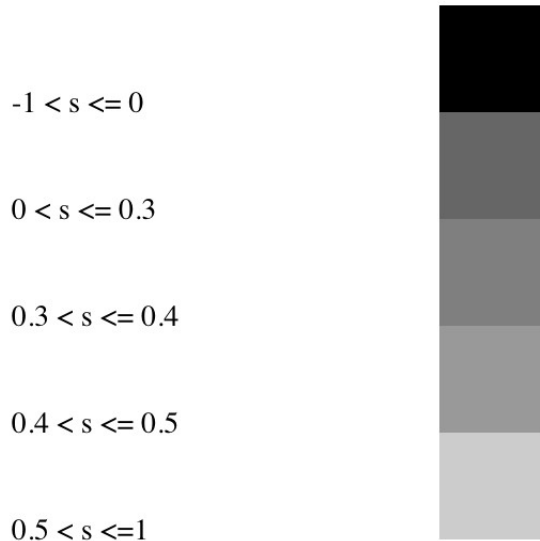


Figure 4.7: Legend for the shading of Figures 4.5 and 4.6,  $s = \sigma(\mathbf{u}_k, \mathbf{s}_k) - (\text{Udiam}[k] + \text{Sdiam}[k])$ . Dark corresponds to obstructions to defining a cone field preserved by  $Df$ .

forms defined in Section 4.2.3. Since the ratio of the metric constants determines the angle width of the cones, even if  $[\sigma(\mathbf{u}_k, \mathbf{s}_k) - (\text{Udiam}[k] + \text{Sdiam}[k])]$  is bounded away from 0, if the constants  $c_k^u$  and  $c_k^s$  are several orders of magnitude different then the cones will be very thin, thus difficult for the computer to work with. This reiterates the need to find good values of  $L$  and  $M$  to give get a reasonable pair of constants in each box. Figure 4.8 illustrates the many boxes in which the cone check failed for an example in which  $\min_k \{\sigma(\mathbf{u}_k, \mathbf{s}_k) - (\text{Udiam}[k] + \text{Sdiam}[k])\} > 0.1$ .

It is theoretically possible to use **BetterMetric** (Section 3.5.2) to improve the metric on the unstable and/or stable directions, with the hopes that the resulting cones would be more robust. However, in practice for a large graph this runs pretty slowly (on average, fixing one edge multiplier per minute). Thus it would take much longer than our patience would hold in order to improve a metric considerably (examine one dimensional example of **BetterMetric** in Section 3.6). However, after **BetterMetric** runs, it marks the boxes in the weakest cycles found, which could be useful for later subdividing procedure We discuss this further in Example 4.4.4.

After testing box-hyperbolicity and gathering the corresponding data, if the cone check fails the user has several options for choosing which boxes to subdivide, including many uses of the data collected in the box-hyperbolicity test:

1. All boxes, or
2. **Option B**: boxes seemingly in sink basin (evals. of  $D_{z_m} H \circ D_{z_{m-1}} H \circ \dots \circ D_{z_0} H$  less than one), or

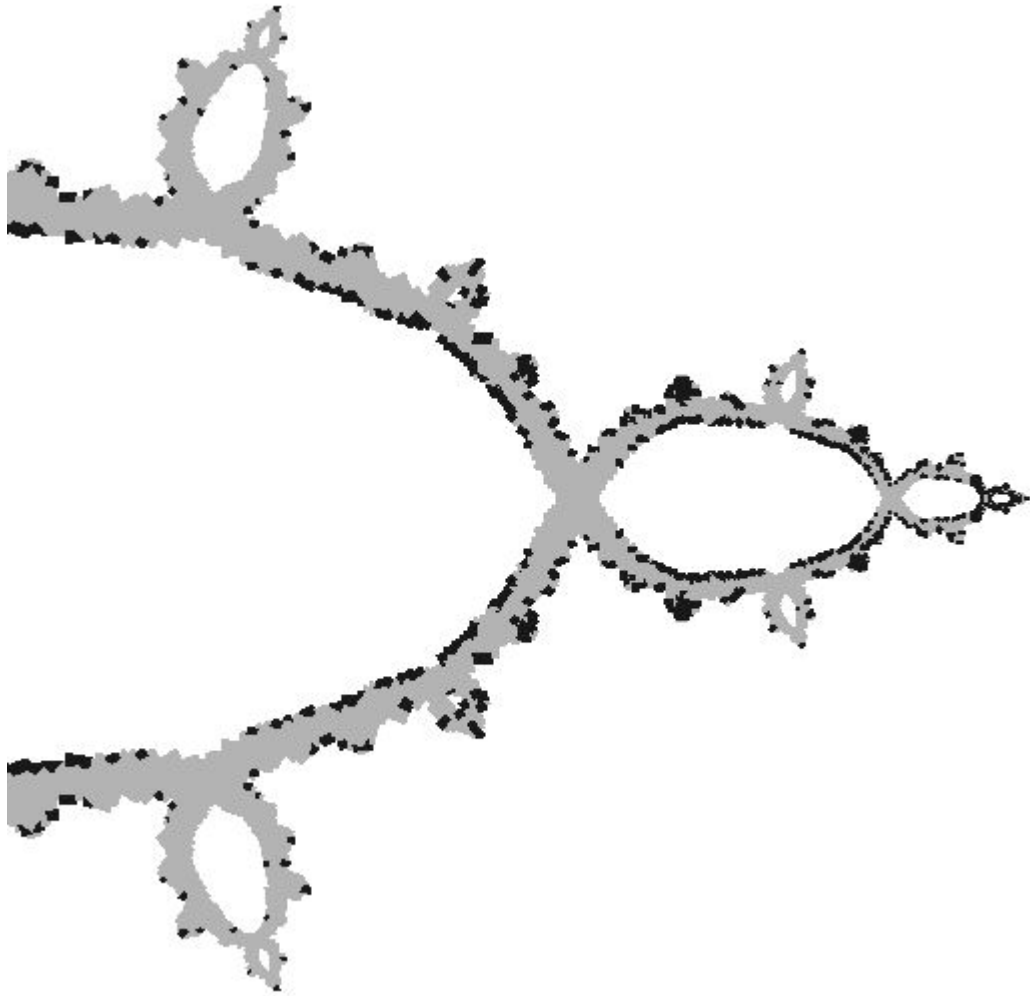


Figure 4.8: The darkest shading in this box cover shows the boxes in which the cone condition failed,  $H_{a,c}$ ,  $c = -1.05$ ,  $a = .05$ , for boxes of side length  $2R/2^7$  and  $2R/2^8$ .

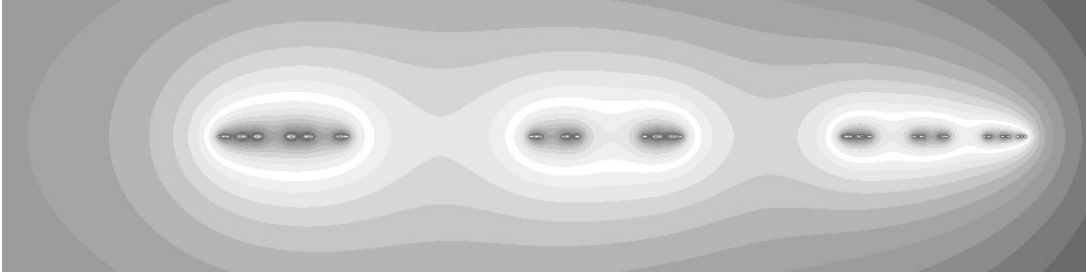


Figure 4.9: A FractalAsm picture of  $W_p^u \cap K^+$  for  $H_{a,c}$ ,  $c = -3$ ,  $a = -.25$

3. Boxes with  $(\text{Udiam}[k] < D)$  and/or  $(\text{Sdiam}[k] < D)$ , *e.g.*,  $D = .25$ , and/or
4. Boxes with  $[\sigma(\mathbf{u}_k, \mathbf{s}_k) - (\text{Udiam}[k] + \text{Sdiam}[k])] < \delta$ , *e.g.*,  $\delta = 0$ , and/or
5. Boxes in which the cone check failed, and/or
6. Boxes found in weak cycles by **BetterMetric**.

#### 4.4.2 Box-hyperbolic Hénon diffeomorphisms

In this section we give detailed data on examples for which *Hypatia* proved box-hyperbolicity. Recall  $V = \mathcal{N}_\infty(0, R'_{a,c})$  is a box neighborhood of 0 which contains the chain recurrent set,  $\mathcal{R}$ .

**Example 4.4.2.** The Hénon diffeomorphism  $H_{a,c}$  with  $c = -.3$ ,  $a = .1$  has an attracting fixed point. *Hypatia* proved that this diffeomorphism is hyperbolic, by using a cover of  $J$  from an evenly subdivided  $(2^7)^4$  grid on  $V$ , finding  $M$  first with bisection, then using  $L = |a|/M$ . Figure 4.1 is the box-hyperbolic cover. See Table 4.1 for all of the data for this example.

**Example 4.4.3.** The Hénon diffeomorphism  $H_{a,c}$  with  $c = -3$ ,  $a = -.25$  is a real horseshoe, *i.e.*, the Julia set is a Cantor set and  $H_{a,c}|_J$  is conjugate to the full 2-shift. *Hypatia* proved this diffeomorphism is hyperbolic, by using a cover of  $J$  from an evenly subdivided  $(2^7)^4$  grid on  $V$ , finding  $M$  first with bisection then using  $L = |a|/M$ . Figure 4.9 is a FractalAsm picture. This kind of picture is really the best to see a Cantor set. See Table 4.1 for all the data for this example.

#### 4.4.3 Describing box covers which are not box-hyperbolic

Next we examine some examples which *Hypatia* cannot show are box-hyperbolic. In some cases, the finest box cover we could compute using current computer resources is not box-hyperbolic due to the dynamical obstructions of Propositions 4.2.1 and 4.2.2. In other examples, there are no obvious obstructions, but

Table 4.1: Data from verifying hyperbolicity with *Hypatia*.

params.	$c$	−.3	−3
	$a$	.1	−.25
sink period		1	N/A (horseshoe)
box size		$1.43/2^6 = 0.022$	$2.57/2^6 = 0.04$
# $\Upsilon$ boxes (1000s)	original	245	20
	V-ck. kills	187	15
$\Upsilon$ size (1000s)	boxes	59	4
	edges	2,300	120
$\Gamma'$ size (1000s)	boxes	32	2.4
	edges	1,250	75
$\sigma(\mathbf{u}, \mathbf{s})$ (in $[0, \pi/2]$ )	min.	0.94	0.6
	avg.	1.09	1.2
Udiam (in $[0, \pi/2]$ )	max.	0.015	0.13
	avg.	0.03	0.023
Sdiam (in $[0, \pi/2]$ )	max.	0.0008	0.11
	avg.	0.0003	0.01
$\sigma(\mathbf{u}, \mathbf{s}) - (\text{Udiam} + \text{Sdiam})$ (in $[0, \pi/2]$ )	min.	0.9	0.47
	avg.	1.07	1.15
$M$	(bisection)	0.05957	0.111328
$c_k^s$ (in $(0, 1]$ )	min.	0.034	0.046
	avg.	0.152	0.096
$L$	(= $ a /M$ )	1.67869	2
$c_k^u$ (in $(0, 1]$ )	min.	0.072	0.033
	avg.	0.158	0.09
box-hyp?		YES	YES
runtime (minutes)		30	< 1
memory used (MB)		220	20

Table 4.2: Data on subdivision for Example 4.4.4.

params.	$c$	-1.05
	$a$	0.05
sink period		2
box size		$1.78/2^6 = 0.03,$ $1.78/2^7 = 0.016$
# $\Upsilon$ boxes (1000s)	original	570
	V-ck. kills	432
$\Upsilon$ size (1000s)	boxes	141
	edges	5,000
$\Gamma'$ size (1000s)	boxes	88
	edges	3,150
runtime thus far (minutes)		12
memory used thus far (MB)		500

still the box cone field constructed by *Hypatia* is not preserved by  $Df$ . In this latter case, we explain a few questions whose answers might help in constructing a cover which is more likely to be box-hyperbolic.

**Example 4.4.4.** The Hénon diffeomorphism  $H_{a,c}$  with  $c = -1.05, a = .05$  appears to be conjugate to the inverse limit of the basilica ( $c = -1$ ), so has a period two sink. Separating the sink from  $J$  required a  $(2^7)^4$  grid on  $V = \mathcal{N}_\infty(0, 1.78)$  if uniformly subdividing the boxes. Alternatively, subdividing uniformly up to a  $(2^6)^4$  grid and then invoking **Option B** (to subdivide only boxes seeming to be in the sink basin) also separated the sink from  $J$ , and used much less memory (about half). After this, we went one step further and had the program (uniformly) subdivide once more all of the boxes in the cover of  $J$ . Shorthand for this choice of subdividing is:

Refine:  $n = 6$ , **Option B** ( $n = 1, m = 2$ ),  $n = 1$ .

Figure 4.2 shows the s.c.c.'s created with this subdivision procedure. Table 4.2 contains the data on the s.c.c.'s.

The program then computed statistics on the directions  $\{\mathbf{u}_k, \mathbf{s}_k\}$ , which are given in Table 4.3. From this data we see there is a definite separation between the directions.

Thus, we next tested box-hyperbolicity for this box cover. First, we tried the option of finding a good  $M$  with bisection, then testing  $L = |a|/M$ . Both metrics

Table 4.3: Data on stable/unstable directions for Example 4.4.4.

params.	$c$	-1.05
	$a$	0.05
$\sigma(\mathbf{u}, \mathbf{s})$ (in $[0, \pi/2]$ )	min.	0.51
	avg.	0.99
Udiam (in $[0, \pi/2]$ )	max.	0.1
	avg.	0.018
Sdiam (in $[0, \pi/2]$ )	max.	0.018
	avg.	0.0023
$\sigma(\mathbf{u}, \mathbf{s}) - (\text{Udiam} + \text{Sdiam})$ (in $[0, \pi/2]$ )	min.	0.44
	avg.	0.97
runtime thus far (minutes)		23
memory used thus far (MB)		530

build successfully, but unfortunately, the cone check failed on (less than) 2% of the edges. Figure 4.8 shows the box cover, with dark shading on the boxes where the cone check failed. Table 4.4 contains the data for the metrics and cone check.

Note that most of the memory usage is for computing s.c.c.'s, while most of runtime is for hyperbolicity testing.

We then tried the alternative to defining the metric constants, in which a good  $L$  is found first, then the stable metric is defined in terms of the unstable metric and the directions:  $c_k^s = |\det[\mathbf{u}_k \ \mathbf{s}_k]| / c_k^u$ . However, this failed dramatically. The unstable directions failed to be box-expansive by  $L = 1.19771$ . The directions were box-expansive by  $L = 1.19770$ , but this defined stable and unstable constants such that the minimum ratio  $c_k^u / c_k^s$  was  $8.7 \times 10^{-7}$ . The cone check failed on nearly every edge. We are perplexed that this method defines such thin cones. Intuitively, it seems more reasonable than defining the metrics independently, at least in the case of small Udiam and Sdiam.

**Question:** Why does the method for defining stable metric constants in terms of the other information produce such extreme cones? Can it be fixed?

In an attempt to improve the metric, we ran **BetterMetric** on this cover, just trying  $L_1 = 1.2$ . After about nine hours, it had still not successfully built a better metric, and had fixed 300 edge multipliers. Figure 4.10 is a picture of which boxes were in these weakest cycles. The placement of these boxes in the picture raises some interesting questions. Recall that a Hénon diffeomorphism has two fixed points, and since this parameter has simply a period two sink, it has two

Table 4.4: Data on first metric and cones for Example 4.4.4.

params.	$c$	-1.05
	$a$	0.05
$M$	(bisection)	0.041992
$c_k^s$ (in $(0, 1]$ )	min.	$9.5 \times 10^{-5}$
	avg.	0.004
$L$	(= $ a /M$ )	1.1907
$c_k^u$ (in $(0, 1]$ )	min.	$8.4 \times 10^{-4}$
	avg.	0.012
box-hyp?		NO
cone check failed (1000s)	boxes	9 (out of 88)
	edges	53 (out of 3,500)
runtime (minutes)		45
memory used (MB)		530

saddle fixed points. The “pinch” points of the Julia set in this unstable manifold picture are precisely the points which also lie in the stable manifold for the other saddle fixed point. Notice these boxes of weakest unstable direction expansion are those near the sink basin and the stable manifold of the other saddle fixed point. *Hypatia*’s algorithm used the first saddle fixed point’s eigenvectors to determine the unstable and stable directions  $\{\mathbf{u}_k, \mathbf{s}_k\}$ . Thus perhaps this did not create ideal conditions for points near the other saddle fixed point. However, consulting Figure 4.8 shows that the cone check did succeed in this area. We wonder:

**Question.** Will developing a method to use both saddle points information improve likelihood of box-hyperbolicity?

**Example 4.4.5.** Recall the Hénon diffeomorphism  $H_{a,c}, c = -1.1875, a = .15$  of Example 1.3.19. It appears to be hyperbolic with a period two attracting cycle, but not exhibit one dimensional behavior.

We found the quickest subdivision procedure to separate the sink from  $J$  was to:

Refine:  $n = 6$ , **Option B** ( $n = 1, m = 5$ ).

Figure 4.3 shows the s.c.c.’s created with this subdivision procedure. Table 4.5 gives the data for this cover.

The program then computed the statistics on the directions  $\{\mathbf{u}_k, \mathbf{s}_k\}$ , given in Table 4.3, and we see this data is quite unsatisfactory, with a large maximum

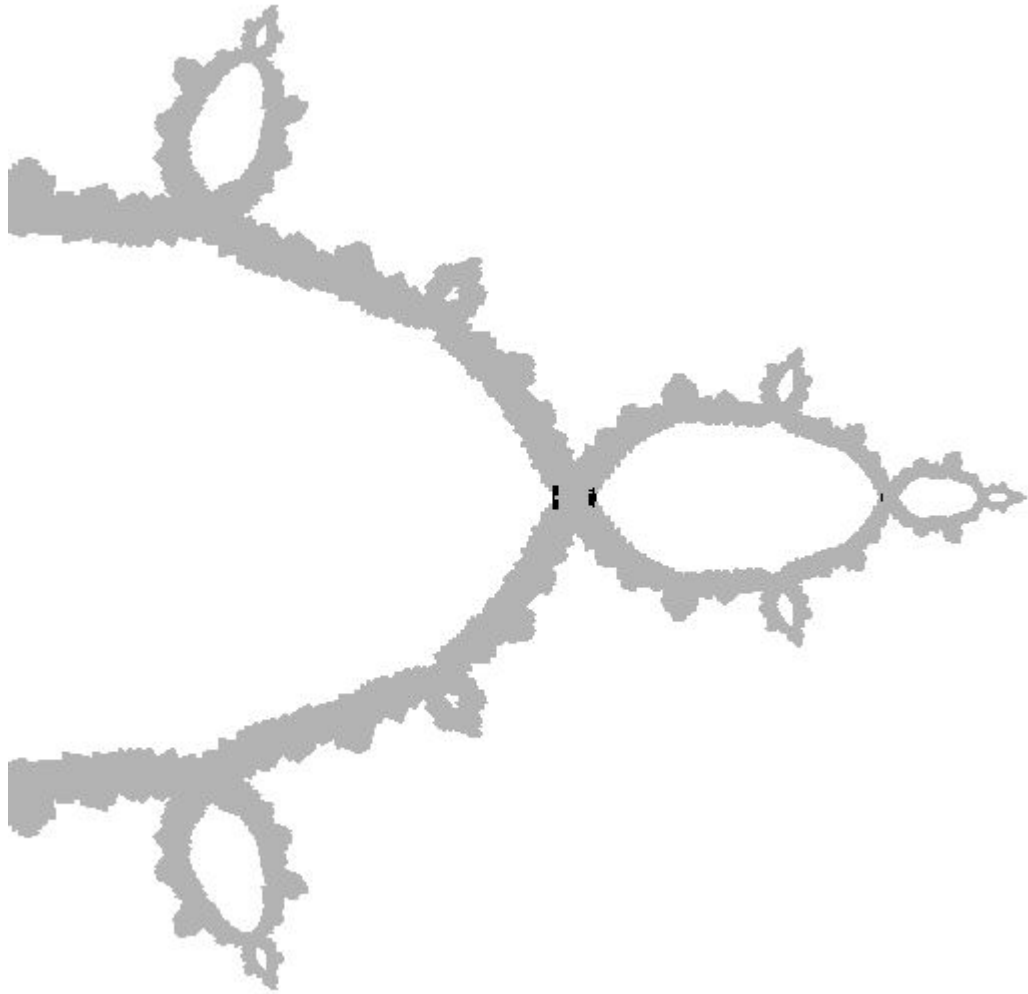


Figure 4.10: The darkest shading in this box cover shows boxes  $B_k$  in cycles with the weakest expansion on the unstable directions,  $\{\mathbf{u}_k\}$ , for  $H_{a,c}, c = -1.05, a = .05$ , with boxes of side length  $2R/2^7$  and  $2R/2^8$ .

Table 4.5: Data on subdivision for Example 4.4.5.

params.	$c$	-1.1875	
	$a$	0.15	
sink period		2	
box size		$1.9/2^5 = 0.06,$	$1.9/2^6 = 0.03,$
		$1.9/2^6 = 0.03$	$1.9/2^7 = 0.015$
# $\Upsilon$ boxes (1000s)	original	184	682
	V-ck. kills	116	417
$\Upsilon$ size (1000s)	boxes	68	265
	edges	2,500	12,400
$\Gamma'$ size (1000s)	boxes	53	182
	edges	2,500	7,800

Sdiam, and a  $\sigma(\mathbf{u}, \mathbf{s}) - (\text{Udiam} + \text{Sdiam})$  as small as  $-1.3$ . Figure 4.5 is shaded to illustrate  $\sigma(\mathbf{u}, \mathbf{s}) - (\text{Udiam} + \text{Sdiam})$  for each box.

It appears that the most worrisome places are in the sink basin, thus we had the program subdivide again with **Option B** ( $n = 1, m = 5$ ). Figure 4.4 shows this finer box cover, and Table 4.5 gives some data for the cover. The program computed the unstable and directions and their statistics, given in Table 4.6, but unfortunately, we see that there are still many boxes in this cover with  $\sigma(\mathbf{u}, \mathbf{s}) - (\text{Udiam} + \text{Sdiam})$  negative. *Thus by Propositions 4.2.1 and 4.2.2, the map is not box-hyperbolic on this cover.*

Figure 4.6 is shaded to illustrate  $\sigma(\mathbf{u}, \mathbf{s}) - (\text{Udiam} + \text{Sdiam})$  for each box in this cover.

**Question** What selective subdivision procedure would be most effective for eliminating boxes in which  $\sigma(\mathbf{u}, \mathbf{s}) - (\text{Udiam} + \text{Sdiam}) < 0$ ?

**Example 4.4.6.** Another type of diffeomorphism from our list of motivating examples, Example 1.3.21, is a horseshoe. It seems rather difficult to find a horseshoe not in the range of Theorem 1.3.18 which is in a large region of stability (thus robust and easier to compute). Using the program SaddleDrop for exploration, Hubbard and Papadantonakis suggest the example  $H_{a,c}$ ,  $c = -3.5$ ,  $a = .57$  ([1]).

We tested this diffeomorphism with *Hypatia*, and the results were quite similar to Example 4.4.5, *i.e.*, bad direction statistics. Though the previous examples only had bad Sdiam, whereas this example seems to have bad Udiam as well as Sdiam. *So again by Propositions 4.2.1 and 4.2.2, the map is not box-hyperbolic on this cover.*

Table 4.6: Data on stable/unstable directions for Example 4.4.5.

params.	$c$	-1.1875	
	$a$	0.15	
box size		$1.9/2^5 = 0.06,$ $1.9/2^6 = 0.03$	$1.9/2^6 = 0.03,$ $1.9/2^7 = 0.015$
$\sigma(\mathbf{u}, \mathbf{s})$ (in $[0, \pi/2]$ )	min.	0.04	0.044
	avg.	0.94	0.92
Udiam (in $[0, \pi/2]$ )	max.	0.55	0.42
	avg.	0.055	0.03
Sdiam (in $[0, \pi/2]$ )	max.	1.55	1.53
	avg.	0.023	0.011
$\sigma(\mathbf{u}, \mathbf{s}) - (\text{Udiam} + \text{Sdiam})$ (in $[0, \pi/2]$ )	min.	-1.31	-0.71
	avg.	0.86	0.88
runtime (minutes)			55
memory used (MB)			900

Table 4.7: Data on subdivision for Example 4.4.6.

params.	$c$	-3.5	
	$a$	-.57	
sink period		N/A (horseshoe)	
box size		$2.9/2^7 = 0.022,$	$2.9/2^8 = 0.011,$
# $\Upsilon$ boxes (1000s)	original	200	457
	V-ck. kills	141	315
$\Upsilon$ size (1000s)	boxes	59	142
	edges	2,600	6,500
$\Gamma'$ size (1000s)	boxes	29	63
	edges	1,300	3,000

For horseshoe diffeomorphisms, there is no sink. Thus there are fewer options for selective subdivision. To study this diffeomorphism, we simply had the program uniformly subdivide the boxes, testing first a  $(2^8)^4$  grid on  $V = \mathcal{N}_\infty(0, 2.9)$ , then a  $(2^9)^4$  grid.

Table 4.7 contains the data on the s.c.c.'s for both box covers. Table 4.8 contains the data on the directions for both covers.

**Question.** What is the most effective selective subdivision procedure for a horseshoe Hénon diffeomorphism?

For comparison purposes, Table 4.9 lists side by side all the data for the smallest box level tested for the diffeomorphisms of Examples 4.4.5 and 4.4.6.

Table 4.8: Data on stable/unstable directions for Example 4.4.6.

params.	$c$	-3.5	
	$a$	-.57	
box size		$2.9/2^7 = 0.022,$	$2.9/2^8 = 0.011,$
$\sigma(\mathbf{u}, \mathbf{s})$ (in $[0, \pi/2]$ )	min.	0.014	0.008
	avg.	1.04	1.06
Udiam (in $[0, \pi/2]$ )	max.	1.47	1.5
	avg.	0.033	0.018
Sdiam (in $[0, \pi/2]$ )	max.	1.1	1.52
	avg.	0.043	0.311
$\sigma(\mathbf{u}, \mathbf{s}) - (\text{Udiam} + \text{Sdiam})$ (in $[0, \pi/2]$ )	min.	-.72	-0.95
	avg.	0.97	1.01
runtime (minutes)			24
memory used (MB)			700

Table 4.9: Data comparing Examples 4.4.5 and 4.4.6.

params.	$c$	-1.1875	-3.5
	$a$	0.15	-.57
sink period		2	N/A (horseshoe)
box size		$1.9/2^7 = 0.015$ , $1.9/2^8 = 0.00075$	$2.9/2^9 = 0.0057$ ,
# $\Upsilon$ boxes (1000s)	original	682	457
	V-ck. kills	417	315
$\Upsilon$ size (1000s)	boxes	265	142
	edges	12,400	6,500
$\Gamma'$ size (1000s)	boxes	182	63
	edges	7,800	3,000
$\sigma(\mathbf{u}, \mathbf{s})$ (in $[0, \pi/2]$ )	min.	0.044	0.008
	avg.	0.94	1.06
Udiam (in $[0, \pi/2]$ )	max.	0.42	1.5
	avg.	0.03	0.018
Sdiam (in $[0, \pi/2]$ )	max.	1.55	1.52
	avg.	0.023	0.311
$\sigma(\mathbf{u}, \mathbf{s}) - (\text{Udiam} + \text{Sdiam})$ (in $[0, \pi/2]$ )	min.	-.71	-0.95
	avg.	0.88	1.01
runtime (minutes)		55	24
memory used (MB)		900	700

# Chapter 5

## Analysis of *Hypatia's* performance

In this chapter, we reflect on the process of using a computer to study the chain recurrent set. In the first section we compute estimates, in the case of a Hénon diffeomorphism with fixed sink, showing for what box size we can guarantee separation between the box-chain transitive components for the sink and  $J$ . We give a conclusion for the thesis in Section 5.2.

### 5.1 Separating $J$ from a fixed sink

Throughout this section, let  $H$  be a Hénon diffeomorphism,  $H(x, y) = (x^2 + c - ay, x)$ , with an attracting fixed point  $p = (z, z)$ . Our goal is to quantify box size needed to get the fixed sink in a separate s.c.c. from  $J$ , which we reach in Proposition 5.1.10. This quantification will be in terms of  $a, c$ , and the eigenvalues,  $\lambda_1 \neq \lambda_2$ , of  $D_p H$ , and  $\lambda = \max(\lambda_1, \lambda_2)$ .

The example that motivates this analysis is:

**Example 5.1.1 (The 3-1 map).** Recall that the Hénon map with  $c = -1.17, a = .3$  is an interesting example because it appears to have has two attracting periodic cycles, one of period three and one of period one. This is not a phenomenon which appears in  $z^2 + c$ . Unfortunately, we could not even begin hyperbolicity testing on this map with *Hypatia*, because the algorithm to find the box cover failed to separate the sinks from  $J$  before running out of the 4 GB of RAM available on our computer.

In an attempt to find a good cover, we used our program to uniformly subdivide all boxes to obtain a  $(2^7)^4$  grid on  $V$ , with box side length  $2R/2^7 = 0.03$ . Then we used Option B, which subdivided about half of the boxes, presumably those closest to the sinks. At this point, the smallest boxes had side length  $2R/2^8 = 0.015$ . The s.c.c. graph  $\Gamma$  was composed of 944,000 boxes and 66,500,000 edges. This used approximately 3.2 GB of RAM, thus it seemed we could not subdivide significantly farther.

We also tried uniformly subdividing to obtain a  $(2^6)^4$  grid on  $V$ , then invoking Option B twice, to get some boxes as small as above. However, this did not significantly decrease the amount of memory used.

Shown in Figure 5.1 is the unstable manifold slice of the cover for a  $(2^7)^4$  grid on  $V$ . We were initially surprised that we could not achieve this separation. This example is what motivated the estimates of this section.

First we find a euclidean disk lying in the sink basin, to prove Proposition 5.1.7. Second, we quantify where a region exists near the sink containing non  $\epsilon$ -chain recurrent points, yielding Proposition 5.1.9. We use this to derive Proposition 5.1.10, calculating a bound on the side length of boxes in the cover such that if boxes are

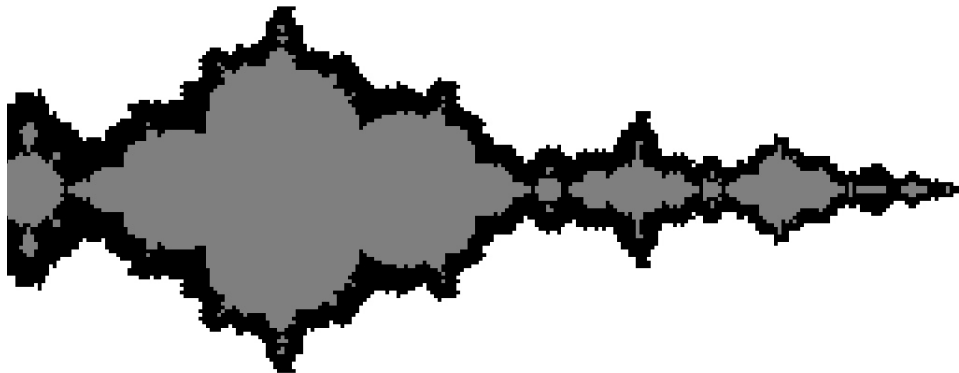


Figure 5.1: A box cover of  $\mathcal{R}$  for  $H_{a,c}$ ,  $c = -1.17$ ,  $a = .3$ , boxes of side length  $2R/2^7$  and  $2R/2^8$ . Lighter gray is approximately in  $K^+$ .

smaller than this bound, then the s.c.c for the fixed sink and the s.c.c. for  $J$  will be different. Finally, we apply our estimates to the 3-1 map.

## A dynamically significant norm

To quantify the dynamical notations of interest, we need to start with a metric which respects the dynamics.

**Definition 5.1.2.** Note the Jacobian is

$$D_p H = \begin{bmatrix} 2z & -a \\ 1 & 0 \end{bmatrix}$$

Suppose  $\lambda_1 \neq \lambda_2$  are the eigenvalues of  $D_z H$ . Let  $\lambda = \max(|\lambda_1|, |\lambda_2|)$ . Note that since  $p$  is a fixed sink,  $|\lambda| < 1$ . Let  $\mathcal{W} = \{\mathbf{v}_1, \mathbf{v}_2\}$  be the basis of eigenvectors, where we choose  $\mathbf{v}_j = (\lambda_j, 1)$ . Then  $\mathbf{A} = [\mathbf{v}_1 \ \mathbf{v}_2]$  is the change of basis matrix, *i.e.*, if  $\{\mathbf{e}_1, \mathbf{e}_2\}$  is the standard basis in  $\mathbb{C}^2$ , then  $\mathbf{A}\mathbf{e}_j = \mathbf{v}_j$ . Let  $\|\cdot\|_e$  be the euclidean norm in  $\mathbb{C}^2$ . Define the norm  $\|\cdot\|_{\mathcal{W}}$  by

$$\|\mathbf{u}\|_{\mathcal{W}} = \|\mathbf{A}^{-1}\mathbf{u}\|_e.$$

We show below that  $H$  is contracting with respect to  $\|\cdot\|_{\mathcal{W}}$  in a neighborhood of  $p$ .

First, we show this metric is uniformly equivalent to euclidean, and compute the constants of equivalence.

**Lemma 5.1.3.** For all  $\mathbf{u} \in \mathbb{C}^2$ ,

$$C \|\mathbf{u}\|_{\mathcal{W}} \leq \|\mathbf{u}\|_e \leq D \|\mathbf{u}\|_{\mathcal{W}},$$

where  $C, D$  are positive constants given by

$$C = \frac{|\lambda_1 - \lambda_2|}{\sqrt{2 + |\lambda_1| + |\lambda_2|}}, \quad D = \sqrt{2 + |a| + \lambda^2}.$$

*Proof.* First, we compute  $C$ . Since we chose eigenvectors  $\mathbf{v}_j = (\lambda_j, 1)$ , we have

$$\mathbf{A} = \begin{bmatrix} \lambda_1 & \lambda_2 \\ 1 & 1 \end{bmatrix}, \quad \text{and} \quad \mathbf{A}^{-1} = \frac{1}{\lambda_1 - \lambda_2} \begin{bmatrix} 1 & -\lambda_2 \\ -1 & \lambda_1 \end{bmatrix}.$$

Now let  $(x, y)$  be any vector in  $\mathbb{C}^2$ . Then

$$\left\| \begin{bmatrix} x \\ y \end{bmatrix} \right\|_{\mathcal{W}} = \left\| \mathbf{A}^{-1} \begin{bmatrix} x \\ y \end{bmatrix} \right\|_e = \frac{1}{|\lambda_1 - \lambda_2|} (|x - \lambda_2 y|^2 + |-x + \lambda_1 y|^2)^{1/2}.$$

Using the triangle inequality, we get

$$\begin{aligned} |\lambda_1 - \lambda_2|^2 \left\| \mathbf{A}^{-1} \begin{bmatrix} x \\ y \end{bmatrix} \right\|_e^2 &= |x - \lambda_2 y|^2 + |-x + \lambda_1 y|^2 \\ &\leq |x|^2 + |\lambda_2|^2 |y|^2 + 2|x||y||\lambda_2| \\ &\quad + |x|^2 + |\lambda_1|^2 |y|^2 + 2|x||y||\lambda_1|. \end{aligned}$$

Observe the useful bound:

$$0 \leq (|x| - |y|)^2 \quad \text{implies} \quad 2|x||y| \leq |x|^2 + |y|^2. \quad (5.1)$$

Applying this to the above, we get

$$\begin{aligned} |\lambda_1 - \lambda_2|^2 \left\| \mathbf{A}^{-1} \begin{bmatrix} x \\ y \end{bmatrix} \right\|_e^2 &\leq |x|^2 + |\lambda_2|^2 |y|^2 + (|x|^2 + |y|^2) |\lambda_2| \\ &\quad + |x|^2 + |\lambda_1|^2 |y|^2 + (|x|^2 + |y|^2) |\lambda_1| \\ &= |x|^2 (2 + |\lambda_1| + |\lambda_2|) + |y|^2 (|\lambda_1|^2 + |\lambda_2|^2 + |\lambda_1| + |\lambda_2|). \end{aligned}$$

Since the eigenvalues have modulus less than one, we conclude

$$|\lambda_1 - \lambda_2|^2 \left\| \mathbf{A}^{-1} \begin{bmatrix} x \\ y \end{bmatrix} \right\|_e^2 \leq (|x|^2 + |y|^2)(2 + |\lambda_1| + |\lambda_2|).$$

Thus we see that we can set  $C$  by

$$C = \frac{|\lambda_1 - \lambda_2|}{\sqrt{2 + |\lambda_1| + |\lambda_2|}}.$$

Next, we compute  $D$ . We do this in a parallel way to the above, using  $\mathbf{A}$  instead of  $\mathbf{A}^{-1}$ . We want  $D$  so that for all  $(z, w)$  in  $\mathbb{C}^2$ ,  $\|(z, w)\|_e \leq D \|(z, w)\|_{\mathcal{W}}$ . Since

$\mathbf{A}$  is invertible, we can instead consider all  $(x, y) \in \mathbb{C}^2$  and let  $(z, w) = \mathbf{A}(x, y)$ . Then we need  $D$  so that  $\|\mathbf{A}(x, y)\|_e \leq D \|\mathbf{A}(x, y)\|_{\mathcal{W}} = D \|(x, y)\|_e$ .

So let  $(x, y)$  be any vector in  $\mathbb{C}^2$ . Then

$$\left\| \mathbf{A} \begin{bmatrix} x \\ y \end{bmatrix} \right\|_e = (|\lambda_1 x + \lambda_2 y|^2 + |x + y|^2)^{1/2}.$$

Using the triangle inequality again, we get:

$$\left\| \mathbf{A} \begin{bmatrix} x \\ y \end{bmatrix} \right\|_e \leq |\lambda_1|^2 |x|^2 + |\lambda_2|^2 |y|^2 + 2|x||y||\lambda_1||\lambda_2| + |x|^2 + |y|^2 + 2|x||y|.$$

Then using Equation 5.1, we reduce this to:

$$\left\| \mathbf{A} \begin{bmatrix} x \\ y \end{bmatrix} \right\|_e \leq |x|^2 (|\lambda_1|^2 + |\lambda_1||\lambda_2| + 2) + |y|^2 (|\lambda_2|^2 + |\lambda_1||\lambda_2| + 2).$$

Recall we defined  $\lambda = \max(|\lambda_1|, |\lambda_2|)$ . Also, note that  $\det(DH) = a$ , thus  $|\lambda_1||\lambda_2| = |a|$ . Hence, we see we can set  $D$  by:

$$D = \sqrt{2 + |a| + \lambda^2}.$$

□

*Remark.* Since the eigenvectors are  $(\lambda_j, 1)$ , the difference  $|\lambda_1 - \lambda_2|$  is the determinant of  $\mathbf{A}$ . This is small if the angle difference between the eigenvectors is small. In this case,  $C$  captures that the metric is skewed far from euclidean, so only a very small euclidean ball will fit inside a  $\mathcal{W}$ -ball. Note also that  $D$  will be large only when the eigenvalues are large. Thus  $D$  captures the strength of the contraction.

## Estimating the size of the sink basin

Now that we know how to convert between the two norms, we are ready to take some measurements in the sink basin. To do so, we will approximate  $H$  by its linearization at  $p = (z, z)$ . Recall that

$$L_p \begin{bmatrix} x \\ y \end{bmatrix} = H \begin{bmatrix} z \\ z \end{bmatrix} + D_p H \begin{bmatrix} x - z \\ y - z \end{bmatrix} = \begin{bmatrix} z^2 + c - 2z(x - z) - ay \\ x \end{bmatrix}.$$

We first bound the error between  $H$  and  $L_p$  in the  $\mathcal{W}$ -norm.

### Lemma 5.1.4.

$$\text{If } \left\| \begin{bmatrix} x - z \\ y - z \end{bmatrix} \right\|_{\mathcal{W}} = r, \text{ then } \left\| H \begin{bmatrix} x \\ y \end{bmatrix} - L_p \begin{bmatrix} x \\ y \end{bmatrix} \right\|_{\mathcal{W}} \leq r^2 \left( \frac{D^2}{C} \right).$$

*Proof.* Let  $(x, y) \in \mathbb{C}^2$  be such that

$$\left\| \begin{bmatrix} x - z \\ y - z \end{bmatrix} \right\|_{\mathcal{W}} = r.$$

It is easy to compute the quadratic error in approximating  $H$  with  $L_p$  in the euclidean metric, since

$$H \begin{bmatrix} x \\ y \end{bmatrix} - L_p \begin{bmatrix} x \\ y \end{bmatrix} = \begin{bmatrix} (x - z)^2 \\ 0 \end{bmatrix}.$$

We then convert to the  $\mathcal{W}$ -norm, using Lemma 5.1.3 twice, to get

$$\begin{aligned} \left\| \begin{bmatrix} (x - z)^2 \\ 0 \end{bmatrix} \right\|_{\mathcal{W}} &\leq \frac{1}{C} \left\| \begin{bmatrix} (x - z)^2 \\ 0 \end{bmatrix} \right\|_e = \frac{1}{C} |x - z|^2 \\ &\leq \frac{1}{C} |x - z|^2 + |y - z|^2 = \frac{1}{C} \left\| \begin{bmatrix} x - z \\ y - z \end{bmatrix} \right\|_e^2 \\ &\leq \frac{D^2}{C} \left\| \begin{bmatrix} x - z \\ y - z \end{bmatrix} \right\|_{\mathcal{W}}^2 = \left( \frac{D^2}{C} \right) r^2. \end{aligned}$$

□

Next, we show that in the  $\mathcal{W}$ -norm, the linearization moves points closer to  $p$  by a linear contraction.

**Lemma 5.1.5.**

$$\text{If } \left\| \begin{bmatrix} x - z \\ y - z \end{bmatrix} \right\|_{\mathcal{W}} = r, \text{ then } \left\| L_p \begin{bmatrix} x \\ y \end{bmatrix} - \begin{bmatrix} z \\ z \end{bmatrix} \right\|_{\mathcal{W}} \leq \lambda r.$$

*Proof.* Since  $p$  is fixed,

$$L_p \begin{bmatrix} x \\ y \end{bmatrix} - \begin{bmatrix} z \\ z \end{bmatrix} = D_p H \begin{bmatrix} x - z \\ y - z \end{bmatrix}.$$

Now to work with  $D_p H$ , note that since the columns of  $\mathbf{A}$  are the eigenvectors of  $D_p H$ , we have

$$\mathbf{A}^{-1} D_p H \mathbf{A} = \begin{bmatrix} \lambda_1 & 0 \\ 0 & \lambda_2 \end{bmatrix}.$$

We use this to compute that

$$\begin{aligned} \left\| D_p H \begin{bmatrix} x - z \\ y - z \end{bmatrix} \right\|_{\mathcal{W}} &= \left\| \mathbf{A}^{-1} D_p H \begin{bmatrix} x - z \\ y - z \end{bmatrix} \right\|_e = \left\| \begin{bmatrix} \lambda_1 & 0 \\ 0 & \lambda_2 \end{bmatrix} \mathbf{A}^{-1} \begin{bmatrix} x - z \\ y - z \end{bmatrix} \right\|_e \\ &\leq \lambda \left\| \mathbf{A}^{-1} \begin{bmatrix} x - z \\ y - z \end{bmatrix} \right\|_e = \lambda \left\| \begin{bmatrix} x - z \\ y - z \end{bmatrix} \right\|_{\mathcal{W}} = \lambda r, \end{aligned}$$

where recall  $\lambda = \max\{|\lambda_1|, |\lambda_2|\}$ .

□

Now we can combine the above two lemmas to estimate  $H$  in the sink basin.

**Lemma 5.1.6.**

$$\text{If } \left\| \begin{bmatrix} x - z \\ y - z \end{bmatrix} \right\|_{\mathcal{W}} = r, \text{ then } \left\| H \begin{bmatrix} x \\ y \end{bmatrix} - \begin{bmatrix} z \\ z \end{bmatrix} \right\|_{\mathcal{W}} \leq \lambda r + r^2 \left( \frac{D^2}{C} \right).$$

*Proof.* This follows immediately from Lemmas 5.1.4 and 5.1.5 and the triangle inequality.  $\square$

We now have the tools we need to estimate the euclidean size of the sink basin.

**Proposition 5.1.7.** *Let*

$$\tau = \frac{|\lambda_1 - \lambda_2|^2}{(2 + |\lambda_1| + |\lambda_2|)(2 + \lambda^2 + |a|)}.$$

*Then the euclidean disk centered at  $p$  of radius  $r_p = \tau(1 - \lambda)$  is contained in the immediate sink basin of  $p$ .*

*Proof.* Note  $C^2/D^2 = \tau$ .

We first show that the  $\mathcal{W}$ -disk centered at  $p$  of radius  $s_p = (1 - \lambda)(C/D^2)$ ,  $\mathbb{D}_{\mathcal{W}}(p, s_p)$ , is contained in the sink basin. For, if  $\|(x - z, y - z)\|_{\mathcal{W}} = r \leq s_p$ , then by Lemma 5.1.6,

$$\left\| H \begin{bmatrix} x \\ y \end{bmatrix} - \begin{bmatrix} z \\ z \end{bmatrix} \right\|_{\mathcal{W}} \leq \lambda r + r^2(D^2/C) \leq r.$$

Thus  $H$  maps the disk  $\mathbb{D}_{\mathcal{W}}(p, s_p)$  into itself, and every point in it closer to  $p$  in the  $\mathcal{W}$ -norm. Thus this disk is contained in the immediate sink basin.

Now we simply use Lemma 5.1.3 to convert to a euclidean statement. Let  $r_p = s_p C$ . Then if  $\|(x - z, y - z)\|_e \leq r_p$ , we have

$$\|(x - z, y - z)\|_{\mathcal{W}} \leq \frac{1}{C} \|(x - z, y - z)\|_e \leq \frac{r_p}{C} = s_p.$$

Thus,  $\mathbb{D}_e(p, r_p) \subset \mathbb{D}_{\mathcal{W}}(p, s_p) \subset \{\text{immediate sink basin}\}$ , and

$$r_p = C s_p = (1 - \lambda) \frac{C^2}{D^2} = (1 - \lambda) \tau.$$

$\square$

## Separating the box-chain transitive components

We now investigate the box-chain transitive components of the chain recurrent set. First, given  $\xi$  sufficiently small, we compute a region  $\mathcal{A}_\xi$ , contained in the immediate sink basin in which the contraction toward the fixed point makes a jump of more than  $\xi$ . This will imply that  $\mathcal{A}_\xi$  is not in the  $\xi$ -chain recurrent set with respect to the  $\mathcal{W}$ -norm, and hence this region separates  $\xi$ -chain components.

**Lemma 5.1.8.** *Let  $\xi > 0$  be small enough that*

$$\xi < \frac{(1 - \lambda)^2 C}{4 D^2}.$$

*Then, in the  $\mathcal{W}$ -norm, the  $\xi$ -chain transitive component that contains the sink is separated from the  $\xi$ -chain transitive component of any other invariant set by a distance of  $(1 - \lambda)C/D^2$ .*

*Proof.* Define  $\mathcal{A}_\xi$  by

$$\mathcal{A}_\xi = \left\{ \begin{bmatrix} x \\ y \end{bmatrix} : r_- < \left\| \begin{bmatrix} x \\ y \end{bmatrix} \right\|_{\mathcal{W}} < r_+ \right\},$$

where

$$r_{\pm} = \frac{C}{2D^2} \left( (1 - \lambda) \pm \sqrt{(1 - \lambda)^2 - 4\xi D^2/C} \right).$$

We show that if  $(x_0, y_0) \in \mathcal{A}_\xi$ , it is not  $\xi$ -chain recurrent with respect to  $\|\cdot\|_{\mathcal{W}}$ .

Note that  $r_{\pm}$  are the roots of the polynomial

$$q(r) = (D^2/C)r^2 - (1 - \lambda)r + \xi.$$

Thus  $\xi < C(1 - \lambda)^2/4D^2$  is precisely the condition that needs to hold in order to be positive. Thus for  $r \in (r_-, r_+)$ , we have  $q(r) < 0$ .

Now let  $(x, y) \in \mathcal{A}_\xi$ , so that  $r = \|(x, y)\|_{\mathcal{W}} \in (r_-, r_+)$ . Then by Lemma 5.1.6 and the triangle inequality, we get

$$\begin{aligned} \left\| \begin{bmatrix} x \\ y \end{bmatrix} - H \begin{bmatrix} x \\ y \end{bmatrix} \right\|_{\mathcal{W}} &\geq \left\| \begin{bmatrix} x \\ y \end{bmatrix} - \begin{bmatrix} z \\ z \end{bmatrix} \right\|_{\mathcal{W}} - \left\| \begin{bmatrix} z \\ z \end{bmatrix} - H \begin{bmatrix} x \\ y \end{bmatrix} \right\|_{\mathcal{W}} \\ &\geq r - (\lambda r + r^2 (D^2/C)) \\ &= \xi - q(r) \geq \xi. \end{aligned}$$

To finish the proof, we show that this  $\xi$  distance between a point and its image is enough to block  $\xi$ -chain recurrence, since we are in a region of strict contraction. Suppose  $(x_0, y_0) \in \mathcal{A}_\delta$ , with  $\|(x_0, y_0)\|_{\mathcal{W}} = r$ . Let  $n \in \mathbb{N}$  and  $\{(x_1, y_1), \dots, (x_{n-1}, y_{n-1})\}$  be any points s.t.  $\|(x_{j+1}, y_{j+1}) - H(x_j, y_j)\|_{\mathcal{W}} < \xi$ , for  $0 \leq j \leq n - 1$ . To show  $\|(x_0, y_0) - H(x_{n-1}, y_{n-1})\|_{\mathcal{W}} \geq \xi$ , we will first show inductively that for  $0 \leq j \leq n - 1$ ,

$$\left\| \begin{bmatrix} x_j \\ y_j \end{bmatrix} - \begin{bmatrix} z \\ z \end{bmatrix} \right\|_{\mathcal{W}} \leq r, \text{ hence by Lemma 5.1.6, } \left\| H \begin{bmatrix} x_j \\ y_j \end{bmatrix} - \begin{bmatrix} z \\ z \end{bmatrix} \right\|_{\mathcal{W}} \leq \lambda r + r^2(D^2/C). \quad (5.2)$$

We have (5.2) for  $j = 0$  already. Now let  $0 < j < n - 1$ , and suppose we know (5.2) for  $(x_j, y_j)$ . Then, by choice of  $(x_{j+1}, y_{j+1})$ , we get

$$\begin{aligned} \left\| \begin{bmatrix} x_{j+1} \\ y_{j+1} \end{bmatrix} - \begin{bmatrix} z \\ z \end{bmatrix} \right\|_{\mathcal{W}} &\leq \left\| \begin{bmatrix} x_{j+1} \\ y_{j+1} \end{bmatrix} - H \begin{bmatrix} x_j \\ y_j \end{bmatrix} \right\|_{\mathcal{W}} + \left\| H \begin{bmatrix} x_j \\ y_j \end{bmatrix} - \begin{bmatrix} z \\ z \end{bmatrix} \right\|_{\mathcal{W}} \\ &\leq \xi + \lambda r + r^2(D^2/C) = q(r) + r \leq r. \end{aligned}$$

Thus induction verifies (5.2). In particular, this statement holds for  $j = n - 1$ . But then

$$\begin{aligned} \left\| \begin{bmatrix} x_0 \\ y_0 \end{bmatrix} - H \begin{bmatrix} x_{n-1} \\ y_{n-1} \end{bmatrix} \right\|_{\mathcal{W}} &\geq \left\| \begin{bmatrix} x_0 \\ y_0 \end{bmatrix} - \begin{bmatrix} z \\ z \end{bmatrix} \right\|_{\mathcal{W}} - \left\| H \begin{bmatrix} x_{n-1} \\ y_{n-1} \end{bmatrix} - \begin{bmatrix} z \\ z \end{bmatrix} \right\|_{\mathcal{W}} \\ &\geq r - \lambda r - r^2(D^2/C) = \xi - q(r) \geq \xi. \end{aligned}$$

□

This lemma leads directly to:

**Proposition 5.1.9.** *Let*

$$\tau = \frac{|\lambda_1 - \lambda_2|^2}{(2 + |\lambda_1| + |\lambda_2|)(2 + \lambda^2 + |a|)}.$$

*Let  $\eta > 0$  be small enough that  $\eta < \tau(1 - \lambda)^2/4$ . Then the  $\eta$ -chain transitive component containing the sink is separate from the  $\eta$ -chain transitive component of any other invariant set.*

*In particular, there exists a connected set  $\mathcal{S}_\eta$  in the immediate sink basin which lies in  $\mathbb{C}^2 \setminus \mathcal{R}_\eta$ , i.e., the complement of the  $\eta$ -chain recurrent set.*

*Proof.* Note  $C^2/D^2 = \tau$ .

We simply convert Lemma 5.1.8 to euclidean estimates, using Lemma 5.1.3. Let  $\eta = \xi C$ , so that

$$\eta = \xi C < \frac{(1 - \lambda)^2 C^2}{4 D^2} = \frac{(1 - \lambda)^2}{4} \tau.$$

Define the set  $\mathcal{S}_\eta$  to be simply the set  $\mathcal{A}_\xi$ , from the proof of Lemma 5.1.8. Let  $(x_0, y_0) \in \mathcal{S}_\eta$ , and let  $n \in \mathbb{N}$  and  $\{(x_1, y_1), \dots, (x_{n-1}, y_{n-1})\}$  be any points such that

$$\left\| \begin{bmatrix} x_{j+1} \\ y_{j+1} \end{bmatrix} - H \begin{bmatrix} x_j \\ y_j \end{bmatrix} \right\|_e < \eta, \quad 0 \leq j \leq n - 1.$$

Then

$$\left\| \begin{bmatrix} x_{j+1} \\ y_{j+1} \end{bmatrix} - H \begin{bmatrix} x_j \\ y_j \end{bmatrix} \right\|_{\mathcal{W}} < \eta/C = \xi.$$

Thus by Lemma 5.1.8,

$$\left\| \begin{bmatrix} x_0 \\ y_0 \end{bmatrix} - H \begin{bmatrix} x_{n-1} \\ y_{n-1} \end{bmatrix} \right\|_e \geq C \left\| \begin{bmatrix} x_0 \\ y_0 \end{bmatrix} - H \begin{bmatrix} x_{n-1} \\ y_{n-1} \end{bmatrix} \right\|_{\mathcal{W}} \geq C\xi = \eta.$$

Thus,  $(x_0, y_0)$  is not in  $\mathcal{R}_\eta$ . □

Now we apply the estimates of Proposition 5.1.9 to guarantee when the Julia set s.c.c. will be separated from the s.c.c. for the fixed sink, to prove Proposition 5.1.10. Recall the box-chain transitive components are precisely the s.c.c.'s.

**Proposition 5.1.10.** *Suppose  $\mathcal{V}_\epsilon$  is a box cover of  $\mathcal{R}$ , corresponding to a box-chain recurrent graph  $\Gamma_\delta$ . Let  $M > 1$  be such that  $\delta < \epsilon/M$ . Let*

$$\begin{aligned}\tau &= \frac{|\lambda_1 - \lambda_2|^2}{(2 + |\lambda_1| + |\lambda_2|)(2 + \lambda^2 + |a|)}, \\ \zeta &= \frac{(1 - \lambda)^2}{4}\tau, \text{ and} \\ \kappa &= \left[1 + 1/M + \max\left(1, (1 - \lambda)\sqrt{\tau} + 2\|p\|_\infty + |a|_\infty\right)\right].\end{aligned}$$

*If  $\epsilon < \frac{1}{2}\left(-\kappa + \sqrt{\kappa^2 + 4\zeta}\right)$ , then the box-chain transitive component of  $\Gamma$  containing  $J$  will be different from the box-chain transitive component of  $\Gamma$  containing the sink  $p$ .*

*Proof.* Note  $C^2/D^2 = \tau$ .

We show that the s.c.c.'s will separate if  $\epsilon > 0$  is small enough that  $\epsilon^2 + \epsilon\kappa < \zeta$ .

To find such  $\epsilon$ , let  $q(\epsilon) = \epsilon^2 + \epsilon\kappa - \zeta$ . Then the roots of  $q$  are  $(-\kappa \pm \sqrt{\kappa^2 + 4\zeta})/2$ . Both roots are real, with one positive and one negative. We seek  $\epsilon > 0$  small enough that  $q(\epsilon) < 0$ , which is the same as  $\epsilon$  smaller than the positive root  $(-\kappa + \sqrt{\kappa^2 + 4\zeta})/2$ .

Now, by Proposition 5.1.9, for  $\eta < (\tau(1 - \lambda)^2/4)$  there will be a connected set  $\mathcal{S}_\eta = \mathcal{A}_\xi$  in the immediate sink basin which lies in  $\mathbb{C}^2 \setminus \mathcal{R}_\eta$ .

Recall that Theorem 2.2.6 calculates an  $\epsilon'$  such that  $\mathcal{B} \subset \mathcal{R}_{\epsilon'}$ . It specifies that  $\epsilon' = \delta + \epsilon + r$ , where  $r$  is computed in Lemma 2.2.4 as  $r = \epsilon^2 + \epsilon(2R^+ + |a|_\infty)$ . Examining the proof of Lemma 2.2.4, we see that in order to apply this to  $\mathcal{A}_\xi$ , we can use a slightly better estimate for  $r$ , so instead of  $\epsilon'$  we get

$$\nu = \epsilon/M + \epsilon + \epsilon^2 + \epsilon \max(1, 2R^+ + |a|_\infty),$$

where  $R^+$  is a bound on the box-norm,  $\|\cdot\|_\infty$ , of a point in  $\mathcal{A}_\xi$ , which we calculate below. Then for  $\mathcal{B} = \mathcal{B}(\mathcal{V}_\epsilon)$ , we get  $\mathcal{B} \cap \mathcal{A}_\xi \subset \mathcal{R}_\nu$ . Hence if  $\nu \leq \eta$ , then  $\mathcal{R}_\nu \subset \mathcal{R}_\eta$ . But since  $\mathcal{S}_\eta = \mathcal{A}_\xi$ , by Proposition 5.1.9, we get

$$\mathcal{S}_\eta \cup \mathcal{B} \subset \mathcal{S}_\eta \cup \mathcal{R}_\eta = \emptyset.$$

Thus the cover does not intersect  $\mathcal{S}_\eta$ .

Now since  $\mathbb{D}_{\mathcal{W}}(p, s_p)$  is mapped into itself by  $H$ , there will be no edges from boxes inside  $\mathbb{D}_{\mathcal{W}}(p, s_p)$  to those outside of  $\mathbb{D}_{\mathcal{W}}(p, s_p)$ . Since  $\mathcal{S}_\eta \subset \mathbb{D}_{\mathcal{W}}(p, s_p)$ , the s.c.c. containing the sink will not be part of the s.c.c. containing  $J$ , whenever the box size  $\epsilon$  is small enough that  $\nu \leq \eta < (\tau(1 - \lambda)^2/4)$ . To maximize the box side length  $\epsilon$ , we use the bound that  $\eta < (\tau(1 - \lambda)^2/4)$ .

We need to compute that  $R^+$ , a bound on the norm of a point in  $\mathcal{A}_\xi$ , with respect to  $\|\cdot\|_\infty$ , is

$$R^+ = (1 - \lambda)\sqrt{\tau}/2 + \|p\|_\infty.$$

Substituting this value of  $R^+$  into the definition of  $\nu$ , and requiring  $\nu < (\tau(1 - \lambda)^2/4)$  will finish the proof.

To compute  $R^+$ , we use that  $\mathcal{A}_\xi$  in the  $\mathcal{W}$ -norm is centered at the point  $p$ , and has outer radius  $r_+ = \frac{C}{2D^2} \left( (1 - \lambda) + \sqrt{(1 - \lambda)^2 - 4\xi D^2/C} \right)$ . But at the maximum  $\eta = \xi C$ , the discriminant is zero, so we have  $r_+ \leq \frac{C}{2D^2}(1 - \lambda)$ . Converting to the euclidean norm, we have a bound of  $Dr_+ \leq \frac{C}{2D}(1 - \lambda) = \sqrt{\tau}(1 - \lambda)/2$ . Now since the box-norm is less than euclidean, we get that if  $(x, y) \in \mathcal{A}$ , then  $\|(x, y)\|_\infty \leq \sqrt{\tau}(1 - \lambda)/2 + \|p\|_\infty =: R^+$ .  $\square$

*Remark.* In the above proposition, one does not need all boxes of size  $\epsilon$ , but rather just the boxes in the immediate sink basin, computed in Proposition 5.1.7. Thus a selective subdivision procedure targeting the sink basin could be advantageous for speeding up separation.

## One dimension

Finally, note that all of the work of this section applies to  $P_c(z) = z^2 + c$ , in the case of an attracting fixed sink  $p$  with multiplier  $\lambda = |P'_c(p)|$ . In this case, we do not need the  $\mathcal{W}$ -norm, so take  $\tau = C = D = 1$ . Then conclude that the disk  $\mathbb{D}_\epsilon(p, (1 - \lambda))$  is in the sink basin and for  $\delta < (1 - \lambda)^2/4$  the set:

$$\mathcal{A}_\delta = \{z : r_- < |z - p| < r_+\},$$

where

$$r_\pm = \frac{1}{2} \left( (1 - \lambda) \pm \sqrt{(1 - \lambda)^2 - 4\delta} \right),$$

is in  $\mathbb{C} \setminus \mathcal{R}_\delta$ . Then we see that in order to guarantee separation of  $J$  from the sink, for

$$\kappa = (1 + 1/M + (1 - \lambda) + 2|p|), \text{ and } \zeta = (1 - \lambda)^2/4,$$

we need boxes of side length  $\epsilon$  satisfying

$$\epsilon < \left( -\kappa + \sqrt{\kappa^2 + 4\zeta} \right) / 2.$$

## The 3-1 map

We now apply our estimates to the  $(c = -1.17, a = .3)$  example, to determine how much smaller the boxes would need to be to get separation of  $J$  from the fixed sink. Table 5.1 shows the values of the constants involved in the estimates.

Thus, we would need a box side length less than 0.00004 to get just the fixed sink separated from  $J$ . But this is several orders of magnitude smaller than the best we could compute with current resources (0.015). Also, note that the guaranteed euclidean disk contained in the sink basin is only of radius 0.0034. But visually inspecting this example using FractalAsm suggests the immediate basin seems much larger.

Table 5.1: Constants for sink/ $J$  separation estimates for Example 5.1.1.

$p$	$=$	$(-0.612, -0.612)$
$\lambda_1$	$=$	$-.885$
$\lambda_2$	$=$	$-.34$
$\lambda$	$=$	$.885$
$\tau$	$=$	$0.029871571$
$\tau(1 - \lambda)$	$=$	$0.0034352307$
$\kappa$	$=$	$2.5448759$
$\zeta$	$=$	$9.876288 \times 10^{-5}$
$\epsilon$	$<$	$3.880793 \times 10^{-5}$

## 5.2 Conclusions

The motivation for this thesis was to write a program testing hyperbolicity of a complex Hénon map using basic computer-friendly notions, such as the chain recurrent set, and the cone field condition to check for hyperbolicity. We had some measure of success in this. The program verifies hyperbolicity for some diffeomorphisms.

One goal for this project was the exploration of the behavior of certain complex Hénon diffeomorphisms which cannot be described in terms of one dimensional phenomena, as described in Section 1.3. Unfortunately, the diffeomorphisms for which we can verify hyperbolicity are not of this type.

We found that one of the key issues which determines success or failure of the hyperbolicity test is a clear separation of the sinks from the Julia set, in fact more separation is needed than we had originally guessed. For example, as discussed in Example 4.4.4, Figure 4.8 shows that most of the places where the cone check failed were those closest to the sink basin. Another indicator is Example 4.4.5, in which Figures 4.5 and 4.6 show that the boxes in which the unstable and stable directions were not separated enough to define cones preserved by the diffeomorphism were in the sink basin. Also, merely getting the box cover refined sufficiently that the sink s.c.c. was separate from the Julia set s.c.c. was surprisingly difficult, as discussed in Example 5.1.1, Figure 5.1. This example shows the limitations of finding the chain recurrent set.

Developing a finer cover with subdivision of all boxes leads to exponential

increase in computer resources. The alternative is choosing only a small fraction of the boxes to be subdivided, and hoping that the right choice will help eliminate undesirable boxes from the cover. However, as discussed in Section 4.4.3, it is not clear which boxes to choose, or that subdividing only a few boxes will even eliminate enough boxes to make a difference in the cover.

This work demonstrates that computer programs can be useful in rigorously describing behavior of hyperbolic complex Hénon diffeomorphisms. The approach we adopted is straightforward. Our work suggests that either new approaches or significantly greater computer resources are required to verify hyperbolicity of the motivating examples of Section 1.3. We look forward to exploring other techniques.

# Appendix A

## Interval arithmetic

In order to genuinely prove dynamical properties, *Hypatia* uses a method of controlling round-off error in the computations, called *interval arithmetic* (IA). This method was recommended to us by Warwick Tucker, who used it in his recent computer proof that the Lorenz differential equation has the conjectured geometry ([64, 63]).

In fact we use IA not only to control error, but take advantage of the structure of this method in the algorithm of *Hypatia*. We thus give a very brief description of IA below, and refer the interested reader to [63, 51, 52, 18].

On a computer, we cannot work with real numbers, but rather we work over the finite space  $\mathbb{F}$  of numbers representable by binary floating point numbers no longer than a certain length. For example, since the number 0.1 is not a dyadic rational, it has an infinite binary expansion. So the computer cannot encode exactly this number. Instead, the basic objects of arithmetic are not real numbers, but rather closed intervals,  $[a, b]$ , with end points in  $\mathbb{F}$ . We denote this space of intervals by  $\mathbb{IF}$ . So to encode the number 0.1, IA use the idea of *directed rounding*:

$$x \in [\downarrow x \downarrow, \uparrow x \uparrow],$$

where  $\downarrow x \downarrow$  is the largest number in  $\mathbb{F}$  that is strictly less than  $x$  (*i.e.*,  $x$  rounded down), and  $\uparrow x \uparrow$  is the smallest number in  $\mathbb{F}$  that is strictly greater than  $x$  (*i.e.*,  $x$  rounded up).

If the user is interested in a computation involving real numbers, then IA performs the computation using intervals in  $\mathbb{IF}$  which contain those real numbers, and gives the answer as an interval in  $\mathbb{IF}$  which contains the real answer.

Consider for example the operation of addition of two intervals  $[a, b], [c, d] \in \mathbb{IF}$ . IA defines addition by:

$$[a, b] + [c, d] = [\downarrow a + c \downarrow, \uparrow b + d \uparrow].$$

Hence if  $x \in [a, b]$  and  $y \in [c, d]$ , then  $x + y \in [a, b] + [c, d]$ .

The other operations are defined analogously:

$$\begin{aligned} [a, b] - [c, d] &= [\downarrow a - d \downarrow, \uparrow b - c \uparrow] \\ [a, b] \times [c, d] &= [\downarrow \min(ac, ad, bc, bd) \downarrow, \uparrow \max(ac, ad, bc, bd) \uparrow] \\ [a, b] \div [c, d] &= [a, b] \times [\downarrow 1/d \downarrow, \uparrow 1/c \uparrow], \text{ if } 0 \notin [c, d]. \end{aligned}$$

In higher dimensions, IA operations can be carried out component-wise, on *interval vectors*. Given  $X$  a number in  $\mathbb{C}^n$ , or an interval vector in  $\mathbb{R}^{2n} = \mathbb{C}^n$ , we denote by  $\text{Hull}(f(X))$  the interval vector computed by IA which contains the image of  $X$  under a polynomial map or diffeomorphism,  $f$ .

In the main body of the dissertation, we almost never mention explicitly how we are using interval arithmetic, despite the fact that one must think carefully about

how to use IA in each situation. It tends to create problems with propagating increasingly large error bounds if not handled carefully. For example, iterating a polynomial map or diffeomorphism like  $P_c$  or  $H_{a,c}$  on an interval vector which is not very close to an attracting period cycle will give a tremendously large interval vector after only a few iterates. That is, if  $B = [a, b] \times [c, d]$  is an interval vector in  $\mathbb{C}$ , and one attempts to compute a box containing  $P_c^{10}(B)$  by:

```

for (j = 1) to (j = 10) do
  B = P_c(B)
  j = j + 1

```

then the box  $B$  will likely grow so large that its defining bounds become machine  $\infty$ , *i.e.*, the largest floating point in  $\mathbb{F}$ . Similarly, one would also never want to try to compute:

$$D_{B_n}H \circ \cdots \circ D_{B_1}H \circ D_{B_0}H(\mathbf{u}),$$

for a vector  $\mathbf{u} \in \mathbb{C}^2$ , since the entries would blow up.

*Hypatia* uses IA for all of its rigorous computations. The IA routines were all provided by the PROFIL/BIAS package, available at [58].

# Appendix B

## Pseudo-code

The algorithm **fExpands** below is described in Section 3.2. Here we provide its pseudo-code.

### Algorithm B.0.1.

**fExpands**( $\Gamma', L$ ):  
do SpanTree(vertex 0 of  $\Gamma'$ )  
for every edge  $(u, v)$  in the graph  $\Gamma'$   
    if (Check[ $u$ ][ $v$ ] = 0) then (*if edge not in spanning tree*)  
        set Check[ $u$ ][ $v$ ] = 1  
        if (FixMetricEdge( $u, v, u, L$ ) = 0) then return 0  
return 1 (*successful*)

**SpanTree**( $v$ ):  
set Color[ $v$ ] to Gray  
for each vertex  $w$  in Adjacency list of  $v$  do  
    if Color[ $w$ ] is White  
        set Check[ $v$ ][ $w$ ] = 1 (*to note that we've checked edge  $(v, w)$* )  
        set  $c_w = Lc_v/\lambda_v$   
        do SpanTree( $w$ )  
set Color[ $v$ ] =Black

**FixMetricEdge**( $a, b, u, L$ ):  
if ( $c_b \geq Lc_a/\lambda_a$ ) then return 1 (*edge  $(a, b)$  OK*)  
else if ( $b = u$ ) then return 0 (*cannot increase  $c_u$ , so fails*)  
else  
    set  $c_b = Lc_a/\lambda_a$  (*increase  $c_b$* )  
    for each  $w$  in adjacency list of  $b$  do  
        if (Check[ $b$ ][ $w$ ] = 1) then  
            if (FixMetric( $b, w, u, L$ ) = 0) then return 0  
return 1 (*if get here, it worked*)

The **Bisection** method is mentioned in Section 3.4.2. Below we give pseudo-code for it.

### Algorithm B.0.2.

**Bisection**( $\Gamma'$ )  
set  $L = 2$ ; hi $L = 2$ ; lo $L = 1$   
for  $k = 0$  to  $k = M$  do  
    if (fExpands( $\Gamma', L$ )=1) then (*try raising  $L$* )

```

    set hiL = L; loL = L; L = (hiL + L)/2
  else (try lowering L)
    set hiL = L; L = (loL + L)/2
  increment k = k + 1

```

Below, a slightly modified **fExpands** (needed in Section 3.4.2) stores the bad cycle, in case of failure to expand, and computes the product of the multipliers along the cycle as it unravels the recursive function calls after the failure.

**Algorithm B.0.3.**

**CheckCycles**( $\Gamma', \delta$ ):

```

set L = 2
while (L > 1) do
  if (fExpands( $\Gamma', L$ ) = 1) then return 1 (i.e., expansion successful)
  else if (multiplier  $\leq$  1) then return 0 (cannot show box-exp. on  $\Gamma'$ )
  else (try to show box-exp. by lower L)
    set L = min(multiplier, L -  $\delta$ )
return 0 (if reached this, unsuccessful. maybe  $\delta$  too large)

```

**fExpands**( $\Gamma', L$ ):

```

do SpanTree(Vertex 0 of  $\Gamma'$ )
for every edge (u, v) in the graph  $\Gamma'$ 
  if (Check[u][v] = 0) (i.e., if edge not in spanning tree)
    set Check[u][v] = 1
    if (FixMetricEdge(u, v, u, L) = 0) (found bad cycle and multiplier)
      compute n = length(badcycle)
      set multiplier = (multiplier)1/n
      return 0
return 1

```

**FixMetricEdge**(a, b, u, L):

```

if ( $c_b \geq Lc_a/\lambda_a$ ) then return 1. (edge (a, b) is OK)
else if (b = u) then (cannot increase  $c_u$ , so fails)
  put b in badcycle (or edge  $b \rightarrow u$ , and set multiplier =  $\lambda_b$ )
  return 0
else
  set  $c_b = Lc_a/\lambda_a$  (i.e., increase  $c_b$ )
  for each w in adjacency list of b
    if (Check[b][w] = 1) then
      if (FixMetric(b, w, u, L) = 0), then do
        put a in badcycle (or edge  $a \rightarrow b$ )
        set multiplier = multiplier *  $\lambda_a$ 
        return 0

```

return 1 (*if get here, it worked*)

**BetterMetric** is first used in Section 3.5.2. Here is the pseudo-code description:

**Algorithm B.0.4.**

**BetterMetric**( $\Gamma', L_0$ ):  
 initialize  $\text{edgeL}[u][v] = 0$  for all edges  $(u, v)$   
 set  $\text{edgeL}[u][v] = L_0$  for edges in badcycle  
 set  $M =$  some cap for number of attempts  
 set  $k = 0$  and  $\text{full} = 0$   
 set  $\text{loL} = L_0$  and  $L = \text{loL} + \delta$   
 while ( $k < M$  and  $\text{full} = 0$ )  
   if (**BetterfExpands**( $\Gamma', L$ ) = 0)  
     for each edge  $(u, v)$  in badcycle do  
       if ( $\text{edgeL}[u][v] = 0$ ) then set  $\text{edgeL}[u][v] = \text{loL}$   
     else (*metric built!*)  
       print/store information on new metric constants  
       if ( $\text{edgeL}[u][v] \neq 0$  on all edges) then set  $\text{full} = 1$   
         (*all edges marked, so stop*)  
       else set  $\text{loL} = L$  and  $L = L + \delta$  (*try larger L*)  
     increment  $k = k + 1$

**BetterfExpands** is exactly the same as **fExpands**, except that it calls **BetterSpanTree** and **BetterFixMetricEdge**. The only difference in these last two is that we replace each instance of using  $L$  on edge  $(u, v)$  to compute the metric with:

if ( $\text{edgeL}[u][v] \neq 0$ ) then use  $\text{edgeL}[u][v]$   
 else use  $L$

## REFERENCES

- [1] Dynamics at Cornell. [<http://www.math.cornell.edu/~dynamics>].
- [2] E. Bedford, M. Lyubich, and J. Smillie. Distribution of periodic points of polynomial diffeomorphisms of  $\mathbf{C}^2$ . *Invent. Math.*, 114(2):277–288, 1993.
- [3] Eric Bedford and John Smillie. Real polynomial diffeomorphisms with maximal entropy: Tangencies. to appear, preprint available at [<http://xxx.arxiv.org>].
- [4] Eric Bedford and John Smillie. Fatou-Bieberbach domains arising from polynomial automorphisms. *Indiana Univ. Math. J.*, 40(2):789–792, 1991.
- [5] Eric Bedford and John Smillie. Polynomial diffeomorphisms of  $\mathbf{C}^2$ : currents, equilibrium measure and hyperbolicity. *Invent. Math.*, 103(1):69–99, 1991.
- [6] Eric Bedford and John Smillie. Polynomial diffeomorphisms of  $\mathbf{C}^2$ . II. Stable manifolds and recurrence. *J. Amer. Math. Soc.*, 4(4):657–679, 1991.
- [7] Eric Bedford and John Smillie. Polynomial diffeomorphisms of  $\mathbf{C}^2$ . III. Ergodicity, exponents and entropy of the equilibrium measure. *Math. Ann.*, 294(3):395–420, 1992.
- [8] Eric Bedford and John Smillie. Polynomial diffeomorphisms of  $\mathbf{C}^2$ . V. Critical points and Lyapunov exponents. *J. Geom. Anal.*, 8(3):349–383, 1998.
- [9] Eric Bedford and John Smillie. Polynomial diffeomorphisms of  $\mathbf{C}^2$ . VI. Connectivity of *J. Ann. of Math. (2)*, 148(2):695–735, 1998.
- [10] Eric Bedford and John Smillie. Polynomial diffeomorphisms of  $\mathbf{C}^2$ . VII. Hyperbolicity and external rays. *Ann. Sci. École Norm. Sup. (4)*, 32(4):455–497, 1999.
- [11] Eric Bedford and John Smillie. Polynomial diffeomorphisms of  $\mathbf{C}^2$ . VIII. Quasi-Expansion. *Amer. J. Math.*, 124(2):221–271, 2002.
- [12] Paul Blanchard, Robert L. Devaney, and Linda Keen. The dynamics of complex polynomials and automorphisms of the shift. *Invent. Math.*, 104(3):545–580, 1991.
- [13] B. Branner and J. H. Hubbard. The iteration of cubic polynomials. I. The global topology of parameter space. *Acta Math.*, 160(3-4):143–206, 1988.
- [14] B. Branner and J. H. Hubbard. The iteration of cubic polynomials. II. Patterns and parapatterns. *Acta Math.*, 169(3-4):229–325, 1992.
- [15] H Brolin. Invariant sets under iteration of rational functions. *Ark. Mat.*, 6:103–144, 1965.

- [16] Gregory T. Buzzard. Kupka-Smale theorem for automorphisms of  $\mathbf{C}^n$ . *Duke Math. J.*, 93(3):487–503, 1998.
- [17] Gregory T. Buzzard and Kaushal Verma. Hyperbolic automorphisms and holomorphic motions in  $\mathbf{c}^2$ . *Michigan Math. J.*, 49(3):541–565, 2001.
- [18] Interval Computations. [<http://www.cs.utep.edu/interval-comp/>].
- [19] C. Conley. Isolated invariant sets and morse index. *Amer. Math. Soc. CBMS*, 38, 1978.
- [20] T. Cormen et al. *Introduction to Algorithms*. The MIT Electrical Engineering and Computer Science Series. The MIT Press and McGraw-Hill Book Company, 1990.
- [21] A. Douady and J.H. Hubbard. Étude dynamique des polynômes complexes. *Publications mathématiques d'Orsay*, 1984-85.
- [22] Adrien Douady and John H. Hubbard. A proof of Thurston's topological characterization of rational functions. *Acta Math.*, 171(2):263–297, 1993.
- [23] John Erik Fornæss and Nessim Sibony. Complex Hénon mappings in  $\mathbf{C}^2$  and Fatou-Bieberbach domains. *Duke Math. J.*, 65(2):345–380, 1992.
- [24] John Erik Fornæss and Nessim Sibony. Critically finite rational maps on  $\mathbf{P}^2$ . In *The Madison Symposium on Complex Analysis (Madison, WI, 1991)*, pages 245–260. Amer. Math. Soc., Providence, RI, 1992.
- [25] John Erik Fornæss and Nessim Sibony. Complex dynamics in higher dimension. I. *Astérisque*, (222):5, 201–231, 1994. Complex analytic methods in dynamical systems (Rio de Janeiro, 1992).
- [26] John Erik Fornæss and Nessim Sibony. Complex dynamics in higher dimensions. In *Complex potential theory (Montreal, PQ, 1993)*, pages 131–186. Kluwer Acad. Publ., Dordrecht, 1994. Notes partially written by Estela A. Gavosto.
- [27] John Erik Fornæss and Nessim Sibony. Classification of recurrent domains for some holomorphic maps. *Math. Ann.*, 301(4):813–820, 1995.
- [28] John Erik Fornæss and Nessim Sibony. Complex dynamics in higher dimension. II. In *Modern methods in complex analysis (Princeton, NJ, 1992)*, pages 135–182. Princeton Univ. Press, Princeton, NJ, 1995.
- [29] John Erik Fornæss and Nessim Sibony. Oka's inequality for currents and applications. *Math. Ann.*, 301(3):399–419, 1995.
- [30] John Erik Fornæss and Nessim Sibony. Fatou and Julia sets for entire mappings in  $\mathbf{C}^k$ . *Math. Ann.*, 311(1):27–40, 1998.

- [31] John Erik Fornæss and Nessim Sibony. Hyperbolic maps on  $\mathbf{P}^2$ . *Math. Ann.*, 311(2):305–333, 1998.
- [32] John Erik Fornæss and Nessim Sibony. Complex dynamics in higher dimension. In *Several complex variables (Berkeley, CA, 1995–1996)*, pages 273–296. Cambridge Univ. Press, Cambridge, 1999.
- [33] John Erik Fornæss and Nessim Sibony. Dynamics of  $\mathbf{P}^2$  (examples). In *Laminations and foliations in dynamics, geometry and topology (Stony Brook, NY, 1998)*, pages 47–85. Amer. Math. Soc., Providence, RI, 2001.
- [34] John Erik Fornæss and Nessim Sibony. Some open problems in higher dimensional complex analysis and complex dynamics. *Publ. Mat.*, 45(2):529–547, 2001.
- [35] Shmuel Friedland and John Milnor. Dynamical properties of plane polynomial automorphisms. *Ergodic Theory Dynamical Systems*, 9(1):67–99, 1989.
- [36] George Grätzer. *Math into L<sup>A</sup>T<sub>E</sub>X 2<sub>ε</sub> Third edition*. Birkhäuser Springer, 2000.
- [37] M. Hénon. Numerical study of quadratic area preserving mappings. *Q. Appl. Math.*, 27:291–312, 1969.
- [38] M. Hénon. A two-dimensional mapping with a strange attractor. *Commun. Math. Phys.*, 50:69–77, 1976.
- [39] Kenneth Hoffman and Ray Kunze. *Linear Algebra Second Edition*. Prentice Hall, 1971.
- [40] L. Hörmander. *An Introduction to complex analysis in several variables*. North-Holland, 1973.
- [41] John Hubbard and Karl Papadantonakis. Exploring the parameter space of complex hénon mappings. *Journal of Experimental Mathematics*, to appear.
- [42] John Hubbard, Peter Papadopol, and Vladimir Veselov. A compactification of Hénon mappings in  $\mathbf{C}^2$  as dynamical systems. *Acta Math.*, 184(2):203–270, 2000.
- [43] John H. Hubbard and Ralph W. Oberste-Vorth. Hénon mappings in the complex domain. I. The global topology of dynamical space. *Inst. Hautes Études Sci. Publ. Math.*, (79):5–46, 1994.
- [44] John H. Hubbard and Ralph W. Oberste-Vorth. Hénon mappings in the complex domain. II. projective and inductive limits of polynomials. In B. Branner and P. Hjorth, editors, *Real and Complex Dynamical Systems*, volume 464 of *NATO Adv. Sci. Inst. Ser. C Math. Phys. Sci.*, pages 89–132. Kluwer Acad. Publ., Dordrecht, 1995.

- [45] John H. Hubbard and Peter Papadopol. Superattractive fixed points in  $\mathbf{C}^n$ . *Indiana Univ. Math. J.*, 43(1):321–365, 1994.
- [46] John H. Hubbard and Dierk Schleicher. The spider algorithm. In *Complex dynamical systems (Cincinnati, OH, 1994)*, pages 155–180. Amer. Math. Soc., Providence, RI, 1994.
- [47] A. Katok and B. Hasselblatt. *Introduction to the Modern Theory of Dynamical Systems*, volume 54 of *Encyclopedia of Mathematics and its Applications*. Cambridge University Press, Cambridge, Mass., 1995.
- [48] R. Mañé, P. Sad, and D. Sullivan. On the dynamics of rational maps. *Ann. Sci. École Norm. Sup. (4)*, 16(2):193–217, 1983.
- [49] A. Manning. The dimension of the maximal measure for a polynomial map. *Ann. Math.*, 119:425–430, 1984.
- [50] J. Milnor. *Dynamics in One Complex Variable. Introductory Lectures*. Friedr. Vieweg and Sohn, Braunschweig, 1999.
- [51] R. E. Moore. *Interval Analysis*. Prentice-Hall, Englewood Cliffs, New Jersey, 1966.
- [52] R. E. Moore. *Methods and Applications of Interval Analysis*. SIAM Studies in Applied Mathematics, Philadelphia, 1979.
- [53] S. Morosawa, Y. Nishimura, M. Taniguchi, and T. Ueda. *Holomorphic dynamics*. Cambridge University Press, Cambridge, 2000. Translated from the 1995 Japanese original and revised by the authors.
- [54] S. Newhouse. Lectures on dynamical systems. In *Dynamical Systems (C.I.M.E. Summer School, Bressanone, 1978)*, volume 8 of *Progress in Mathematics*, pages 1–114. Birkhäuser, Boston, Mass., 1980.
- [55] S. Newhouse and J. Palis. Bifurcations of Morse-Smale dynamical systems. In *Dynamical systems (Proc. Sympos., Univ. Bahia, Salvador, 1971)*, pages 303–366. Academic Press, New York, 1973.
- [56] Ralph W. Oberste-Vorth. *Complex horseshoes and the dynamics of mappings of two complex variables*. PhD thesis, Cornell University, 1987.
- [57] Ricardo Oliva. *On the combinatorics of external rays in the dynamics of the complex Hénon map*. PhD thesis, Cornell University, 1998.
- [58] PROFIL/BIAS Interval Arithmetic Package.  
[<http://www.ti3.tu-harburg.de/Software/PROFILEnglisch.html>].
- [59] F Przytycki. Hausdorff dimension of the harmonic measure on the boundary of an attractive basin for a holomorphic map. *Invent. math.*, 80:161–179, 1985.

- [60] Clark Robinson. *Dynamical systems*. CRC Press, Boca Raton, FL, second edition, 1999. Stability, symbolic dynamics, and chaos.
- [61] Michael Shub, Albert Fathi, and Rémi Langevin. *Global stability of dynamical systems*. Springer-Verlag, New York, 1987. Translated from the French by Joseph Christy.
- [62] John Smillie. The entropy of polynomial diffeomorphisms of  $\mathbf{C}^2$ . *Ergodic Theory Dynam. Systems*, 10(4):823–827, 1990.
- [63] Warwick Tucker. A rigorous ode solver and Smale’s 14th problem. Preprint available at [<http://www.math.uu.se/~warwick/papers.html>].
- [64] Warwick Tucker. The Lorenz attractor exists. *C. R. Acad. Sci. Paris Sér. I Math.*, 328(12):1197–1202, 1999.